Summer 7-1-2017

Oxygen Isotope Composition of Water in Martian Meteorites

Oleg Vitalivich Maltsev
University of New Mexico

Oleg Maltsev
Candidate

Earth and Planetary Science
Department

This dissertation is approved, and it is acceptable in quality and form for publication:

Approved by the Dissertation Committee:

Karen Ziegler   , Chairperson

Zachary Sharp

Carl Agee

OXYGEN ISOTOPE COMPOSITION OF WATER IN MARTIAN METEORITES

BY

Oleg Vitalivich Maltsev

B.S. Earth and Planetary Science, University of New Mexico, 2014

B.A. Media Arts, University of New Mexico, 2011

THESIS

Submitted in Partial Fulfillment of the

Requirements for the Degree of

Master of Science

Earth and Planetary Science

The University of New Mexico

Albuquerque, New Mexico

July 2017

DEDICATION

I dedicate this work to my mother Faina Fialkovskaya. Thank you for never giving up.

OXYGEN ISOTOPE COMPOSITION OF WATER IN MARTIAN METEORITES

Oleg Vitalivich Maltsev

M.S. Earth and Planetary Science, University of New Mexico, 2017

B.S. Earth and Planetary Science, University of New Mexico, 2014

B.A. Media Arts, University of New Mexico, 2011

Abstract

The oxygen isotope composition of water extracted from Martian meteorites appears not to be in isotopic equilibrium with the silicate portion of the meteorites. This disequilibrium suggests the existence of multiple distinct oxygen isotope reservoirs on planet Mars. Here we present oxygen isotope measurements of waters extracted from Martian shergottites Tissint, Zagami and NWA-7042 and from nakhlite NWA-10153. These waters were extracted by stepwise heating to preserve segregation between low temperature adsorbed waters, intermediate temperature mineral waters and the high temperature mineral structural OH groups. The results of our study, analyzed cooperatively with previous work by Karlsson et al., (1992) and Agee et al., (2013), show that two isotopically distinct water reservoirs exist on Mars. The isotopic influence of these two reservoirs is preserved in two distinct groups of Martian meteorites. Martian shergottites preserve the isotopic composition of Martian mantle waters while nakhlites and Chassigny preserve a contribution from a reservoir elevated in ^{17}O. The presence of low temperature aqueous alteration minerals in nakhlites and Chassigny suggests that the elevated ^{17}O component is sourced from Martian near-surface waters. Based on oxygen

isotope measurements of ^{17}O enriched waters extracted from Martian meteorites we propose that the Martian near-surface waters must have a $\Delta'^{17}O$ of at least 0.89‰ or greater.

TABLE OF CONTENTS

1. Introduction and Background Information

1.1 Introduction

The presence of water in Martian meteorites provides a unique glimpse into the evolution of water on Mars. Previous studies (Karlsson et al., 1992; Agee et al., 2013; Ziegler et al., 2013) have shown that the oxygen extracted from water in Martian meteorites is not in isotopic equilibrium with the bulk silicate rock phases. This disequilibrium suggests that isotopically different reservoirs of oxygen exist on Mars. It has been proposed (Karlsson et al. 1992; Agee et al., 2013) that the mantle, lithosphere, hydrosphere and possibly the atmosphere represent isotopically distinct oxygen reservoirs on Mars, but no end member compositions have been suggested. Studies of hydrous minerals within Martian meteorites have produced a range of hydrogen isotope values from δD of -150 to 4300‰ (Usui et al., 2012). This further supports the possibility that Martian meteorites preserve a history of interaction with different Martian water reservoirs.

In this study, we analyzed the oxygen isotope composition of water extracted from Martian shergottites Tissint, Zagami and NWA-7042 and one nakhlite, NWA-10153. These meteorite samples were generously provided by the Institute of Meteoritics, University of New Mexico (Tissint, Zagami and NWA-10153) and by The Royal Ontario Museum, Toronto (NWA-7042). To facilitate these analyses a specialized water extraction and fluorination line was built at the Center for Stable Isotopes, University of New Mexico. The design of this specialized line was based on work by Karlsson et al. (1992) and O'Neal and Epstein (1966). Certain design modifications were added in this study to improve performance. Oxygen released by fluorination was extensively purified prior to analysis.

The oxygen purification line used in this work followed the design of Sharp et al, (1996). The water was extracted from the samples using a stepwise heating technique. This allowed for the extraction of water over different temperature ranges to preserve segregation between absorbed water, low temperature mineral water and high temperature mineral hydroxyl groups.

Extensive work was done on terrestrial samples to standardize the rock-water oxygen isotope ratio measurement technique. First the method of water fluorination using BrF$_5$ was used to make high precession measurements of the oxygen isotope composition of Vienna Standard Mean Ocean Water (VSMOW) and Standard Light Antarctic Precipitation (SLAP) water standards. These measurements were then used to do a VSMOW/SLAP scale calibration of the instrumentation and to calibrate the in-house laboratory water and silicate standards. To calibrate rock-water extraction, several terrestrial samples were analyzed. Water extracted from terrestrial basalt, metasomatized peridotite and serpentinite was routinely fluorinated and measured relative the VSMOW. Oxygen isotope analyses of the water extracted from these terrestrial samples showed that water extraction by heating was a highly kinetic process and an appropriate fractionation slope for calculating ^{17}O surplus was determined based on terrestrial measurements.

An experiment to evaluate the effect of terrestrial moisture contamination on Martian samples was conducted. Aliquots of terrestrial rock-water standards were placed in a sealed environment containing isotopically enriched (^{17}O and ^{18}O) moisture and allowed to exchange for one year at room temperature. After one year, the "contaminated" samples were extracted and the oxygen isotope composition of the water within the samples was measured. This experiment showed the degree of possible terrestrial contamination to

the different rock-water reservoirs (absorbed or low/high temperature structural). Experiments to negate the effects of the contamination were also carried out.

This work is a culmination of all these various experiments and the data which was produces. All the technical aspects of the experimental systems as well as the methods are described in detail in the following chapters. Oxygen isotope composition data of water from Martian meteorites, collected during this work, is presented cooperatively with previous work done on the subject by Karlsson et al. (1992) and Agee et al. (2013). This approach is essential since meteorite water measurements are difficult to make and require a very large sample size.

1.2 Background Information

1.2.1 Water on Mars

1.2.1.1 At the present

Surface water on Mars exists in the atmosphere, surface regolith and the polar ice caps (Kuzmin et al., 2007). The atmosphere of Mars is estimated to have a water vapor partial pressure of about 10^{-3} mbar (<0.1 wt%), about 10^4 times less than Earth (Jakosky and Phillips, 2001). Because average temperatures on Mars are bellow 273 K and the atmospheric pressure is at, or below the triple point of water, it is not likely that any permanent liquid water exists on the surface of Mars today (Malin and Edgett, 2000). In areas along the equator where temperatures rise above 273 K liquid water could exist as a transient phase but would quickly evaporate into the dry atmosphere to eventually freeze out at colder high latitudes (Jakosky and Phillips, 2001). Analysis of Martian surface amorphous component (Martian dust) at Rocknest by the SAM (Sample Analysis at Mars)

instrument aboard the Curiosity rover show H_2O content between 3 and 6 wt% (Leshin, et al., 2013).

Measurements of the hydrogen content in the subsurface soils made by the Mars Odyssey neutron spectrometer indicate the presence of up to 8 wt% H_2O in some low latitude regions of the Martian surface (Feldman et al., 2004). Similarly, data from the Curiosity rover shows subsurface water content of as much as 4 wt% (Mitrofanov et al., 2013; Hardgrove et al., 2013). Subsurface orbital and rover measurements are limited to the upper ½ meter or less of the Martian surface. Because of this limitation, no constraint has been placed on the amount of water in the crust of Mars. The Martian crust could contain liquid water and this crustal water likely undergoes exchanges with surface regolith and atmospheric H_2O (Jakosky and Phillips, 2001).

The mantle of Mars is another key reservoir of water. It has been proposed that the Martian mantle could have H_2O concentrations equivalent to that of the mantle of Earth (Trieman, 1985; Johnson et al., 1991; McSween et al., 2001; McCubbin et al., 2012; Gross et al., 2013). Based on experimental results for water partitioning into olivine and its high-pressure polymorphs wadsleyite, ringwoodite and bridgemanite (Inoue et al., 2010) the upper level estimate for the H_2O content of the Martian mantle could be as high as 1 wt%. Alternatively, a low Martian mantle water content of 1-36 ppm has also been suggested (Dreibus and Wänke, 1987; Wänke and Dreibus, 1988; Filiberto and Treiman, 2009). In any case, the Martian mantle is a key component in the study of water on Mars.

1.2.1.2 In the past

The geologic history of Mars is divided into three periods: The Nochian, Hesperian and the Amazonian (Carr, 2012). These periods are primarily defined by the degree of surface cratering and the relative age of such events determined by cratering chronology (Hartmann and Neukum, 2001). The Nochian is a period of heavy meteorite bombardment of Mars and ranges from 4.6 to 3.7 Ga (Hartmann and Neukum, 2001). The Hesperian period ranges from 3.7 to 2.9 Ga and the Amazonian is from 2.9 Ga to the present (Hartmann and Neukum, 2001).

Bibring et al., (2006) defined the geologic history of Mars in terms of mineralogical epochs based on global mineralogical mapping of Mars done by the OMEGA instrument on board the European Space Agency's Mars Express spacecraft. This mineralogical approach to defining the geological history of Mars is ideal for this study because the index mineral assemblages are often directly related to the history of water on the surface of Mars. Figure 1.1 shows how the mineralogical epochs defined by Bibring et al., (2006) correlate to the crater chronology based geologic history of mars. Bibring et al., (2006) divide the history of Mars into three mineralogical epochs, the phyllosian (4.6-4.1 Ga), theiikian (3.8-3.5 Ga) and siderikian (3.5 Ga to present).

Figure 1.1. Geologic history of Mars with mineralogical epochs defined by Bibring et al. (2006). Figure from Bibring et al. (2006)
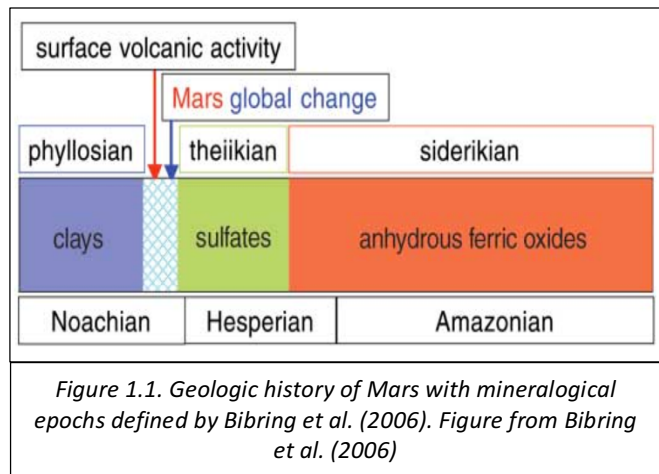
Phyllosian is defined by the presence of phillosilicates (clays) and carbonate deposits, which are a record of nonacidic aqueous alteration (Bibring et al., 2006). The formation of phillosilicates and carbonates would have required a dense atmosphere

capable of sustaining liquid water at the surface of Mars (Chauffray et al., 2007). It has been proposed that most of this early Martian surface water was lost to space due to heavy meteorite bombardment and hydrodynamic escape (Jakosky and Phillips, 2001). Similarly, much of the early atmosphere of Mars was also removed by the heavy meteorite bombardment and hydrodynamic escape during the phyllosian era (Chauffray et al., 2007).

After the phyllosian, during the Middle to late Noachian (4.1 to 3.8 Ga), the outgassing of the Tharsis volcanoes (Phillips et al., 2001; Anderson et al., 2001) may have created a secondary atmosphere capable of sustaining liquid water (Jakosky and Phillips, 2001). Many of the valley networks in the vicinity of the Tharsis rise have been observed to preferentially follow the slopes that resulted from the heavy loading of the lithosphere due to the formation of Tharsis volcanic pile (Jakosky and Phillips, 2001). This indicates that a significant amount of liquid water existed on the surface of Mars after the emplacement of the Tharsis rise in the late Noachian (Phillips et al., 2001). The end of the Noachian is marked by the loss of the Martian magnetic field which made it possible for the solar wind to strip away most of the Martian atmosphere (Jakosky and Phillips, 2001; Chauffray et al., 2007).

The theiikian era (3.8-3.5 Ga) is characterized by the presence of sulfates, which formed as acidic aqueous alterations (Bibring et al., 2006). During this time, any contribution to the atmosphere of Mars from outgassing was likely countered by solar wind removal (Jakosky and Phillips, 2001). Therefore, an atmosphere of a density like that of the early Noachian could not form. However, there is evidence of catastrophic flood events that date back to the late Hesperian (Tanaka et al., 2005). These events are preserved in the form of colossal outflow channels, most of which are found around the Chryse basin in the

Northern Hemisphere (Carr, 2012). Several mechanisms have been proposed for the formation of outflow channels on Mars. Most of these mechanisms advocate for some form of tectonic interactions with groundwater reservoirs (Carr, 1979; Hanna and Phillips, 2005; Andrews-Hanna and Phillips, 2007).

The siderikian is characterized by ferric oxides likely produced by atmospheric aqueous-free alteration (Bibring et al., 2006). The siderikian era starts prior to and spans the entire range of the Amazonian period (Bibring et al., 2006) and represents Martian surface conditions that are like what is observed on Mars at the present.

1.2.2 Martian Meteorites

Martian meteorites are an invaluable resource in our efforts to understand the planet Mars. Laboratory analysis of Martian meteorites provides us with geochemical and mineralogical data of greater detail than what can currently be achieved with robotic missions. In some cases, such laboratory work is key to understanding the data returned from robotic missions.

Except for Allan Hills (ALH)84001 and the basaltic breccia NWA 7034 all other Martian meteorites are classified as shergottites, nakhlites and chassignites (the SNC meteorite group). The classification of Martian meteorites is based on the mineralogy and rock type.

Shergottites are the most common type of Martian meteorite. Shergottites are subdivided into basaltic, lherzolitic, olivine-phyric and olivine-orthopyroxene-phyric groups based on petrography and chemical composition (McSween and Treiman, 1998;

Goodrich, 2002; Irving, 2012). Shergottites are also classified as depleted, intermediate and enriched based on their rare-earth element (REE) composition. Based on variability in the REE composition of shergottites it has been proposed that different silicate reservoirs must exist on Mars (Borg et al., 1997; Brendon et al., 2000; Debaille et al., 2008; Papike et al., 2008; Brandon et al., 2012). By studying shergottites we can learn about the composition of the different silicate reservoirs on mars. For example, it has been proposed that shergottite Y 980459 is most representative of the primitive depleted Martian mantle (Koizumi et al., 2004; Usui et al., 2008). It is also possible that the geochemical composition of enriched shergottites represents assimilation of Martian crust into the primitive melt (Herd et al., 2002; Usui et al., 2012).

Nakhlites are cumulate clinopyroxenites composed primarily of subcalcic augite and include olivine, plagioclase, K-feldspar, Fe-Ti oxides, pyrite chalcopyrite and hydrated alteration phases (Bunch and Reid, 1975; Treiman, 2005). K-Ar and Rb-Sr ratios of nakhlites indicate a crystallization age of around 1.3 Ga (Treiman, 2005) The presence of pre-terrestrial clay-rich alteration product iddingsite as well as halite and oxy-hydroxides in nakhlites (Ashworth and Hatchison, 1975, Bunch and Reid, 1975; Treiman et al., 1993; Bridges and Grady, 1999) indicates that these samples interacted with extraterrestrial near-surface water (Reid and Bunch, 1975; Gooding et al., 1991; Sawyer et al., 2000; Bridges et al., 2001).

Chassignites are dunites composed of greater than 90% cumulate olivine with minor plagioclase and Hi-Ca pyroxene components (Papike et al., 2009). Chassignites also contain low temperature alteration minerals including carbonates, sulfates and oxides (Bridges et al., 2001).

Orthopyroxenite ALH84001 is the oldest known (bulk rock age) Martian meteorite based on lutetium-hafnium (Lu-Hf) isotope data. The age of this meteorite was determined by Lapen et al. (2010) to be 4.091Ga. It is composed mostly of orthopyroxene with minor chromite, maskelynite, augite, apatite, pyrite and carbonate components (Mittlefehldt, 1994). The Carbonate component of ALH84001 amounts to about 1wt% of the sample and based on oxygen isotope composition has been determined to not be in isotopic equilibrium with the bulk rock (Romanek et al., 1994). The isotopic composition of the carbonate suggests that the carbonate is most likely a product of low temperature fluid alteration (Romanek et al., 1994; McSween and Harvey, 1998; Eiler et al., 2002; Halevy et al., 2011; Melwani Daswani et al., 2013).

Basaltic breccia NWA 7034 is a porphyritic basaltic breccia dominated by low-Ca pyroxene, pigeonite and augite clasts. Initial Rb-Sr analysis indicated an age of 2.089 ±0.081 Ga for NWA 7034 (Agee et al., 2013) yet ^{147}Sm-^{143}Nd and ^{146}Sm-^{142}Nd analysis of various lithological components of the breccia have produced age estimates as old as 4.44 Ga (Nyquist et al., 2016)NWA 7034 is the most geochemically enriched of Martian meteorites found to date and shows the best match to the bulk chemical data collected by orbital and lander missions on Mars (Agee et al., 2013). Base on the elevated H_2O content of 6000ppm (Agee et al., 2013) this meteorite is ideal for studying aqueous fluid alteration at or near the Martian surface (Muttik et al., 2014).

1.2.3 Water in Martian Meteorites

All Martian meteorites have been found to contain water in varying amounts. The water within a Martian meteorite is likely stored in several reservoirs. These reservoirs include (i) absorbed H_2O on grain surfaces and boundaries, (ii) hydrated minerals and (iii) water trapped as inclusions within glass and mineral grains (Karlsson et al., 92). The waters in these different storage sites likely originate from different Martian reservoirs such as mantle, crust, hydrosphere and atmosphere. The existence and possible isotopic diversity within these different storage sites is the reason for why stepwise heating is used to extract the water in this work.

1.2.3.1 Absorbed water

Absorbed water represents H_2O molecules stored on the surfaces and boundaries of the grains, which make up the sample. Most absorbed water is evolved from the sample at temperatures below 150°C (Karlsson et al., 1992). Absorbed water is prone to low temperature exchanges and is therefore most vulnerable to terrestrial contamination. However, the lowest temperature water evolved from NWA 7034 (below 50°C) had a distinctly extraterrestrial $\Delta^{17}O$ (concentration of ^{17}O, relative to ^{16}O and ^{18}O) value (Agee et al., 2013). The same behavior was also observed for many of the samples analyzed by Karlsson et al. (1992). The extraterrestrial $\Delta^{17}O$ values of absorbed water in Martian meteorites suggests that useful data can be produced from this water storage reservoir.

1.2.3.2 Hydrated minerals

Hydrated minerals are the largest storage of H_2O and HO in Martian meteorites. Water bearing minerals found in Martian meteorites include primary phases biotite, amphibole (hornblend), apatite and secondary minerals gypsum, iddingsite, clay minerals (smectite, nontronite, kaolinite, stilphomelane), iron oxy-hydroxides, salts, carbonate, and serpentinite (Romanek et al., 1994; McSween and Treiman, 1998; Bridges and Grady, 2000; Bridges et al., 2001; Eiler et al., 2002; Murchie et al., 2009; Agee et al., 2013; Kuebler, 2013; Muttik et al., 2014). Each hydrous mineral will break down and release water within a specific temperature range. Therefore, general predictions can be made as to the mineralogical source of water for a temperature range. For example, gypsum will completely dehydrate at temperatures below 230°C (Gooding et al., 1991). Iddingsite and clay minerals (phyllosilicates) will start to lose interlayer H_2O at relatively low temperatures ($\approx$100°C) and will begin to lose structural hydroxyl at temperatures above 400°C (Grim and Kulbicki, 1961; Bishop et al., 1994; Frost et al., 2000). Amphibole, apatite and micas will lose structural hydroxyl at temperatures above 600°C (Smekatz-Kloss, 1974; Norman and Palin, 1982; Mason et al., 2009).

1.2.3.3 Water inclusions

Water inclusions in glass and mineral grains will break down at temperatures above 600°C (Karlsson et al., 1992). It is difficult to predict the occurrence of water inclusions in a bulk sample but if they do exist they will likely be volumetrically small and their effect on the isotopic composition will only be observed at the highest temperature water release step.

1.2.4 Stable Isotope Composition of Water in Martian Meteorites

The application of stable isotope systems to planetary science is one of the most powerful tools in our understanding of the solar system. By applying our knowledge of oxygen and hydrogen isotopic systems to water in Martian meteorites we can unravel much detail about the origin and evolution of those waters.

1.2.4.1 Oxygen

Since the discovery of the ^{17}O anomaly in the solar nebula by Robert Calyton, in the early 1970s, oxygen isotope analyses have been fundamental to planetary science. Most studies of oxygen isotope composition of Mars have focused on the bulk silicate rock composition. Most Martian meteorites (SNCs and ALH84001) have $\Delta^{17}O$ values of +0.3‰ (Clayton and Mayeda, 1983; Franchi et al., 1999). Terrestrial materials by definition have a $\Delta^{17}O$ value of 0.0‰ so a $\Delta^{17}O$ values of +0.3‰ indicates a significant ^{17}O enrichment in the Martian samples.

Despite all the oxygen isotope work that has been done on Martian meteorites the water component has received little attention. To date, only two studies by Karlsson et al. (1992) and Agee et al. (2013) have analyzed the isotopic composition of the water in Martian meteorites. Both studies have shown that the water in Martian meteorites is not in isotopic equilibrium with the bulk rock. This disequilibrium, observed between the bulk rock $\Delta^{17}O$ values and water $\Delta^{17}O$ values, suggests that multiple distinct oxygen isotope

sources exist on Mars. So far, no end member isotopic compositions have been proposed for the different oxygen reservoirs (mantle, crust, hydrosphere and atmosphere).

1.2.4.2 Hydrogen

Hydrogen is another isotopic system that has been widely used in planetary science. Due to its volatility and the large mass difference between protium (1amu) and deuterium (2amu), the hydrogen isotopic system is very good at recording fractionation events. Much work has already been done on constraining the hydrogen isotope composition of the different reservoirs on Mars (mantle, crust, hydrosphere and atmosphere). Hallis et al. (2012) reported the δD value of the Martian mantle to be between -111 and +155‰. In comparison, Earth's mantle δD values range from -80 to -40‰ (Lécuyer et al., 1998). On the other hand, the water in the Martian atmosphere is enriched in deuterium and has a δD value of 780‰ (Owen et al., 1988). An even more deuterium-enriched ($\delta D > 4000‰$) component of the Martian atmosphere has also been proposed (Bjoraker et al., 1989; Leshin and Vicenzi, 2006). The deuterium enrichment of the Martian atmosphere is caused by the preferential loss of the light isotope of hydrogen to space via thermal escape (Owen et al., 1988; Donahue, 1995) and preferential removal of protium by solar wind (Bjoraker et al., 1989; Owen, 1992). Martian magmatic waters have been reported to have δD values of around +900‰ (Leshin, 2000).

δD measurements of water from primary and secondary minerals have yielded values ranging from -150 to +4300‰ (Usui et al., 2012). This δD range indicates that the various minerals within Martian meteorites are indeed sampling the entire range of Martian

hydrogen in different reservoirs. This fact is very relevant to this study because it underscores the isotopic variability of the hydrous phases in Martian meteorites.

Most of the hydrogen isotope studies of Martian materials have been done *in-situ* on individual mineral grains and alteration phases. Only a few studies done by Leshin et al. (1996), Eiler et al. (2002), and Agee et al. (2013) have studied the δD composition of water evolved from Martian meteorites, both in bulk and by step-wise heating. These studies showed a degree of variability between the δD values evolved at different temperatures. Agee et al. (2013) analysis of NWA 7034 by step-wise heating produced water with a δD value as high as +327‰ while bulk δD analysis yielded a value of +46‰. This variability indicates that different hydrous storage sites (absorbed and low/high mineral water) are preserving different δD values, which are likely representative of different Martian reservoirs (mantle, crust, hydrosphere and atmosphere).

2. Oxygen isotope composition of water in Martian meteorites

2.1 Abstract

The oxygen isotope composition of water extracted from Martian meteorites appears not to be in isotopic equilibrium with the silicate portion of the meteorites. This disequilibrium suggests the existence of multiple distinct oxygen isotope reservoirs on planet Mars. Here we present oxygen isotope measurements of waters extracted from Martian shergottites Tissint, Zagami and NWA-7042 and from nakhlite NWA-10153. These waters were extracted by stepwise heating to preserve segregation between low temperature adsorbed waters, intermediate temperature mineral waters and the high temperature mineral structural OH groups. The results of our study, analyzed cooperatively with previous work by Karlsson et al., (1992) and Agee et al., (2013), show that two isotopically distinct water reservoirs exist on Mars. The isotopic influence of these two reservoirs is preserved in two distinct groups of Martian meteorites. Martian shergottites preserve the isotopic composition of Martian mantle waters while nakhlites and Chassigny preserve a contribution from a reservoir elevated in ^{17}O. The presence of low temperature aqueous alteration minerals in nakhlites and Chassigny suggests that the elevated ^{17}O component is sourced from Martian near-surface waters. Based on oxygen isotope measurements of ^{17}O enriched waters extracted from Martian meteorites we propose that the Martian near-surface waters must have a $\Delta'^{17}O$ of at least 0.89‰ or greater.

2.2 Introduction

The elevated concentration of ^{17}O, relative to ^{16}O and ^{18}O, in waters extracted from many Martian meteorites indicates that these samples contain extraterrestrial waters (Karlsson et al., 1992; Agee et al., 2013; Ziegler et al., 2013). The planet Mars is the most likely origin of these waters. By studying the oxygen isotope composition of the waters extracted from Martian meteorites the $\Delta^{17}O$ (concentration of ^{17}O, relative to ^{16}O and ^{18}O) of water on Mars can be constrained. A tighter constraint on the $\Delta^{17}O$ value of water on Mars coupled with possible mechanisms for mass and non-mass dependent isotopic fractionation provides additional insight into the complex history of the evolution of water on planet Mars.

2.2.1 Brief history of water on Mars

Presently the average temperatures on Mars are below 273 K and the atmospheric pressure is at, or below the triple point of water, making it unlikely that any permanent liquid water exists on the surface of Mars (Malin and Edgett, 2000). In areas along the equator where temperatures rise above 273 K liquid water could exist as a transient phase but would quickly evaporate into the dry atmosphere to eventually freeze out at colder high latitudes (Jakosky and Phillips, 2001). However, analysis of Martian surface amorphous component (Martian dust) at Rocknest by the SAM (Sample Analysis at Mars) instrument aboard the Curiosity rover show H_2O content between 3 and 6 wt% (Leshin, et al., 2013).

The discovery of phillosilicates and carbonate deposits in some of the most ancient terrains on Mars by the OMEGA instrument on board the European Space Agency's Mars Express spacecraft, indicates that early on (4.6-4.1 Ga) Mars had a dense atmosphere capable of sustaining liquid water at the surface (Bibring et al., 2006; Chauffray et al., 2007). It has been proposed that most of this early Martian surface water was lost to space due to heavy meteorite bombardment and hydrodynamic escape (Jakosky and Phillips, 2001). During the Middle to late Noachian (4.1 to 3.8 Ga), the outgassing of the Tharsis volcanoes (Phillips et al., 2001; Anderson et al., 2001) may have created a secondary atmosphere capable of sustaining liquid water (Jakosky and Phillips, 2001). Many of the valley networks near the Tharsis rise have been observed to preferentially follow the slopes that resulted from the heavy loading of the lithosphere due to the formation of Tharsis volcanic pile (Jakosky and Phillips, 2001). This indicates that a significant amount of liquid water existed on the surface of Mars after the emplacement of the Tharsis rise in the late Noachian (Phillips et al., 2001). The end of the Noachian is marked by the loss of the Martian magnetic field which made it possible for the solar wind to strip away most of the Martian atmosphere (Jakosky and Phillips, 2001; Chauffray et al., 2007). Any subsequent contribution to the atmosphere of Mars from outgassing was countered by solar wind removal making it impossible to form an atmosphere of a density similar to that of the early Noachian (Jakosky and Phillips, 2001).

2.2.2 Martian Meteorites

Martian meteorites are an invaluable resource in our efforts to understand the planet Mars. Laboratory analysis of Martian meteorites provides us with geochemical and mineralogical data of greater detail than what can currently be achieved with robotic missions. In some cases, such laboratory work is key to understanding the data returned from robotic missions. Except for Allan Hills (ALH)84001 and the basaltic breccia NWA 7034 all other Martian meteorites are classified as shergottites, nakhlites and chassignites (the SNC meteorite group). The classification of Martian meteorites is based on the mineralogy and rock type.

Shergottites are the most common type of Martian meteorite. Shergottites are subdivided into basaltic, lherzolitic, olivine-phyric and olivine-orthopyroxene-phyric groups based on petrography and chemical composition (McSween and Treiman, 1998; Goodrich, 2002; Irving, 2012). Shergottites are also classified as depleted, intermediate and enriched based on their rare-earth element (REE) composition. Based on variability in the REE composition of shergottites it has been proposed that different silicate reservoirs must exist on Mars (Borg et al., 1997; Brendon et al., 2000; Debaille et al., 2008; Papike et al., 2008; Brandon et al., 2012). By studying shergottites we can learn about the composition of the different silicate reservoirs on mars. For example, it has been proposed that shergottite Y980459 is most representative of the primitive depleted Martian mantle (Koizumi et al., 2004; Usui et al., 2008). It is also possible that the geochemical composition of enriched shergottites represents assimilation of Martian crust into the primitive melt (Herd et al., 2002; Usui et al., 2012).

Nakhlites are cumulate clinopyroxenites composed primarily of subcalcic augite and include olivine, plagioclase, K-feldspar, Fe-Ti oxides, pyrite chalcopyrite and hydrated

alteration phases (Bunch and Reid, 1975; Treiman, 2005). K-Ar and Rb-Sr ratios of nakhlites indicate a crystallization age of around 1.3 Ga (Treiman, 2005) The presence of pre-terrestrial clay-rich alteration product iddingsite as well as halite and oxy-hydroxides in nakhlites (Ashworth and Hatchison, 1975, Bunch and Reid, 1975; Treiman et al., 1993; Bridges and Grady, 1999) indicates that these samples interacted with extraterrestrial near-surface water (Reid and Bunch, 1975; Gooding et al., 1991; Sawyer et al., 2000; Bridges et al., 2001).

Chassignites are dunites composed of greater then 90% cumulate olivine with minor plagioclase and Hi-Ca pyroxene components (Papike et al., 2009). Chassignites also contain low temperature alteration minerals including carbonates, sulfates and oxides (Bridges et al., 2001).

Orthopyroxenite ALH84001 is the oldest known (whole rock) Martian meteorite. Based on lutetium-hafnium (Lu-Hf) isotope data, the age of this meteorite was determined by Lapen et al. (2010) to be 4.091Ga. It is composed mostly of orthopyroxene with minor chromite, maskelynite, augite, apatite, pyrite and carbonate components (Mittlefehldt, 1994). The carbonate component of ALH84001 amounts to about 1 wt% of the sample and based on oxygen isotope composition has been determined to not be in isotopic equilibrium with the bulk rock (Romanek et al., 1994). The isotopic composition of the carbonate suggests that the carbonate is most likely a product of low temperature fluid alteration (Romanek et al., 1994; McSween and Harvey, 1998; Eiler et al., 2002; Halevy et al., 2011; Melwani Daswani et al., 2013).

Basaltic breccia NWA 7034 is a porphyritic basaltic breccia dominated by low-Ca pyroxene, pigeonite and augite clasts. Initial Rb-Sr analysis indicated an age of 2.089

±0.081 Ga for NWA 7034 (Agee et al., 2013) yet ^{147}Sm-^{143}Nd and ^{146}Sm-^{142}Nd analysis of various lithological components of the breccia have produced age estimates as old as 4.44 Ga (Nyquist et al., 2016). NWA 7034 is the most geochemically enriched of Martian meteorites found to date and shows the best match to the bulk chemical data collected by orbital and lander missions on Mars (Agee et al., 2013).

2.2.3 Water in Martian meteorites

All Martian meteorites have been found to contain water in varying amounts. Water within a Martian meteorite is likely stored in several reservoirs. These reservoirs include absorbed H_2O on grains surfaces and boundaries, hydrated minerals and water trapped as inclusions within glass of mineral grains (Karlsson et al., 1992). The waters in these different storage sites likely originate from different Martian reservoirs such as mantle/crust, hydrosphere and possibly the atmosphere. The existence and possible isotopic diversity within these different storage sites is the reason for why stepwise heating is used to extract the water in this work.

Absorbed water represents H_2O molecules stored on the surfaces and boundaries of the grains, which make up the sample. Most absorbed water is evolved from the sample at temperatures below 150°C (Karlsson et al., 1992). Absorbed water is prone to low temperature exchanges and is therefore most vulnerable to terrestrial contamination. However, the lowest temperature water evolved from NWA 7034 (below 50°C) had a distinctly extraterrestrial $\Delta^{17}O$ value (Agee et al., 2013). The same behavior was also observed for many of the samples analyzed by Karlsson et al. (1992). The extraterrestrial

Δ^{17}O of absorbed water in Martian meteorites suggests that useful data can be produced from this water storage reservoir.

Hydrated minerals are the largest storage of H_2O and HO in Martian meteorites. Water bearing minerals found in Martian meteorites include primary phase biotite, amphibole (hornblende), apatite and secondary minerals gypsum, iddingsite, clay minerals (smectite, nontronite, kaolinite, stilpnomelane), iron oxy-hydroxides, salts, carbonate, and serpentinite (Romanek et al., 1994; McSween and Treiman, 1998; Bridges and Grady, 2000; Bridges et al., 2001; Eiler et al., 2002; Murchie et al., 2009; Agee et al., 2013; Kuebler, 2013; Muttik et al., 2014). Each hydrous mineral will break down and release water within a specific temperature range. Thus, general predictions can be made as to the mineralogical source of water for a temperature range. For example, gypsum will completely dehydrate at temperatures below 230°C (Gooding et al., 1991). Iddingsite and clay minerals (phyllosilicates) will start to lose interlayer H_2O at relatively low temperatures (≈100°C) and will begin to lose structural hydroxyl at temperatures above 400°C (Grim and Kulbicki, 1961; Bishop et al., 1994; Frost et al., 2000). Amphibole, apatite and micas will lose structural hydroxyl at temperatures above 600°C (Smekatz-Kloss, 1974; Norman and Palin, 1982; Mason et al., 2009).

Water inclusions in glass and mineral grain will be released at temperatures above 600°C (Karlsson et al., 1992). It is difficult to predict the occurrence of water inclusions in a bulk sample but if they do exist they will likely be volumetrically small and their effect on the isotopic composition will only be observed at the highest temperature water release step.

2.2.4 Prior work on water from Martian meteorites

The oxygen isotope composition of water extracted from Martian meteorites has been investigated by only two studies, Karlsson et al., (1992) and Agee et al., (2013). Both studies found that the water extracted form Martian meteorites is not in isotopic equilibrium with the bulk rock silicate portion. Measurements of the silicate portion of Martian SNC (Shergottites, Nakhlites and Chassignites) group meteorites show remarkable oxygen isotope heterogeneity in terms of $\Delta'^{17}O$ ($\Delta'^{17}O = \delta'^{17}O - \theta*\delta'^{18}O$). Note that prime notation ($\Delta'^{17}O$, $\delta'^{18}O$ and $\delta'^{17}O$) indicates that the data has been linearized according to Miller, (2002). The purpose of linearization is discussed in the following sections. All meteorites in the SNC group have a $\Delta'^{17}O$ value of $\approx$0.3‰ (Clayton and Mayeda, 1983; Franchi et al., 1999; Rumble and Irving, 2009). However, waters extracted from SNC meteorites span a large $\Delta'^{17}O$ range from -0.2‰ to 0.9‰ (Karlsson et al., 1992). Similar disequilibrium was also observed in Martian meteorite NWA-7034 by Agee et al., (2013). $\Delta'^{17}O$ values of the water extracted from NWA-7034 were lower than the $\Delta'^{17}O$ values of the bulk silicate portion.

It has been proposed that the observed oxygen isotope disequilibrium between the silicate rock of Martian meteorites and the water extracted from them is due to existence of isotopically distinct/different water reservoirs on planet Mars (Karlsson et al., 1992; Agee et al., 2013; Ziegler et al., 2013). It is likely that interaction with such isotopically different water reservoirs has affected the oxygen isotope composition of the water preserved in Martian meteorites and is responsible for the observed disequilibrium. The existence of an isotopically exotic water reservoirs on Mars is possible since much of the

water originally found on Mars was lost to space. The vast loss of surface water to space through various mechanisms can account for extreme isotopic fractionation of the remaining water.

2.2.5 $\Delta'^{17}O$ relevance and notation

Since the discovery of the ^{17}O anomaly in the solar nebula by Clayton *et al.*, (1973), oxygen isotope analyses have been fundamental to planetary science. Most studies of oxygen isotope composition of Mars have focused on the bulk silicate rock. Most Martian meteorites (SNCs and ALH84001) have $\Delta^{17}O$ values of $\approx 0.3‰$ (Clayton and Mayeda, 1983; Franchi et al., 1999). Terrestrial materials, by definition, have a $\Delta^{17}O$ value of 0.0‰. $\Delta^{17}O$ values of +0.3‰ indicate a significant ^{17}O enrichment in the Martian samples relative to Earth. $\Delta^{17}O$ is a measure of surplus/deficit of mass seventeen oxygen within a sample relative to a known standard which, in planetary studies, is Earth. Since the ratio of ^{17}O to ^{16}O and ^{18}O varies thoughout the solar system, $\Delta^{17}O$ measurements provide a robust mechanism for identifying and grouping planetary materials. $\Delta^{17}O$ measurements are, for example, one of the most definitive methods for identifying a Martian meteorite. If a meteorite is identified as a potential Martian sample the oxygen isotope composition of the silicate portion of the sample is measured to verify that the sample is in fact Martian. If the $\Delta^{17}O$ of the sample falls in the normal SNC range ($\approx 0.3‰$) the sample is most likely Martian. If the $\Delta^{17}O$ value of the sample is something other than 0.3‰ ±0.05, the sample is likely from another differentiated planetary body. The prime notation ($\Delta'^{17}O$) indicates

that the oxygen isotope data has been linearized according to Miller, (2002). Calculations for determining $\Delta^{17}O$ and data linearization will be discussed in detail in the next section.

2.2.6 VSMOW-SLAP water standard calibration

Oxygen isotope measurements are reported in standard δ notation where $\delta = \left(\frac{R_{Sample}}{R_{Standard}} - 1\right) \times 1000$ and where R is the ratio of the heavy isotope to the light isotope, as in $R=(^{18}O/^{16}O)$. By definition, the $\delta^{18}O$ of VSMOW is equal to 0‰ and SLAP has a $\delta^{18}O$ value of -55.5‰ (Hut, 1987; Coplen, 1994). Because of the large spread in $\delta^{18}O$ values between VSMOW and SLAP the two standards are used in tandem as a two-point calibration system. The measured $\delta^{18}O$ of VSMOW is used to calibrate the $\delta^{18}O=0‰$ of the $\delta^{18}O$ scale and the measured $\delta^{18}O$ of SLAP is used to determine the squeeze/stretch factor of the $\delta^{18}O$ scale for an experimental system.

Measurements of $\delta^{17}O$ have been crucial to the study of extraterrestrial materials since extraterrestrial materials often show large ^{17}O anomalies (McKeegan and Leshin, 2001). Data in triple oxygen isotope space is presented in terms of $\delta^{18}O$ (domain) vs. $\delta^{17}O$ (range). Since ^{16}O is included in the calculation of both the $\delta^{17}O$ and $\delta^{18}O$ values, the data can be plotted on a simple x-y graph. It has been proposed that VSMOW and SLAP water standards should also be used to define a reference line for terrestrial water mass-dependent fractionation between mass 17 and mass 18 isotopes of oxygen relative to the mass 16 isotope (Barkan and Luz, 2012; Schoenemann et al., 2013). The slope (θ) of the fractionation line within the triple oxygen space can be calculated as $\theta_{A-B} = \left(\frac{\delta^{17}O_A - \delta^{17}O_B}{\delta^{18}O_A - \delta^{18}O_B}\right)$, where point A is the measured values of VSMOW and point B the measured

value of SLAP. Applying this procedure to measured VSMOW and SLAP values yields a θ value of 0.528 (Schoenemann et al., 2013). Using this known θ slope, a theoretical $\delta^{17}O$ value can be calculated from any $\delta^{18}O$ measurement using the formula $\delta^{17}O=\theta\times\delta^{18}O$. This deviation from the theoretical value is known as $\Delta^{17}O$ and is defined as $\Delta^{17}O=\delta^{17}O-\theta\times\delta^{18}O$.

The $\Delta^{17}O$ of VSMOW is =0‰ since $\Delta^{17}O=\delta^{17}O-\theta\times\delta^{18}O$ and both $\delta^{17}O$ and $\delta^{18}O$ of VSMOW are equal to 0. Similarly, the $\Delta^{17}O$ of SLAP is also =0‰ because the measured $\delta^{17}O=29.7‰$ and $\delta^{18}O=55.5‰$ were used to constrain the slope of the terrestrial fractionation line θ. Using the calculated θ=0.528 value, any sample analyzed for oxygen isotope composition can be compared to the theoretical norm established by the VSMOW and SLAP standards. However, there is a linearity consideration that must be addressed when working in the triple oxygen space. The identity $\Delta^{17}O=\delta^{17}O-\theta\times\delta^{18}O$ is an approximation derived from the power law $\alpha_{17/16}=(\alpha_{18/16})^{\theta}$ (Clayton and Mayeda, 1996; Miller, 2002). For the data to correctly plot as a linear function it must be linearized using the following equation $\delta' = 1000 \ln\left(\left(\frac{\delta}{1000}\right) + 1\right)$ (Miller, 2002). Note that delta prime (δ' or Δ') notation indicates that the data has been linearized.

2.2.7 Water fluorination

It has been demonstrated that the only way to obtain precise $\delta^{17}O$ measurements is by mass spectrometric analysis of pure O_2 (Barkan and Luz, 2012). Direct water fluorination with BrF_5 is an established method used to break the OH bond and produce O_2 from water without fractionation. Direct BrF_5 fluorination of water was first done by

O'Neal and Epstein (1966). The procedure was based on previous work by Hoekstra and Katz (1953), who used BrF_5 fluorination to measure total oxygen in metal and mineral oxides, as well as the work of Clayton and Mayeda (1963) who used the process to liberate oxygen from mineral samples. Water Fluorination with BrF_5 proceeds per the following reaction: $BrF_5 + H_2O \rightarrow BrF_3 + 2HF + \frac{1}{2}O_2$ (O'Neal and Epstein, 1966). In the original work by O'Neal and Epstein (1966) the liberated O_2 was converted to CO_2 prior to making isotopic ratio measurements. This approach was suitable since the authors were only measuring $\delta^{18}O$ of the samples. However, the conversion to CO_2 makes it impossible to accurately measure $\delta^{17}O$ due to mass interference from other isotopes (^{13}C and ^{18}O) which combine to make CO_2 molecules of atomic mass 45. Direct analysis of pure O_2 extracted from water was first done by Jabeen and Kusakabe (1997) and their work greatly improved the accuracy of the direct water fluorination method, yielding $\delta^{17}O$ and $\delta^{18}O$ precession of approximately 0.1 ‰ ($\sigma 1$) and 0.15‰ ($\sigma 1$) respectively.

2.2.8 Possible issues

Little work has been done on measuring the isotopic composition of water in bulk rock samples, thus no universally accepted rock water standard currently exists. This had to be addressed prior to measuring Martian samples. Karlsson et al, (1992) mention the use of a terrestrial basalt as a working standard but no identifying details or actual measurement data were reported. Another concern is the lack of understanding of what effect heat extraction of water has on the slope theta (θ) of the oxygen isotonic fractionation line. Karlsson et al, (1992) used a kinetic value of 0.52 for θ, arguing that the heat extraction

process is kinetic in nature. In our study, we wanted to further evaluate this claim and determine if this value is in fact appropriate.

The effects of terrestrial contamination of water in extraterrestrial samples is another concern that has not received much attention. It is often speculated that low temperature (absorbed/grain boundary) waters experience terrestrial contamination while water extracted at high temperature preserve the extraterrestrial isotopic signature. We wanted to test this assumption experimentally and to determine if high temperature hydrous phases can be affected by terrestrial contamination. Another concern is whether a small aliquot of a sample is representative of the entire meteorite. We wanted to address this issue by doing a statistical analysis of the distribution of hydrous mineral phases within a sample on centimeter to micrometer scale. Martian shergottite Zagami was used for this work.

2.2.9 Distribution and composition of hydrous phases in Martian meteorite Zagami

The main mass of Zagami consists of several distinct lithologies. Most of the sample is dominated by the fine to coarse-grained (0.24-0.36mm) basaltic lithology referred to as normal Zagami (Stolper and McSween 1979). Zagami also includes a dark-mottled-lithology which has been found to contain higher concentration of shock melt (Marti et al. 1995) and a Fe-rich lithology which has been described as residual melt by McCoy et al. 1993. All the water oxygen isotope analyses of Zagami have been done on the fine-grained normal Zagami lithology since it is by far the most abundant. For this reason, this study will focus on the fine-grained normal Zagami lithology.

The mineralogy of the fine-grained normal Zagami lithology consists primarily of pyroxene and plagioclase that has been shocked to amorphous maskelynite (Easton and Elliott, 1977). The lithology also contains amphibole (Treiman, 1985a), phosphates (McCoy et al. 1992), sulfides (McCoy et al. 1999), oxides (Stolper and McSween, 1979) and glass veins (McCoy et al. 1992). Amphibole and phosphates are the most important mineral phases for this discussion since they are the only hydrous phases present in the fine-grained normal Zagami lithology. Amphibole is reported to be present in Zagami melt inclusions in the form of kaersutite $((Na)(Ca_2)(Mg_4Ti)(Si_6Al_2)(O_{22})(OH,F)_2))$ and actinolite $((Ca_2)(Fe_5)(Si_8)(O_{22})(OH,F)_2))$ (Treiman, 1985a). Phosphates make up between 0.5 and 1.3 wt% of Zagami and occur as merrillite $(Ca_9NaMg(PO_4)_7)$ and apatite $(Ca_{10}(PO_4)_6(OH,F,Cl)_2)$ (Wang et al. 1999; Shearer et al. 2015). The phosphate assemblage in Zagami is dominated by merrillite. Apatite, which is the only phosphate phase that contains hydroxyl, is relatively rare (Shearer et al. 2015). Karlsson et al. (1992) reported the bulk H_2O content of Zagami to be 430 ppm. This value agrees with H_2O concentrations reported for other Martian shergottites. Based on available mineralogical data most of the 430 ppm H_2O budget of Zagami is likely stored in the minerals kaersutite, actinolite and apatite. Since these minerals have very distinct compositions it was possible to identify them and to map their spatial distribution using an electron microprobe. This data was then used to conduct statistical analysis of the distribution of hydrous minerals within Zagami.

2.3 Procedure

Water and hydroxyl groups were extracted from the samples by means of heating in a He stream. The heating was done in discrete temperature steps (intervals) to preserve
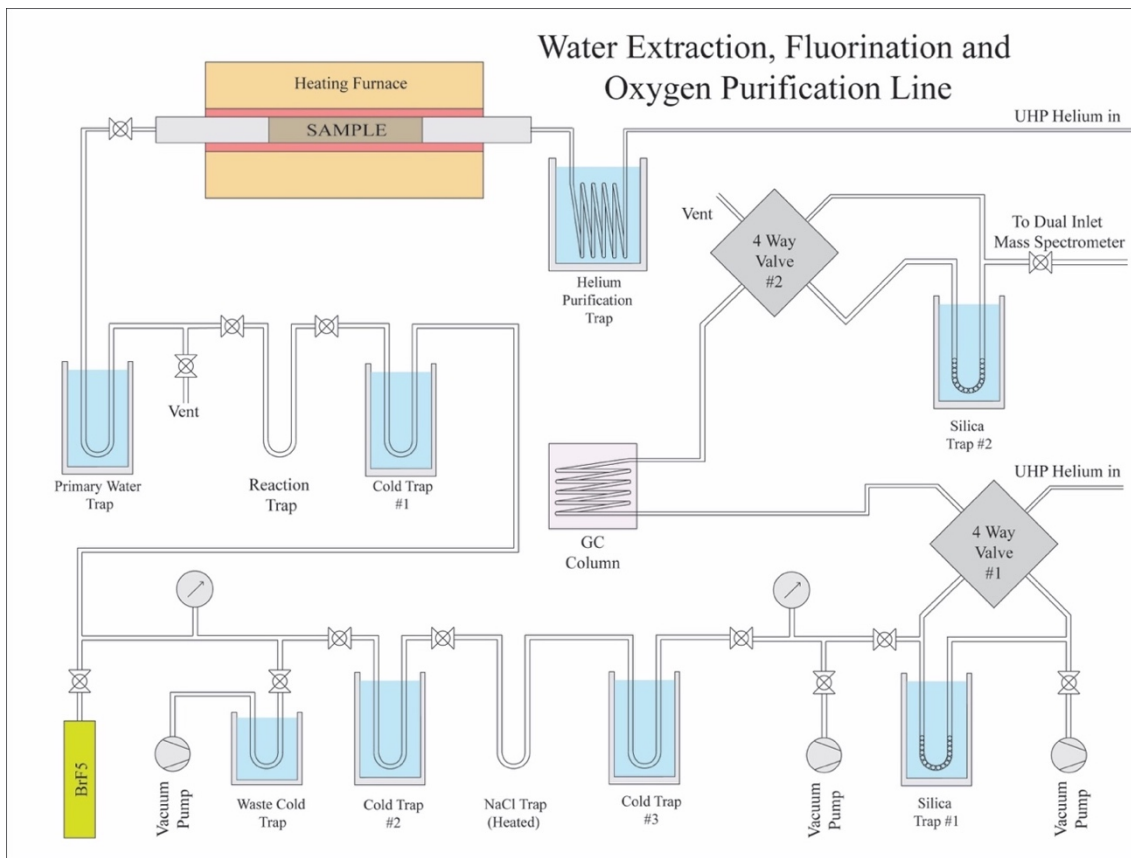
Figure 2.1. Schematic diagram of the water extraction, fluorination and oxygen pirification line.

segregation between low, intermediate and high temperature water/hydroxyl storage sites. The water extracted at each step was collected in a cold trap and fluorinated with high purity BrF_5 to release oxygen. The liberated O_2 was then purified and analyzed using a *ThermoFinnigan MAT 253* gas source dual inlet isotope ratio mass spectrometer. A complete schematic view of the analytical system is shown in figure 2.1.

2.3.1 Water extraction by stepwise heating

The amount of sample material needed for an analysis was determined based on the

wt.% water in each sample. Since Martian meteorites contain between 0.03 and 0.6 wt.% water (Karlsson et al., 1992; Agee et al., 2013; Leshin et al., 1996), sample sizes ranged from 0.6 to 3.5 grams. For terrestrial control samples, much less material was needed (≈0.1-0.5g) due to higher sample water content. For samples with unknown water concentration a small portion (≈2-3mg) was measured for total hydrogen content to determine how much water was present in the sample. This was done using a *ThermoFinnigan* TC/EA (Thermal Combustion Elemental Analyzer) coupled with a *ThermoFinnigan Delta V* isotope ratio mass spectrometer. By measuring the amount of hydrogen within a known mass of sample material relative to known standards the wt.% water of the unknown sample was determined. Once the appropriate amount of sample material was determined the sample was crushed to a fine powder and loaded into a 0.5-inch diameter quartz tube. Prior to sample loading the quartz tube along with quartz wool plugs was heated to 1000°C in an inert gas environment, to expel any trace water contamination. Once the sample was loaded, it was flushed with ultra-high purity helium gas at room temperature for two hours. Prior to entering the sample chamber the helium gas was passed through a silica gel trap held at liquid nitrogen temperature to remove any trace contamination. The sample was then stepwise heated to 50°, 200°, 400°, 700° and 1000°C. The sample was held at each temperature for 45 minutes while the evolved volatiles (mostly water) were collected. The water was entrained in a helium stream (at a flow rate of 120 cm^3/min) and collected in a cold trap held at liquid nitrogen temperature. The cold trap was then isolated from the sample chamber and excess helium was pumped away, leaving behind the water which remained frozen at liquid nitrogen temperature. At this point the water was ready for fluorination.

During the interval of time when the water extracted in the previous temperature interval was being analyzed, the sample (rock/meteorite) temperature was reduced by 50°C and the sample was held in a static inert gas environment. In this study, the volatiles were evolved into a helium stream instead of a vacuum, as was previously done by other workers (Karlsson et al., 1992; Agee et al., 2013). The use of helium was hypothesized to minimize the occurrence of secondary reactions between the evolved water and the rock sample and to minimize the large kinetic isotope effect, which favors light isotopes during the dehydration process (Karlsson et al., 1992). The use of helium gas also had the effect of reducing the chance of external contamination since the sample chamber was held at a positive pressure during stepwise heating and the downtime between temperature steps.

2.3.2 Water fluorination

To insure complete fluorination of water by the reaction $BrF_5 + H_2O \rightarrow BrF_3 + 2HF + \frac{1}{2}O_2$ a stoichiometric excess of BrF$_5$ was used. This excess was kept to approximately four time the stoichiometric balance. Each aliquot of BrF$_5$ was purified before being used in the fluorination reaction by expanding the reagent into a known volume at a predetermined pressure needed to provide the appropriate amount of reagent. The measured amount of BrF$_5$ was then condensed out of the volume into cold trap held at liquid nitrogen temperature. Once the reagent was condensed, the entire volume was open to vacuum and all the non-condensable gases were removed. It was found that prolonged storage of BrF$_5$ in a *Kel-F* (Polychlorotrifluoroethylene) container allowed trace amounts of air to leak in and form a head over the reagent. By purifying the reagent before

every fluorination, the trace contamination was reliably removed. Once the reagent was purified it was admitted into the reaction chamber. Prior to admitting BrF_5 into the reaction chamber the level of liquid nitrogen was raised so that the reagent would condense above the previously frozen water. This averted the possibility of the fluorination reaction starting before the reaction chamber was sealed. With the reactants loaded and the reaction chamber sealed the entire reaction chamber assembly was continually heated for 4 minutes using a heat gun. Care was taken to heat the reaction chamber uniformly to a temperature of approximately 300°C. It was determined from experimentation as well as reports from previous researchers (O'Neal and Epstein, 1966) that 4 minutes was the ideal time to facilitate the reaction. Allowing the reaction to proceed longer had no benefit. Once the reaction was completed, the remaining BrF_5 along with produced BrF_3 and HF were condensed into a cold trap held at liquid nitrogen temperature and the produced O_2 gas was moved into the purification line.

The reaction trap was constructed from ¼ inch OD pure nickel (nickel 200 alloy) tubing with a wall thickness of 0.022 inch. Internally electro-polished stainless steel tubing was originally used for the reaction chamber but yielded inconsistent results. Pure nickel appeared to be the ideal material for containing the water fluorination reaction. It is important to mention that each new nickel reaction chamber did require "conditioning" prior to correct operation. The conditioning process consisted of about 7 to 10 back-to-back water fluorination reactions.

2.3.3 Oxygen purification

A schematic diagram of the oxygen purification line is included in figure 2.1. The oxygen purification line follows the design described by Sharp et al, (1996). To remove remaining contaminants produced during fluorination, oxygen was expanded into another cold trap held at liquid N_2 temperature and then passed through a heated NaCl trap to neutralize any molecular fluorine gas (F_2) potentially produced during the fluorination reaction. Since fluorine gas has a condensation temperature lower than the temperature of liquid nitrogen it had to be captured by the reaction $2NaCl_{(solid)}+F_{2(gas)} \rightarrow 2NaF_{(solid)}+Cl_{2(gas)}$. The Chlorine gas produced by this reaction was collected in another cold trap. The purified oxygen was then collected in molecular sieve trap held at liquid nitrogen temperature. Once the oxygen was collected in the molecular sieve trap the trap was isolated from the rest of the purification line. UHP (Ultra-High Purity) helium was then used to transport the oxygen sample through a 5 Å mol sieve GC (Gas Chromatograph) column. The purpose of the GC column was to separate the O_2 from any potential NF_3 contamination. Removal on NF_3 form the sample was essential because during ionization in the mass spectrometer NF_3 can break down into NF and create interference at atomic mass 33. Since accurate measurements of mass 33 were essential to determining the $\delta^{17}O$ of the sample any NF_3 contamination had to be removed. It is important to mention that prior to use the UHP helium had to be further purified by passing through a molecular sieve trap held at liquid nitrogen temperature to remove any traces of O_2 in the He (Not shown in Figure 2.1). To monitor the movement of gas through the GC column a Thermal Conductivity Detector (TCD) was installed inline following the GC column. By monitoring the output of the TCD the arrival and passage of the O_2 peak was observed. Once all the O_2 gas had cleared the GC column it was trapped in a second molecular sieve trap held at liquid nitrogen

temperature. Once the O_2 was collected in the second molecular sieve trap the trap was isolated and the incoming helium stream along with any NF_3 contamination was routed to the vent port. The second molecular sieve trap was held at liquid nitrogen temperature while the helium was pumped away through the vacuum system of the mass spectrometer. Once the helium was removed the liquid nitrogen was removed from the second molecular sieve trap and the trap was heated using a heat gun freeing the oxygen. The oxygen was then admitted into the sample bellows of the dual inlet isotope ratio mass spectrometer.

2.3.4 Isotope ratio mass spectrometer configuration

All the oxygen isotope ratio measurements were made at the Center for Stable Isotopes, University of New Mexico. A *ThermoFinnigan MAT 253* IRMS (Isotope Ratio Mass Spectrometer) was used to make the high precision isotopic measurements of the water extracted from Martian meteorites. A dual inlet configuration was used to allow for multiple sample/reference comparisons. For each of the measurements care was taken to balance the pressure of the sample and the reference. This approach reduced the signal amplitude mismatch during sequential sample/reference comparisons and made it possible to continuously run 20 back-to-back comparison cycles with no analytical drift. After 20 sample/reference comparisons the pressures of the sample was again adjusted to match the reference and another set of 20 sample/reference comparisons was carried out. This was repeated two to five times for a total of 40-100 sample reference comparisons. A 20 second integration time was used for each comparison cycle. Using such a long integration time greatly reduced the standard error of the measurements.

2.3.5 High precision VSMOW-SLAP triple oxygen isotope calibration

A full VSMOW-SLAP triple oxygen isotope calibration was done to evaluate $\Delta'^{17}O$ accuracy of the analytical system. VSMOW and SLAP water standards were measured for calibration. These water standards were handled and used with utmost care to prevent isotopic fractionation due to evaporation or equilibration with atmospheric H_2O. An injection port was fitted to the fluorination line (described above) to allow liquid water to be injected into the fluorination line. 1 micro liter (μL) of water was used when measuring water standards. Injections were made using *Hamilton* model 7102 2μL trough-the-needle plunger syringes. The needle would remain in the injection port for approximately 30 seconds while the injection port was heated using a heat gun. The injected water vapor was then condensed in the reaction chamber of the fluorination line by cooling the reaction chamber to liquid nitrogen temperature. The water was then fluorinated, using the procedure described above, and the liberated oxygen was then purified and analyzed.

2.3.6 Terrestrial rock water sample calibration

During this work, waters from three terrestrial rock samples were routinely extracted and analyzed for oxygen isotope composition. This was done to evaluate the reproducibility of the analytical system and to collect the data necessary to determine the most appropriate fractionation slope (θ) for temperature extracted waters. The three terrestrial standards included basalt, metasomatized peridotite and serpentinite. Hydrogen

isotope ratio analysis were done on these terrestrial standards to determent the wt.% water present in each of the standards. By knowing the total amount of water in each aliquot of sample the performance of the analytical system could be further evaluated and monitored.

2.3.7 Contamination experiment

To evaluate the potential effects of terrestrial contamination on extraterrestrial waters within Martian meteorites, an oxygen isotope exchange experiment was conducted on terrestrial rock water standards. A 10g solid sample of terrestrial basalt standard was placed in a sealed container along with an open beaker containing 1ml of ^{18}O enriched water ($\delta^{18}O = 8000‰$). The experimental setup allowed isotopically enriched water vapor to interact with the rock sample at room temperature. The exchange happened through vapor only as the sample basalt and the isotopically spiked water were never in direct contact. The basalt sample remained in the sealed experiment for one year. After one year, the sample was removed, broken into several large pieces and 400mg portions of the material ware prepared for analysis. To remove adsorbed moisture, the samples were placed in a vacuum, heated to 100°C and allowed to dry for 4 hours. The samples were then loaded into the stepwise heating system and again heated to 100°C in a UHP helium stream. The samples remained at 100°C in helium for 24 hours. After the drying procedure, the samples were stepwise heated and the isotopic composition of the waters extracted at each temperature interval was measured. To negate the isotopic memory effect problem, multiple VSMOW water standards were analyzed between each isotopically spiked water measurement (each temperature interval). One portion of isotopically spiked basalt was

dried to a temperature of 350°C prior to analysis to remove all low temperature water. This sample was then stepwise heated from 350 to 600°C and from 600 to 1000°C and the isotopic composition of the water extracted during each interval was measured. VSMOW water standards were again measured after each analysis of isotopically spiked water. This was done to ensure that each measurement was not affected by contamination to the system from a prior analysis (the memory effect).

2.3.8 Martian meteorite sample preparation

The amount of sample material needed from each meteorite was determined based on the total concentration of water in each meteorite. Based on terrestrial standards it was determined that approximately 4μL (microliter) of total water were needed to yield a measurable amount of oxygen at each temperature step. This was not an absolute measure since the abundance of water and OH in different storage sites (low vs high temperature) varies from sample to sample. Therefore, enough material was used from each meteorite sample to yield at least 4μL of water. Once the appropriate amount of material was determined for each sample the material was crushed to a fine powder and loaded into the sample holder of the stepwise heating system (figure 2.1). Prior to water extraction each meteorite sample was dried to remove any adsorbed water. The drying was done at room temperature passing a UHP helium stream through the sample for 24 hours. Samples were not dried at a higher temperature because it has been shown that event the low temperature <50°C waters can preserve an extraterrestrial oxygen isotope signature (Agee et al., 2013). Once the sample was dried it was stepwise heated using the procedure described above and

the oxygen isotope composition of water extracted during each temperature interval was measured.

2.3.9 Distribution and composition of hydrous phases in Martian meteorite Zagami

Six thin sections of Zagami from the University of New Mexico Institute of Meteoritics collection were studied using a petrographic microscope. It was determined that no significant differences existed between the six thin sections. All six thin sections were representative of the fine-grained normal Zagami lithology. Two thin sections (998 and 1094), with the least surface damage, were chosen for microprobe analysis using the *JOEL 8200 electron probe* at the Earth and Planetary Science department of the University of New Mexico. Full thin section qualitative maps of elements Ca, Cl, F, P and Ti were made for both thin sections to identify the minerals of interest for this study (kaersutite, actinolite, merrillite and apatite). *JOEL* software was used to set the mapping conditions for the initial qualitative mapping of the thin sections. The qualitative maps were statistically analyzed using *ImageJ* software to determine the overall distribution of hydrous grains within Zagami.

Using the qualitative date, four areas of interest were identified based on elevated concentration of fluorine and chlorine, elements that are characteristic of kaersutite, actinolite and apatite (Treiman, 1985a; Wang et al. 1999; Shearer et al. 2015). The selected areas were then imaged using BSE (Back Scatter Electrons). The BSE images were linked to the microprobe stage coordinates through *Probe for EPMA ImageSnap* software to allow for more efficient sample navigation and analytical automation. *Probe for EPMA* software

was then used to automate multiple qualitative single-point analysis of various mineral grains to determine the mineral chemistry of the phases. Measured X-ray spectra where compared against known standards by the *Probe for EPMA* software. The average of 29 quantitative single-spot analyses of multiple apatite grains in Zagami was used to determine the actual chemical makeup of the grains. The measured values were normalized to the atomic concentration of oxygen in apatite to calculate normalized abundance for the constituent elements.

2.4 Results

2.4.1 VSMOW-SLAP triple oxygen isotope calibration

The raw measured $\delta^{17}O$ and $\delta^{18}O$, linearized $\delta'^{17}O$ and $\delta'^{18}O$ and the calculated $\Delta'^{17}O$ values of each VSMOW and SLAP analysis are presented in table 2.1. $\Delta'^{17}O$ values shown are calculated by equation $\Delta'^{17}O=\delta'^{17}O-\lambda*\delta'^{18}O$ using a λ value of 0.528. Average $\delta^{17}O$ and $\delta^{18}O$ values of six analyses of VSMOW have a standard deviation of 0.1‰ ($\sigma1$) for $\delta'^{17}O$ and of 0.2% ($\sigma1$) for $\delta'^{18}O$. The standard deviation of the calculated $\Delta'^{17}O$ for measurements of VSMOW is ±0.01‰ ($\sigma1$). Numerous factors during

Table 2.1 Oxygen isotope composition of terrestrial water standards VSMOW and SLAP. $\Delta'^{17}O$ calculated using $\theta=0.528$

VSMOW					
	$\delta^{17}O$	$\delta^{18}O$	$\delta'^{17}O$	$\delta'^{18}O$	$\Delta'^{17}O$
Run #1	-0.16	-0.27	-0.16	-0.27	-0.02
Run #2	-0.01	0.03	-0.01	0.03	-0.03
Run #3	0.00	0.04	0.00	0.04	-0.02
Run #4	-0.27	-0.46	-0.27	-0.46	-0.03
Run #5	-0.03	-0.05	-0.03	-0.05	-0.01
Run #6	-0.03	-0.04	-0.03	-0.04	-0.01
STDEV	0.11	0.20	0.11	0.20	0.01
Average	-0.08	-0.12	-0.08	-0.12	-0.02
SLAP					
	$\delta^{17}O$	$\delta^{18}O$	$\delta'^{17}O$	$\delta'^{18}O$	$\Delta'^{17}O$
Run #1	-29.54	-55.13	-29.98	-56.71	-0.04
Run #2	-29.26	-54.63	-29.70	-56.18	-0.03
Run #3	-29.81	-55.64	-30.26	-57.25	-0.03
Run #4	-29.96	-55.95	-30.42	-57.58	-0.02
Run #5	-29.92	-55.88	-30.38	-57.50	-0.02
STDEV	0.30	0.56	0.30	0.59	0.01
Average	-29.70	-55.45	-30.15	-57.04	-0.03

O_2 extraction and preparation result in measurement variability of $\delta'^{17}O$ and $\delta'^{18}O$. However, since this variability is caused by mass-dependent fractionation it has no effect on the $\Delta'^{17}O$. Thus, the standard deviation of $\Delta'^{17}O$ is smaller than that of $\delta'^{17}O$ and $\delta'^{18}O$. Similarly, $\Delta'^{17}O$ values of SLAP have a standard deviation of only 0.01‰ ($\sigma1$), lower than the standard deviations of the $\delta'^{17}O$ and $\delta'^{18}O$ values. Because the average $\delta^{18}O$ of SLAP was -55.5‰, exactly the same as the accepted value of -55.5‰, no stretching factor correction was needed for the VSMOW-SLAP scale. Note that the non-linearized value of SLAP is used. Originally the VSMOW-SLAP scale was defined using non-linearized values and here we adhere to that convention. However, linearized $\delta'^{17}O$ and $\delta'^{18}O$ values are used in calculating $\Delta'^{17}O$ of SLAP. Using the calculated $\Delta'^{17}O$ values of VSMOW and SLAP (-0.02‰ and -0.03‰ respectively) a correction factor is established for all other $\Delta'^{17}O$ measurements. The correction factor is the offset between the line plotted by $\Delta'^{17}O_{VSMOW}$ and $\Delta'^{17}O_{SLAP}$ from the terrestrial fractionation line. Mathematically the correction can be expressed as $\Delta'^{17}O_{(corrected)}= \Delta'^{17}O+(0.0002*\delta'^{18}O+0.02)$. For most samples ($\delta^{18}O=0‰ \pm10‰$) the application of this correction has the effect of adding approximately 0.02‰ to the measured $\Delta'^{17}O$ value.

2.4.2 Terrestrial standard calibration.

Table 2.2 shows the results of oxygen isotope analysis of waters extracted from terrestrial samples. Measurements of water extracted from terrestrial basalt and peridotite produced slightly positive $\Delta^{17}O$ values of ≈0.04 ‰ for temperatures below 450°C and negative $\Delta^{17}O$ values of ≈ -0.09 ‰ for temperatures above 450°C with a standard deviation

(1σ) of 0.03 ‰. It is likely that the low temperature waters are sampling terrestrial meteoric

waters that have a Δ^{17}O value of ≈0.03‰ (Luz and Barkan, 2010). The negative Δ'^{17}O

values of high temperature waters are consistent with negative Δ'^{17}O estimates of mantle

silicates based on the Δ'^{17}O = -0.054‰ of San Carlos olivine (Sharp et al., 2016). High

temperature waters extracted from serpentinite plotted in the meteoric water range of Δ'^{17}O

≈0.03‰. (Luz and Barkan, 2010).

Table 2.2. Average oxygen isotope composition of waters extracted from terrestrial serpentinite, metasomatized peridotite and basalt rock water standards. Standard deviation (1σ) = 0.03 ‰

Sample	Weight	step	mid-point	δ^{17} O	δ^{18} O	δ'^{17} O	δ'^{18} O	Δ'^{17} O
	[g]	[T_{max} °C]	[T_{mid} °C]					
Setprntinite	0.061	200	125	-2.98	-5.88	-2.99	-5.90	0.08
		400	300	2.43	4.86	2.43	4.85	-0.10
		700	550	1.34	2.53	1.34	2.53	0.03
		1000	850	2.14	4.03	2.14	4.02	0.05
Met. Peridotite	0.365	200	125	-4.19	-8.24	-4.19	-8.27	0.11
		400	300	3.98	7.53	3.97	7.50	0.07
		700	550	5.72	11.15	5.71	11.09	-0.06
		1000	850	7.98	15.66	7.95	15.54	-0.13
Basalt	0.2	50	35	-2.46	-4.80	-2.46	-4.81	0.04
		200	125	-0.43	-0.94	-0.43	-0.94	0.06
		450	325	3.79	7.22	3.78	7.19	0.04
		700	575	8.43	16.43	8.39	16.30	-0.08
		1000	850	2.71	5.41	2.70	5.39	-0.10

It has been observed that water released from bulk rock by heating does not

preserve the δ^{18}O of the original hydroxyl groups of the mineral (Karlsson et al., 1992).

During heat extraction, the water undergoes substantial fractionation. However, since the

fractionation is mass-dependent the ratio between ^{17}O and ^{18}O remains unaffected and by

calculating Δ'^{17}O using the correct fractionation slope for temperature extracted water the

original Δ'^{17}O of the water can be determined. In order to determine the appropriate

fractionation slope (λ) the Δ^{17}O values of terrestrial samples were recalculated relative to

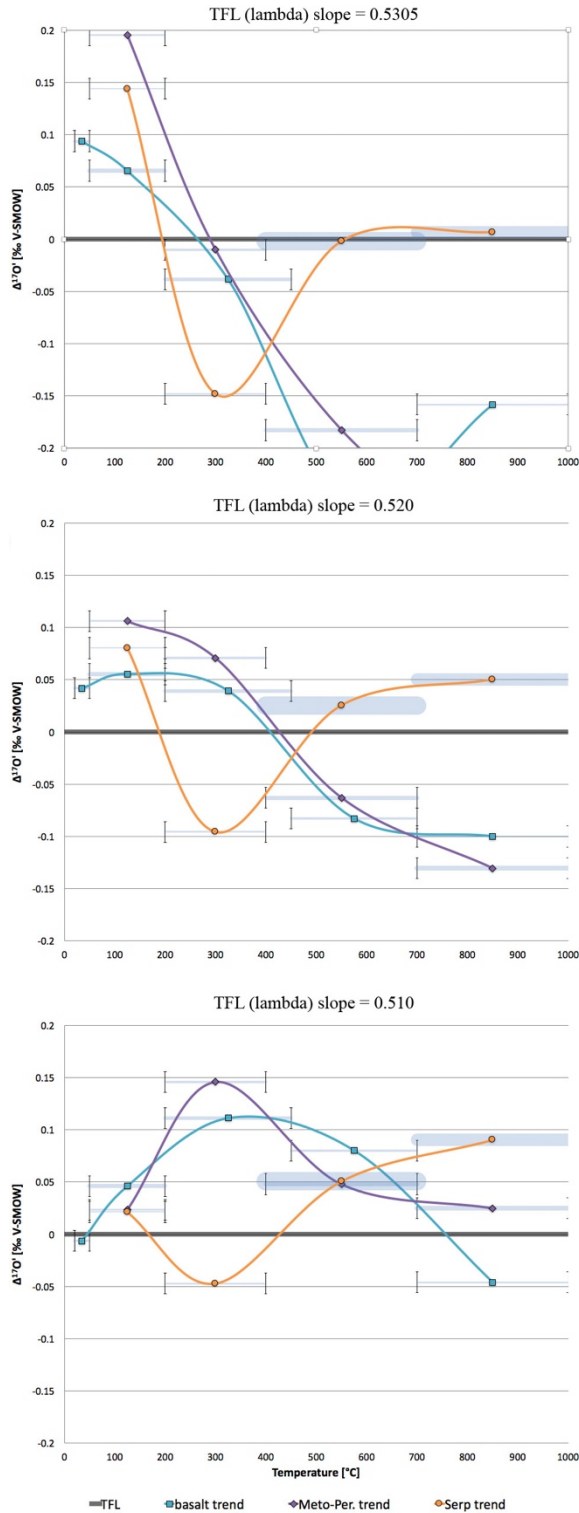different fractionation λ values ranging from 0.5308 to 0.510 using the equation

Figure 2.2 Δ'17O values of waters extracted from terrestrial basalt, metasomatized peridotite and serpentinite. The figures illustrate how the calculated Δ'17O values of waters extracted from terrestrial rock standards change as a function of theta (terrestrial fractionation line slope) in equation Δ'17O= δ'17O-(lambda)*δ'18O.

$\Delta^{17}O'=\delta^{17}O'-\lambda*\delta^{18}O'$ (figure 2.2). The most logical fit of the data to meteoric and mantle oxygen isotope values, was achieved with a λ value of 0.52. This indicates that the release of water during mineral dehydration is a kinetic fractionation process. Karlsson et al. (1992) also used a λ value of 0.52 to calculate $\Delta'^{17}O$. The possibility that the fractionation slope was not a constant throughout the water extraction temperature range was also considered. However, the most logical calculation results for all temperature steps were attained using the value 0.52. For example, an equilibrium lambda of 0.5305 for lower temperature steps 25-150°C yielded $\Delta'^{17}O$ values above 0.1‰ These values do not correlate with the known value for meteoric waters (≈0.03‰) likely to be present as the adsorbed water component. Therefore, it was concluded that a fractionation slope of 0.52 was the most appropriate for all water release

temperature intervals.

2.4.3 Oxygen isotope composition of water in Martian meteorites

As previously reported (Karlsson et al., 1992; Agee et al., 2013; Ziegler et al., 2013), the oxygen isotope composition of waters extracted from Martian meteorites fall outside the SNC bulk rock silicate range. Raw measured $\delta^{17}O$ and $\delta^{18}O$ values, linearized $\delta'^{17}O$ and $\delta'^{18}O$ values and the calculated $\Delta'^{17}O$ for all the samples analyzed in this study along with all other literature data are presented in table 2.3. $\Delta'^{17}O$ data collected as part of this study is corrected using the correction equation $\Delta'^{17}O_{(corrected)}= \Delta'^{17}O+(0.0002*\delta'^{18}O+0.02)$, determined by executing the VSMOW-SLAP triple isotope calibration procedure. Previously reposted literature data is presented as is since the determined correction is only applicable to our analytical system. In this study, the $\Delta'^{17}O$ values of waters extracted from Martian meteorites ranged from -0.02 to 0.55‰. Waters extracted from shergottites (Tissint, NWA-7042, Zagami) showed a deficit of ^{17}O relative to the bulk SNC silicate oxygen isotope composition. Low temperature (<150°C) waters extracted from shergottites generally produced $\Delta'^{17}O$ values similar to terrestrial meteoric waters (0.0-0.03‰). The most elevated concentrations of $\delta^{17}O$, in shergottites were observed in waters extracted between 150 and 600°C. The $\Delta'^{17}O$ values of these waters ranged from 0.08 to 0.23‰. Waters extracted from shergottites at temperatures above 600°C had $\Delta'^{17}O$ values close those of terrestrial samples (0.01 to 0.05‰). For shergottites, the high temperature extraction steps produced the smallest amounts of water (<10µmoles)

Table 2.3. Oxygen isotope composition of water in Martian meteorites. *From Karlsson et al., (1992) with additional unpublished data (***) provided by the authors. **From Agee et al., (2013). All data has been recalculated using θ=0.520

Meteorite	weight	step	mid-point	H_2O yield	$\delta^{18}O$	$\delta^{18}O'$	$\delta^{17}O$	$\delta^{17}O'$	raw $\Delta^{17}O'$ (0.52)	$\Delta^{17}O'$ (0.52)
	[g]	[T_{max} °C]	[T_{mid} °C]	[μmoles]				[‰ V-SMOW]		
Tissint	2.50	50	37.5	7	-3.29	-3.30	-1.67	-1.67	0.04	0.06
		200	125	16	1.06	1.06	0.64	0.64	0.09	0.11
		400	300	15	8.05	8.02	4.39	4.38	0.21	0.23
		700	550	13	13.26	13.17	7.05	7.02	0.17	0.20
		1000	850	8	16.87	16.73	8.77	8.73	0.03	0.05
NWA-10153	2.35	50	40	111	-12.14	-12.21	-6.39	-6.41	-0.06	-0.04
		150	100	143	-4.14	-4.15	-2.15	-2.15	0.01	0.03
		350	250	170	6.51	6.49	3.67	3.66	0.29	0.31
		600	475	58	10.96	10.90	6.17	6.15	0.48	0.50
		1000	800	34	24.52	24.22	13.21	13.13	0.53	0.55
NWA-7042	3.48	50	40	84	-11.30	-11.36	-5.93	-5.95	-0.04	-0.02
		150	100	179	-4.97	-4.98	-2.57	-2.58	0.01	0.03
		350	250	183	6.56	6.53	3.48	3.47	0.08	0.10
		600	475	176	12.54	12.47	6.62	6.60	0.12	0.14
		1000	800	47	14.96	14.85	7.74	7.71	-0.01	0.01
Zagami	3.5	50	40	9	-4.85	-4.86	-2.45	-2.45	0.07	0.09
		150	100	16	4.29	4.28	2.29	2.29	0.06	0.08
		350	250	15	4.50	4.49	2.44	2.44	0.10	0.12
		600	475	20	17.02	16.88	8.90	8.86	0.08	0.11
Chassigny*	2.07	150	88	17.3	5.20	5.19	2.79	2.79	0.09	0.09
		350	250	20.6	-11.67	-11.74	-5.98	-6.00	0.11	0.11
		600	475	16.2	-2.09	-2.09	-0.74	-0.74	0.35	0.35
		1000	800	4.3	-13.37	-13.46	-6.22	-6.24	0.76	0.76
Lafayette*	2.99	150	88	112.8	5.73	5.71	3.09	3.09	0.11	0.11
		350	250	108.6	11.44	11.38	6.22	6.20	0.29	0.29
		600	475	75.1	6.10	6.08	3.75	3.74	0.58	0.58
		1000	800	24.3	5.28	5.27	3.30	3.29	0.56	0.56
Nakhla*	2.09	150	88	24.5	-0.98	-0.98	-0.30	-0.30	0.21	0.21
		350	250	26.3	-3.57	-3.58	-1.48	-1.48	0.38	0.38
		600	475	13.5	3.01	3.01	2.46	2.46	0.89	0.89
	***	1000	800	1.5	2.27	2.27	1.99	1.99	0.81	0.81
Shergotty*	3.09	150	88	13.8	1.76	1.76	1.12	1.12	0.20	0.20
		350	250	19	-10.09	-10.14	-5.14	-5.15	0.12	0.12
		600	475	12.9	-8.16	-8.19	-4.44	-4.45	-0.19	-0.19
		1000	800	9.5	-10.44	-10.49	-5.28	-5.29	0.16	0.16
Zagami-1*	2.93	150	88	11.6	-2.03	-2.03	-0.65	-0.65	0.41	0.41
		350	250	11.8	-11.04	-11.10	-5.43	-5.44	0.33	0.33
		600	475	5.5	-3.28	-3.29	-1.05	-1.05	0.66	0.66
		1000	800	5.1	-15.36	-15.48	-7.48	-7.51	0.54	0.54
Zagami-2*	3.43	150	88	11.8	-3.48	-3.49	-1.58	-1.58	0.23	0.23
		350	250	14.4	-11.02	-11.08	-5.50	-5.52	0.25	0.25
		600	475	7.9	-6.23	-6.25	-3.10	-3.10	0.14	0.14
		1000	800	7.2	-13.47	-13.56	-6.69	-6.71	0.34	0.34
EET-A*	3.06	150	88	22.3	-16.60	-16.74	-8.65	-8.69	0.02	0.02
		350	250	20.5	-16.65	-16.79	-8.64	-8.68	0.05	0.05
		600	475	7.8	-21.13	-21.36	-10.82	-10.88	0.23	0.23
	***	1000	800	4.1	-20.94	-21.16	-10.90	-10.96	0.04	0.04
NWA 7034**	1.23	50	35	21.1		-21.78		-11.05	0.28	0.28
		150	100	18.2		-3.88		-1.79	0.23	0.23
		320	235	7.7		-4.73		-2.14	0.32	0.32
		500	410	3.6		-1.63		-0.48	0.37	0.37
		1000	750			11.02		5.91	0.18	0.18

44

compared to other temperature intervals. The difference in the amount of extracted water between temperature intervals should be considered when interpreting the results.

Analysis of the waters extracted from the Martian nakhlite NWA-10153 revealed a different overall $\Delta'^{17}O$ trend from that of shergottites. The low temperature (<150°C) waters extracted from NWA-10153 showed a relatively terrestrial oxygen isotope signature ($\Delta'^{17}O \approx 0.0$‰). Water extracted from NWA-10153 between 150 and 300°C had a $\Delta'^{17}O$ value of 0.29‰ and is the only water sample in this study to plot in the bulk SNC silicate $\Delta'^{17}O$ range. Waters extracted from NWA-10153 at temperatures above 300°C had $\Delta^{17}O$ values of 0.50-0.55‰, higher than bulk SNC silicate values (see Table 2.3). Unlike the shergottites, the highest temperature water (600-1000°C) extraction from NWA-10153 yielded a large sample (>20μmoles) which had a high $\Delta'^{17}O$ value (0.55‰), the highest $\Delta'^{17}O$ value of any Martian water measured in this study.

2.4.4 Water and hydroxyl oxygen isotope exchange experiment

Low temperature water (100-150°C) extracted from a basalt sample exposed to isotopically spiked water vapor ($\delta^{18}O=8000$‰) had a $\Delta'^{17}O$ value of 515‰. This was expected since adsorbed water readily exchanges with atmospheric moisture. After this low temperature extraction, 5 VSMOW water standard samples were analyzed until most of the isotopic contamination from the spiked sample was removed and $\Delta'^{17}O$ measurements of VSMOW returned to <1.0‰. Oxygen isotope analysis of intermediate temperature water (150-350°C) yielded a $\Delta'^{17}O$ value of 328‰. The contamination was again removed from

the system by analyzing consecutive VSMOW samples until the $\Delta'^{17}O$ returned to <1.0‰. Water extracted from the sample between 350-1000°C had a much higher than expected $\Delta'^{17}O$ value of 86‰. Another portion of the "contaminated" basalt sample, which was dehydrated up to 350°C, was then used to further resolve the degree of contamination in high temperature waters (OH groups). Waters extracted between 350 and 600°C had a $\Delta'^{17}O$ of 187‰ while waters extracted between 600 and 1000°C had a $\Delta'^{17}O$ of 76‰. The data indicates that the effect of water oxygen isotope exchange extends to the high temperature hydroxyl groups of hydrous minerals within the sample. It is not known whether the exchange happens during heating as the water is extracted or at room temperature during the exposure experiment. The result, however, is the same. Rock water exchange with atmospheric moisture extends beyond the adsorbed waters and does influences the isotopic composition of water extracted at high temperature.

2.4.5 Distribution and composition of hydrous phases in Martian meteorite Zagami

Results of statistical analysis of the qualitative maps of Zagami thin sections are reported in Table 2.4 in area percent. Majority of the phosphate assemblage in both thin sections is made up of anhydrous mineral merrillite. 0.17% of the area of the thin sections is occupied by apatite (possibly containing OH). Of the present apatite 0.11A% is Cl-rich apatite while 0.06A% is F-rich apatite. No amphibole minerals were observed on the large-scale qualitative maps of Zagami thin sections 998 and 1094. The mineral grains in the

Table 2.4 Mineral composition of Zagami thin sections 998 and 1094 reported in area percent (A%)

Thin Section	Pyroxene	Maskelynite	Iron-titanium oxides	Phosphate minerals
998	78.23	19	1.27	1.5
1094	78.28	19.1	1.12	1.5

samples showed uniform distribution. Typical fine-grain normal Zagami foliated texture produced by preferential orientation of pyroxene and maskelynite grains, originally reported by Stolper and McSween 1979 and McCoy et al. 1992, was also observed in the samples.

Based on data collected from single-point quantitative analysis a ratio of apatite OH site occupancy in the F-rich portion was calculated to be $OH_{0.122}$, $F_{1.679}$, $Cl_{0.199}$. This indicates that OH sites in the F-rich apatite are occupied by 83.9% fluorine, 6.1% OH and 10% chlorine. By combining the calculated percentage of OH in the F-rich apatite grains and the distribution of F-rich apatite in Zagami, it was determined that F-rich apatite-bound OH makes up 0.013 wt% of Zagami (130 ppm). By applying the same OH occupancy value to the Cl-rich apatite portion of Zagami it was calculated that the Cl-rich portion could store 0.0238 wt% (238 ppm) OH. In total the apatite OH storage capacity in Zagami was determined to be 0.0369 wt% (369 ppm).

2.5 Discussion

2.5.1 Three reservoirs

Measurements of oxygen isotope composition of water extracted from Martian meteorites conclusively support previous reports (Karlsson et al., 1992; Agee et al., 2013; Ziegler et al., 2013) that the water within Martian meteorites is not in isotopic equilibrium with the bulk rock silicate portion. $\Delta'^{17}O$ values of waters extracted from Martian meteorites fall both above and below the SNC silicate oxygen isotope composition range.

This indicates that at least three isotopically distinct reservoirs of water are represented within these samples. The first reservoir is the original Martian mantle water, which is presumably in isotopic equilibrium with the oxygen isotope composition of silicate rock and has a $\Delta'^{17}O$ value of $\approx0.3‰$ (Clayton and Mayeda, 1983; Franchi et al., 1999; Rumble and Irving, 2009). The second reservoir is also Martian in origin but has an elevated $\Delta'^{17}O$ value. The third reservoir is terrestrial water which, by definition, has a $\Delta'^{17}O$ of 0.0‰. The interaction of these three isotopically distinct water reservoirs, two of which are Martian and one terrestrial, defines the isotopic composition of the waters extracted from Martian meteorite samples.

When the results of this study are analyzed cooperatively with work done by Karlsson et al., (1992) and Agee et al., (2013) two clear trends appear based on the oxygen isotope composition of extracted waters (figure 2.3 a and b). In one group of meteorites we see a mixing trend between Martian mantle waters and terrestrial waters (contamination). In the other group, we see the same mixing between Martian mantle waters and terrestrial waters but we also see a contribution from the elevated $\Delta'^{17}O$ Martian water reservoir. The distinction between the two groups is also supported by mineralogy and rock type of the meteorites. The first group, showing two component mixing, is made up only of shergottite. The second group which shows elevated $\Delta'^{17}O$ reservoir contribution includes nakhlites Nakhla, Lafayette and NWA-10153 as well as Chassigny. This suggests a clear correlation between the geologic history of the samples and the oxygen isotope composition of the waters within each sample.

2.5.2 Two component mixing in shergottites.

Except for one single analysis of Martian meteorite Zagami, done by Karlsson et al., (1992), the $\Delta'^{17}O$ of waters extracted from shergottites are below the SNC silicate value (<0.3‰). This trend holds true for all waters extracted at different temperatures from Shergotty, EETA-79001A, Zagami (two different samples), Tissint, and NWA-7042 (figure 2.3a). Based on the water isotopic exchange experiment, done as part of this study, we propose that the $\Delta'^{17}O$ values of the waters extracted from these samples are a product of mixing between Martian mantle water and terrestrial moisture (contamination). Such contamination could easily produce the observed effect. Original Martian mantle water, in isotopic equilibrium with silicate oxygen ($\approx$0.3‰), mixed with terrestrial moisture of $\approx$0.03‰ (Barkan and Luz, 2005) would producing an isotopic composition which falls between the two endmembers. This is exactly what we observe in the isotopic composition of waters extracted from shergottites. The low temperature (<150°C) waters extracted from these samples generally have the lowest $\Delta'^{17}O$ values, similar to those of terrestrial meteoric waters. This is because adsorbed waters readily undergo exchange with terrestrial moisture. Waters extracted between 150 and 600°C generally have the highest $\Delta'^{17}O$ values and the oxygen isotope composition of these waters is close to the SNC silicate oxygen isotope composition. However, the $\Delta'^{17}O$ values of these intermediate temperature waters are <0.3‰ indicating that terrestrial contamination is present. The measured isotopic composition of high temperature waters (>600°C) present a bit of a mystery. Since these high temperature waters (OH groups) are the least likely to experience terrestrial contamination it would be logical to expect these waters to preserve their original isotopic composition. However, the $\Delta'^{17}O$ of these waters span the whole range of $\Delta'^{17}O$ values

from terrestrial 0.03‰ to Martian SNC values of 0.3‰. This observed trend could be due to the small sample size of these high temperature waters. The smaller the original reservoir the more likely it is to be affected by terrestrial contamination both during normal exposure to atmospheric moisture and the water extraction procedure.

The assumption that the original formation waters in shergottites are in isotopic equilibrium with the silicate portion is made based on analysis of terrestrial samples. High temperature waters (>600°C) extracted from terrestrial basalts have negative $\Delta'^{17}O$ values between -0.05 and -0.1‰ ±0.02‰. Work done on terrestrial silicate samples, thought to be representative of Earth mantle values, has yielded a similar range of $\Delta'^{17}O$ (Herwartz et al., 2014; Sharp et al., 2016). This correlation indicates that the high temperature formation waters extracted from terrestrial basalt samples are in isotopic equilibrium with the silicate portion.

Fluorine/chlorine zoning in the Martian basaltic shergottite Zagami presents additional support for isotopic equilibrium between the origin water and the silicate portion. A study by McCubbin et al. (2015) determined that for a basaltic melt the mineral-melt partition coefficients (D values) for OH site elements in apatite are $D_F^{Ap.-melt} = 4.4\text{-}19$, $D_{Cl}^{Ap.-melt} = 1.1\text{-}5$, $D_{OH}^{Ap.-melt} = 0.07\text{-}0.24$. Since F has a much higher partition coefficient than Cl and OH it is preferentially incorporated into the apatite grain as the melt begins to crystalize. Once F is exhausted Cl becomes the dominant element in the OH site of apatite grains. The apatite grains in Zagami are interstitial and element partitioning occurs on a small scale within isolated pockets of grain boundary melt. This produces the irregular zoning characteristics observed in Zagami apatite. Essentially, the distribution of F and Cl follows the cooling history of each individual apatite grain. The partitioning of OH into the

apatite remains relatively constant up to the point where Cl occupancy in the apatite OH site reaches approximately 80% at which point the OH partitioning drastically decreases until Cl is exhausted (McCubbin et al., 2016). Once Cl is exhausted OH dominates the structure of the apatite until OH is no longer available and merrillite ($Ca_9NaMg(PO_4)_7$) becomes the dominant phosphate mineral (McCubbin et al., 2016). This transition to merrillite is exactly what is observed in Zagami and indicates complete removal of the volatile components OH, F and Cl from the melt. Since the available OH in the melt is wholly incorporated into the apatite grains no significant isotopic fractionation should occur. Thus, the OH groups in the sample must initially have had a Martian mantle-like oxygen isotope composition.

Similar two reservoir mixing could be responsible for the $\Delta'^{17}O$ trend of waters extracted from NWA-7034 (Agee et al., 2013). In the case of NWA-7034 the $\Delta'^{17}O$ of the bulk rock silicate portion is elevated relative to SNC group meteorites and the $\Delta'^{17}O$ of the extracted waters group roughly in the bulk SNC range. The average $\Delta'^{17}O$ value of silicate oxygen of NWA-7034 is 0.58‰ while the $\Delta'^{17}O$ values of the extracted water range from 0.18‰ to 0.37‰ (Agee et al., 2013). Even though the actual $\Delta'^{17}O$ values are different, the offset between the water and silicate oxygen isotope composition is comparable to the offset measured in shergottites. It is possible that the Martian water in NWA-7034 was in isotopic equilibrium with the silicate portion but has since experienced exchange with terrestrial water vapor. This exchange has resulted in a $\Delta'^{17}O$ shift of the extracted waters towards more terrestrial values.

The one sample that does not follow this trend is an aliquot of Martian shergottite Zagami measured by Karlsson et al., (1992). Waters extracted from this sample had

elevated $\Delta'^{17}O$ values above bulk SNC $\Delta'^{17}O$ range. It is possible that this aliquot of Zagami contained shock melt inclusions with trapped near-surface Martian waters. Due to the large sample size used (2.93g) it is conceivable that the presence a melt inclusion may have been overlooked during analysis. One other outlier in the dataset is the $\Delta'^{17}O$ of water extracted from Shergotty between 350-600°C by Karlsson et al., (1992). This analysis yielded an extreme negative $\Delta'^{17}O$ outlier of -0.19‰. It is possible that this measurement hints at the existence of a ^{17}O depleted reservoir on Mars. However, as this is the only data point with such a negative value it is possible that it is simply an analytical outlier.
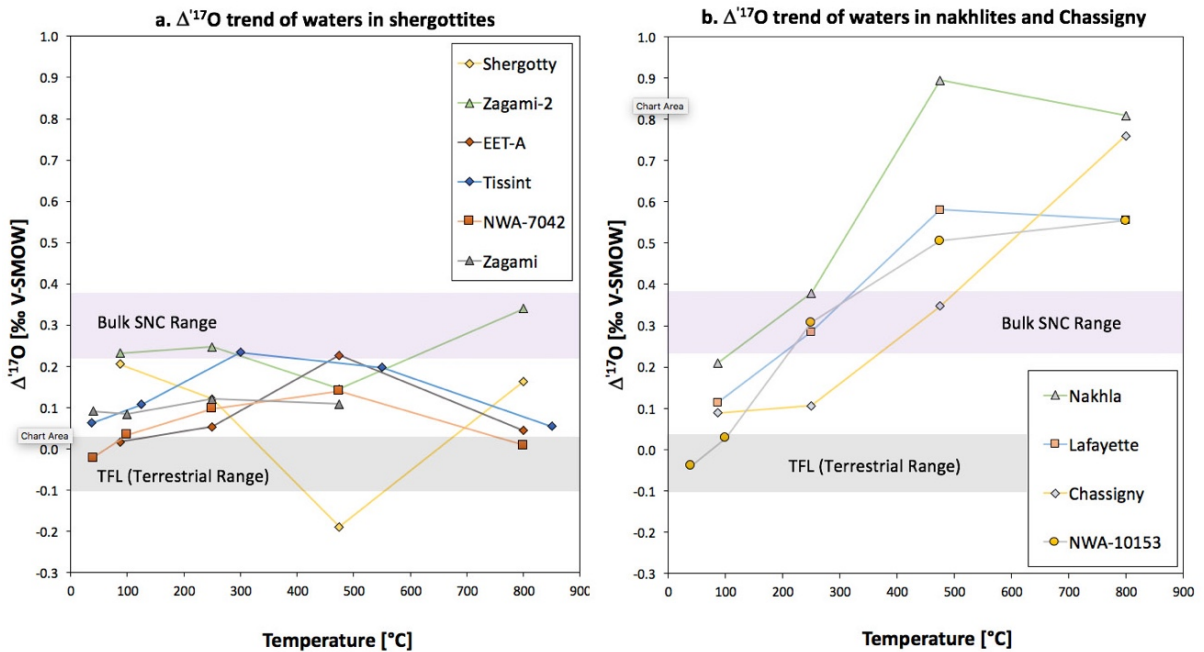
Figure 2.3 Two distinct trends observed in the oxygen isotope composition of waters extracted from Martian meteorites. a) Δ'17O trend of waters extracted from shergottites. b) Δ'17O trend of waters extracted from nakhlites and Chassigny.

2.5.3 Three component mixing in nakhlites and Chassigny

High temperature (>350°C) water extracted from nakhlites and Chassigny have $\Delta'^{17}O$ values that range from 0.48‰ to 0.89‰ (figure 2.3b), significantly higher than the

SNC oxygen isotope composition range. It appears that these high-temperature waters preserve the oxygen isotope contribution from a high $\Delta'^{17}O$ Martian water reservoir. Based on the presence of pre-terrestrial clay-rich alteration product iddingsite, halite and oxy-hydroxides in nakhlites and low temperature alteration carbonates, sulfates and oxides in Chassigny, these samples likely interacted with extraterrestrial near-surface water (Ashworth and Hatchison, 1975, Bunch and Reid, 1975; Reid and Bunch, 1975; Gooding et al., 1991; Treiman et al., 1993; Bridges and Grady, 1999; Sawyer et al., 2000; Bridges et al., 2001) Thus, it is likely that the elevated $\Delta'^{17}O$ value of these high temperature waters is a record of that interaction. The oxygen isotope composition of the near-surface Martian waters is also preserved in the non-water oxygen component of the alteration minerals. Oxygen isotope composition analysis of carbonates and water-soluble sulfates in Nakhla and Lafayette was done by Farquhar and Thiemens (2000). Their work showed that these alteration minerals are enriched in ^{17}O with water-soluble sulfate from Nakhla having the highest $\Delta^{17}O$ values of 1.4‰ (Farquhar and Thiemens, 2000). The water isotopic exchange observed in our experiment, over a course of one year, indicates that long term interaction between rock and water/water moisture can affect the isotopic composition of high temperature waters. By the same mechanism, the original isotopic composition of waters within nakhlites and Chassigny was likely changed by long-term interaction with Martian near-surface waters. It is important to mention that the high temperature water yield from nakhlites and Chassigny is much greater than the high temperature water yield from shergottites.

The measured oxygen isotope composition of waters extracted from nakhlites and Chassigny samples are likely not entirely representative of any one isotopic reservoir. More

realistically, each of the extracted waters records the influence of all three isotopically distinct water reservoirs. The original formation waters in nakhlites and Chassigny were most likely in isotopic equilibrium with the silicate portion and had a $\Delta'^{17}O$ value of approximately 0.3‰. Through hydrothermal interaction with ^{17}O enriched near-surface Martian waters the $\Delta'^{17}O$ of the waters in the samples was elevated. Once the samples arrived on Earth, terrestrial moisture began to exchange with the waters within the samples altering the oxygen isotope composition of the extraterrestrial water. This exchange happens fastest in the adsorbed and low temperature mineral waters. Thus, the low temperature (<150°C) waters extracted from nakhlites and Chassigny show a significant $\Delta'^{17}O$ shift towards terrestrial values. The $\Delta'^{17}O$ values of intermediate temperature waters (150-350°C) extracted from nakhlites and Chassigny range between 0.29‰ and 0.38‰. The isotopic composition of these waters is likely a mixture of the original formation waters (≈0.3‰) the Martian surface waters, elevated in ^{17}O, and of terrestrial moisture contamination (≈0.03‰). The high temperature waters (>350° C) experience the slowest rate of exchange with terrestrial moisture. Thus, they better preserve the extraterrestrial water and the isotopic contribution form the elevated ^{17}O Martian near-surface water reservoir.

2.5.4 $\Delta'^{17}O$ of Martian surface/near-surface waters

The oxygen isotope composition of waters extracted from Martian meteorites represent the mixing of three isotopically distinct reservoirs. The original mineral formation waters, in equilibrium with the silicate portion, the terrestrial contamination

waters and most interestingly the elevated $\Delta'^{17}O$ Martian near-surface waters. As we do not know what percentage of the original high temperature formation waters was replaced by Martian near-surface water we cannot back-calculate the actual $\Delta'^{17}O$ of the Martian near-surface water reservoir. However, the $\Delta'^{17}O$ value of the near-surface Martian water reservoir has to be as high or higher than the highest $\Delta'^{17}O$ measured in waters extracted from Martian meteorites. In this study, the highest $\Delta'^{17}O$ value was measured in the 600-1000°C temperature water extracted from nakhlite NWA-10153. This water sample had a $\Delta'^{17}O=0.55‰$. Therefore, based on our works, the $\Delta'^{17}O$ of the Martian near-surface water reservoir has to be at least 0.55‰ ±0.05‰ or greater. The highest ^{17}O surplus outside our work was measured in water extracted from Nakhla by Karlsson et al, (1992) between temperatures of 350 and 600°C. This water sample had a $\Delta'^{17}O$ of 0.89‰. The second highest $\Delta'^{17}O$ value of 0.73‰ was measured in a water sample extracted from Chassigny at temperatures between 600 and 1000°C (Karlsson et al., 1992). Based on Karlsson et al., (1992) data, the $\Delta'^{17}O$ of the Martian near-surface water reservoir has to be equal to or greater than 0.89‰ ±0.1‰. This estimate is consistent with $\Delta'^{17}O=0.8±0.05‰$ of carbonate minerals in ALH 84001 measured by Farquhar et al., (1998). $\Delta'^{17}O$ of water-soluble sulfate from Nakhla, measured by Farquhar and Thiemens, (2000) suggests that the $\Delta'^{17}O$ of Martian near-surface waters could be as high as 1.4‰.

2.5.5 The origin of ^{17}O surplus in Martian near-surface waters

Evidence for the existence of a ^{17}O enriched reservoir on planet Mars has been identified by several authors in Martian waters and secondary mineral phases (Karlsson et

al., 1992; Romanek et al., 1994; Clayton and Mayeda, 1996; Farquhar et al., 1998; Franchi et al., 1999; Farquhar and Thiemens, 2000; Agee et al., 2013). It has been proposed that the observed ^{17}O excess is representative of the atmosphere and hydrosphere (surface and near-surface waters) of Mars (Farquhar and Thiemens, 2000). This ^{17}O enriched reservoir is distinctly different from the oxygen isotope composition of the silicate portion of Mars. This leads to the big question: how did two reservoirs with such distinct oxygen isotope compositions evolve on planet Mars? To answer this question, we must first define the system boundaries of each reservoir. First, the two reservoirs must be practically isolated from one another with only limited oxygen isotope exchange between the two reservoirs. If this was not true the two reservoirs would equilibrate and no isotopic heterogeneity would be observed. Second, the hydrosphere and atmosphere of Mars should be treated as two parts of a single reservoir. Near surface waters will inevitably interact with the Martian atmosphere and vice versa through evaporation and regolith absorption. Orbital and rover measurements dating back to the Viking mission show evidence for substantial diurnal water vapor exchange between the atmosphere and the regolith of Mars (Farmer et al., 1977; Jakosky and Farmer, 1982; Jakosky et al., 1997; Smith, 2004; Tschimmel et al., 2008; Smith, et all., 2009; Pankine et al., 2010; Maltagliati et al., 2011; Maltagliati et al., 2013; Steele, et al., 2017). The isotopic exchange between these two components is likely relatively slow but significant over long periods of time and affects the isotopic composition of all near surface water on Mars. Based on this framework we can safely make the following speculations. The oxygen isotope composition of silicate rocks on Mars was primarily defined during planetary accretion of Mars and has not changed significantly

though time. The oxygen isotope composition of the Martian atmosphere and near–surface water has evolved over time to its present-day composition defined by a surplus of ^{17}O.

Within the defined framework, we can present several possible mechanisms for ^{17}O enrichment of the Martian atmosphere and near-surface waters. It has been proposed that the observed ^{17}O surplus of the near surface Martian waters is due to cometary influx of water during the planet's history (Farquhar and Thiemens, 2000). Conceptually this mechanism is appealing especially in the context of a solar system $\Delta'^{17}O$ gradient caused by nebular self-shielding during cosmic ray dissociation of oxygen bearing molecules such as CO (Thiemens and Heidenreich, 1983). Because of the mass-impendent fractionation nature of the process, materials which form in the outer solar system would have a surplus of ^{17}O relative to the materials which form near the center of the solar nebula. Thus, outer solar system (Kuiper belt) waters should have a surplus of ^{17}O and if these waters are delivered to a planetary body such as Mars the isotopic signature of those waters will be imprinted on the waters of that planetary body. However, recent work on cometary materials has shown that a significant heterogeneity ($\Delta^{17}O$ from -5‰ to +1‰) in the oxygen isotope composition exists and most cometary materials have negative $\Delta'^{17}O$ values (McKeegan et al., 2006; Nakamura et al., 2008; Ogliore et al., 2012; Nakashima et al., 2012). This data indicates that cometary contribution to Martian waters would not necessarily result in the ^{17}O surplus measured in Martian near-surface waters. Furthermore, cometary water contribution to Mars are estimated (based on data from Grinspoon and Lewis, 1988) to be approximately 0.5m over the planet's surface over a time span of 3.8 billion years (Krasnopolsky, 2002). A relatively small contribution to the total water budget of Mars.

It is more likely that the ^{17}O surplus measured in Matrian waters and secondary minerals is primarily a product of ongoing oxygen isotope fractionation effects happening in the regolith, on the surface and in the atmosphere of Mars. Due to the mass difference between the tree isotopes of oxygen, mass-dependent isotopic fractionation mechanisms follow a predetermined relationship where $\delta^{17}O \approx 0.52 * \delta^{18}O$. Therefore, during equilibrium mass-dependent fractionation no significant enrichment in ^{17}O occurs relative to ^{18}O. Any minute enrichment in ^{17}O by a mass-dependent process would also produce a very high $\delta^{18}O$ value. This has not been observed in any of the Martian waters or secondary alteration minerals studied by Farquhar and Thiemens, (2000) and Farquhar et al., (1998). Therefore, it is not likely that the surplus of ^{17}O in Martian near surface waters is a product of mass-dependent fractionation. Most likely, the ^{17}O surplus of the near-surface Martian waters is a product of mass-independent fractionation.

Many gas phase photochemical reactions have been found to result in mass-independent oxygen isotope fractionations (Thiemens, 1999; Farquhar and Thiemens, 2000; Thiemens et al., 2012). On Earth, many of these chemical reactions are inhibited by the presence of molecular oxygen in the atmosphere. Most of the necessary ultraviolet energy ($\lambda < 310$ nm) needed to initiate such reactions is absorbed by and drives the dissociation of ozone (Ball et al., 1997; Johnston and Thiemens, 1997). In an atmosphere without molecular oxygen however, many other photochemical reactions could take place (Velivetskaya et al., 2016). Of particular interest is the direct photodissociation of H_2O to produce H_2O_2 through the following reactions: *$H_2O + hv(\lambda < 190$ nm$)$ $\rightarrow$ $H + OH$* followed by *$OH + OH \rightarrow H_2O_2$* (Velivetskaya et al., 2016). It has been shown that during photochemical formation of hydrogen peroxide (H_2O_2) oxygen undergoes a significant

mass-independent fractionation (Savarino and Thiemens, 1997; Velivetskaya et al., 2016). H_2O_2 experimentally produced in an oxygen free environment by Velivetskaya et al., (2016) had a significant increase in ^{17}O ($\Delta^{17}O\approx1.4‰$) with no change in $\delta^{18}O$ relative to the original water. Since hydrogen peroxide is an oxidizer it readily reacts with other species and H_2O is a common reaction byproduct. Alternatively, H_2O_2 can dissociate following the reaction $2H_2O_2\rightarrow2H_2O+O_2$. Inevitably the H_2O inherits the ^{17}O enriched isotope signature of the H_2O_2. In the case of planet Mars, this mass-independent fractionation process could have occurred in the atmosphere and even on the planet's surface since there is no O_3 to block the incoming ultraviolet radiation. Over geologic time the effect of this process could have raised the concentration of ^{17}O in Martian near-surface waters. Undoubtedly, this is not the only mass-impendent fractionation process at work on Mars. Many other gas phase chemical reactions have also been proposed as mechanisms to drive ^{17}O enrichment in Martian near–surface waters. These mass-independent fractionation reactions are based on the photochemical effects on various gas phase species such as carbon monoxide (Huff and Thiemens 1998; Rockmann et al., 1998; Thiemens and Heidenreich, 1983), nitrous oxide (Cliff and Theiemens, 1997), sulfate species (Lee et al., 1998) and carbon dioxide (Savarino et al., 1998). In reality the ^{17}O enrichment measured in Martian waters and secondary minerals is most likely a product of all the above-mentioned mechanisms.

Another big question relating to the ^{17}O enrichment of Martian near-surface waters is the fate of the ^{17}O depleted component. From a classical mass balance perspective, any enrichment in one reservoir must be balanced by a depletion in another reservoir. So far, no conclusive evidence of a ^{17}O depleted reservoir has been presented. It has been

suggested that oxidized minerals in the Martian regolith could be a sink of ^{17}O depleted oxygen (Farquhar and Thiemens, 2000). If we consider the decomposition reaction for hydrogen peroxide $2H_2O_2 \rightarrow 2H_2O+O_2$ the oxidation of regolith minerals by released molecular O_2 is a likely possibility. Another possible sink is the direct loss of ^{17}O depleted oxygen/oxygen bearing species to space following mass-independent photochemical reactions. Many of the created/remaining species following photochemical reactions are lighter than the CO_2 dominated atmosphere of Mars (Barth, 1974; Owen et al., 1977; Nair et al., 1994). Thus, it would be possible for these species to remain in the atmosphere and possibly escape into space. This is especially relevant when CO_2 is photolyzed by ultraviolet radiation. After CO_2 is dissociated by UV light (<228 nm) following the reaction $CO_2+hv \rightarrow CO+O,$ CO+O recombination is significantly slower than the reaction between two oxygen atoms to form O_2 (Nair, et al., 1994). Therefore, the Martian atmosphere should contain a significant amount of CO and O_2 but the concentrations of the two species are significantly lower (Nair, et al., 1994). Most investigations of this discrepancy and into the evolution of the atmosphere of Mars agree that a large portion of the molecular oxygen is lost to space (Anderson and Hord, 1971; Lundin et al., 1989; Nair et al., 1994; Brain and Jakosky, 1998; Chassefiere and Leblanco, 2004). Solar wind play a key role in the actual mass removal of oxygen from the Martian atmosphere through ion puck-up (Lundin, et al., 1989; Chassefiere and Leblanco, 2004; Rahmati, et al., 2015). Possible oxygen escape flux, due to solar wind, has been estimated to be as high as $7x10^{27}$ions/second (Lundin, et al., 1989) Even with a more conservative flux estimate and a low atmospheric oxygen (O_2^+) ionization rate, the loss of oxygen to space is substantial and could function as a sink of ^{17}O depleted oxygen.

3. High Precision Triple Oxygen Isotope Calibration of Terrestrial Water Standards VSMOW and SLAP

3.1 Abstract

In order to measure the triple oxygen isotope composition of water a direct water fluorination line was built and calibrated to the VSMOW-SLAP water standard scale. Water was fluorinated using BrF_5 reagent and the liberated O_2 gas was measured using gas source stable isotope ratio mass spectrometry. The analytical procedure was refined to yield a $\Delta^{17}O$ precision of 0.005‰ (1σ) and a $\delta^{18}O$ precession of 0.05‰ (1σ). The system was used to make high-precision measurements of water standards VSMOW and SLAP. $\delta^{18}O$ measurements were used to determine the linearity of the experimental system between 0.0‰ (VSMOW) and the extreme negative outlier SLAP at -55.5‰. The measured $\Delta'^{17}O$ values were used to determine that a 0.02‰ correction was required for all $\Delta'^{17}O$ measurements made with the system. Due to the ever-improving resolution of $\Delta'^{17}O$ measurements, such system/laboratory corrections are crucial to $\Delta'^{17}O$ analysis and inter-laboratory data comparisons. Here it is shown that in addition to establishing $\delta^{18}O$ linearity, the VSMOW-SLAP scale provides a convenient reference for determining system/laboratory $\Delta'^{17}O$ corrections.

3.2 Introduction

Vienna Standard Mean Ocean Water (VSMOW) and Standard Light Antarctic Precipitation (SLAP) are two quintessential isotopic water standards. All laboratory analysis of the isotopic composition of oxygen or hydrogen extracted from water samples must be made relative to these two water standards. For this reason, laboratories that conduct isotopic analysis of water must inevitably calibrate their instrumentation and analytical procedures to VSMOW and SLAP water standards. This work focuses primarily on the relevance of these water standards to isotopic measurements of oxygen. Oxygen isotope measurements are reported in standard δ notation where $\delta = \left(\frac{R_{Sample}}{R_{Standard}} - 1\right) *$ 1000 and where R is the ratio of the heavy isotope to the light isotope, as in $R=(^{18}O/^{16}O)$. By definition the $\delta^{18}O$ value of VSMOW is equal to 0‰ and SLAP has a $\delta^{18}O$ values of -55.5‰ (Hut, 1987; Coplen, 1994). Because of the large spread in $\delta^{18}O$ values between VSMOW and SLAP the two standards are used in tandem as a two-point calibration system. The measured $\delta^{18}O$ value of VSMOW is used to calibrate the $\delta^{18}O=0‰$ of the $\delta^{18}O$ scale and the measured $\delta^{18}O$ value of SLAP is used to determine the squeeze/stretch factor of the $\delta^{18}O$ scale for a particular experimental system.

Measurements of $\delta^{17}O$ have historically been relevant only to extraterrestrial applications since extraterrestrial materials often show large ^{17}O anomalies (McKeegan and Leshin, 2001). In the past terrestrial variability in $\delta^{17}O$ has been largely overlooked because it was below the detection limit of most instruments. However, improvements in the accuracy of isotopic ratio measurements have made it possible to accurately measure terrestrial $\delta^{17}O$ variability. Data in triple oxygen isotope space is presented in terms of $\delta^{18}O$ (domain) vs. $\delta^{17}O$ (range). Since ^{16}O is included in the calculation of both the $\delta^{17}O$ and $\delta^{18}O$ values, the data can be plotted on a simple x-y graph. The slope (θ) of the water

fractionation line within the triple oxygen space can be calculated as $\theta_{A-B} = \left(\frac{\delta^{17}O_A - \delta^{17}O_B}{\delta^{18}O_A - \delta^{18}O_B} \right)$, where point A is the measured values of VSMOW and point B the measured values of SLAP. Applying this procedure to measured VSMOW and SLAP values yields a θ value of 0.528 (Schoenemann et al., 2013). Using this known θ slope, a theoretical $\delta^{17}O$ value can be calculated from any $\delta^{18}O$ water measurement using the formula $\delta^{17}O=\theta*\delta^{18}O$. This deviation from the theoretical value is known as $\Delta^{17}O$ and is defined as $\Delta^{17}O=\delta^{17}O-\theta*\delta^{18}O$.

The $\Delta^{17}O$ value of VSMOW is $=0$‰ since $\Delta^{17}O=\delta^{17}O-\theta*\delta^{18}O$ and both $\delta^{17}O$ and $\delta^{18}O$ of VSMOW are equal to 0. Similarly, the $\Delta^{17}O$ of SLAP is also 0 because the measured $\delta^{17}O=29.7$‰ and $\delta^{18}O=55.5$‰ were used to constrain the slope of the terrestrial fractionation line θ. Using the calculated $\theta=0.528$ value any sample analyzed for oxygen isotope composition can be compared to the theoretical norm established by the VSMOW and SLAP standards. However, there is a linearity consideration that must be addressed when working in the triple oxygen space. The identity $\Delta^{17}O=\delta^{17}O-\theta*\delta^{18}O$ is an approximation derived from the power law $\alpha_{17/16}=(\alpha_{18/16})^{\theta}$ (Clayton and Mayeda, 1996; Miller, 2002). For the data to correctly plot as a linear function it must be linearized using the following equation $\delta' = 1000 \ln \left(\left(\frac{\delta}{1000} \right) + 1 \right)$ (Miller, 2002). Note that delta prime (δ' or Δ') notation indicates that the data has been linearized.

It has been demonstrated that the only way to obtain precise $\delta^{17}O$ measurements is by mass spectrometric analysis of pure O_2 (Barkan and Luz, 2012). Presently there are three established methods for breaking the oxygen-hydrogen bond of water with little to no isotopic fractionation. These methods include electrolysis (Meijer and Li, 1998), direct fluorination by F_2 or BrF_5 (O'Neil and Epstein, 1996) and solid reagent (CoF_3) fluorination

(Lantz, 1967). So far the electrolysis method is insufficient for high precision measurements of $\delta^{17}O$. The best analytical precision for this method to date is 0.07‰ and 0.1‰ for $\delta^{18}O$ and $\delta^{17}O$ respectively (Meijer and Li, 1998). Solid reagent fluorination using CoF_3 has recently become the most widely used of the three methods. The popularity of this approach is largely because CoF_3 is far less hazardous than F_2 and BrF_5 and the fact that the accuracy of this method has been greatly improved notably by Barkan and Luz, (2012). However, despite the recent improvements to the solid reagent fluorination method, direct water fluorination using F_2 or BrF_5 is universally accepted as a reliable method capable of yielding the highest precision.

Direct BrF_5 fluorination of water was first done by O'Neal and Epstein (1966). The procedure was based on previous work by Hoekstra and Katz (1953), who used BrF_5 fluorination to measure total oxygen in metal and mineral oxides, as well as the work of Clayton and Mayeda (1963) who used the process to liberate oxygen from mineral samples. Water Fluorination with BrF_5 proceeds per the following reaction: $BrF_5 + H_2O \rightarrow BrF_3 + 2HF + \frac{1}{2}O_2$ (O'Neal and Epstein, 1966). In the original work by O'Neal and Epstein (1966) the liberated O_2 was converted to CO_2 prior to making isotopic ratio measurements. This approach was suitable since the authors were only measuring $\delta^{18}O$ of the samples. However, the conversion to CO_2 makes it impossible to accurately measure $\delta^{17}O$ due to mass interference from other isotopes (^{13}C and ^{18}O) which combine to make CO_2 molecules of atomic mass 45. To accurately measure $\delta^{17}O$ ratios pure O_2 must be analyzed by isotope ratio mass spectrometry. For water samples this was first done by Jabeen and Kusakabe (1997) and their work greatly improved the accuracy of the direct

water fluorination method, yielding $\delta^{17}O$ and $\delta^{18}O$ precession of approximately 0.1 ‰ and 0.15‰ respectively.

Here we summarize and implement all the improvements made to the direct water fluorination method to date. The VSMOW-SLAP calibration procedure, described herein, was conducted to establish an up to date water standard calibration for the Center for Stable Isotopes at the University of New Mexico and to calibrate laboratory in-house water and silicate standards. The data was also used by Sharp et al., (2016) to further constrain the $\Delta^{17}O$ value of San Carlos olivine standard for inter laboratory comparisons. The analytical goal of this study was to achieve a $\Delta^{17}O$ precision of 0.005‰ (1σ) and a $\delta^{18}O$ precession of 0.05‰ (1σ).

3.3 Procedure

For this work, pristine VSMOW and SLAP water standards were obtained. These water standards were handled and used with utmost care to prevent isotopic fractionation due to evaporation or equilibration with atmospheric H_2O. Water standards were Fluorinated with high purity BrF_5 to break the OH bonds and free the oxygen. The liberated O_2 was then purified and analyzed using a *ThermoFinnigan MAT 253* gas source dual inlet isotope ration mass spectrometer. The analytical procedure is very susceptible to errors and works reliably only when all the details are observed and followed with exactness.

3.3.1 Water fluorination

3.3.1.1 Overview of water fluorination line

Figure 3.1 shows a schematic design view of the water fluorination system. Through experimentation it was found that using U traps instead of "fingers" for both the primary water trap and the reaction chamber (bomb) greatly improved the reproducibility of the process. It is not certain exactly why U traps yielded better reproducibility but they do offer some obvious advantages. When moving water vapor molecules in a vacuum using a temperature gradient, a U trap offers only a single path while a T connection to a cold finger offers an extra path for the randomly moving molecules to follow. The random motion of the molecules will inevitably transport all of water vapor to the cold finger but if the process is rushed some of the vapor molecules may not condensed in the cold finger and fractionation will occur. From a statistical perspective, a U trap greatly reduces this problem. A U trap also provides the advantage of a uniform pressure/vacuum gradient throughout the fluorination line.

The primary water trap was constructed using a ¼ inch OD (Outer Diameter) Cajon glass metal joint and a length of ¼ inch OD Pyrex glass tubing. The glass end of the joint was welded to the glass tubing to make a 12 inch Pyrex glass segment with ¼ inch stainless steel end. The glass portion of the segment was then heated (blown) in order to shape it into a U with the glass end facing straight up and the stainless steel end bent 90 degrees away from the trap (see figure 3.1). A *Cajon Ultra Torr* ¼ inch union was fitted on the glass end of the U trap and a rubber septum was loaded into the outer end of the union. The stainless steel end of the U trap was swaged on to the rest of the line using standard ¼ inch

Swagelok components. Glass construction was chosen for the primary water trap to allow visual monitoring of the injection process.

The reaction trap was constructed from ¼ inch OD pure nickel (nickel 200 alloy) tubing with a wall thickness of 0.022 inch. Internally electro-polished stainless steel tubing was originally used for the reaction chamber but yielded inconsistent results. Pure nickel appeared to be the ideal material for containing the water fluorination reaction. It is important to mention that each new nickel reaction chamber did require "conditioning" prior to correct operation. The conditioning process consisted of about 7 to 10 back-to-back water fluorination reactions.

To contain the water fluorination reaction, two ¼ inch *Swagelok* stainless steel bellows sealed valves with stainless steel tips were used (part SS-4H). These valves have a maximum temperature rating of 315°C and are not damaged by the repeated heating of the fluorination U trap. The stainless steel tip used in these valves resisted corrosion and surface damage by BrF_5 better than alternative valve tip materials. The stainless steel construction of the containment valves did not appear to have an adverse effect on the water fluorination reaction likely because the valves themselves were never heated to as high a temperature as the nickel reaction U trap. All other portions of the water fluorination line were constructed using internally electro-polished stainless tubing and *Swagelok* alloy 400/R-405 (Monel) tube fittings. However, alloy 400/R-405 is not required for the tube fittings and the use of 316 stainless steel would have been acceptable.

3.3.1.2 Water injection

Prior to the injection of water, the entire fluorination line was brought to a high vacuum ($< 1 * 10^{-4}$ mbar) and the entire assembly was heated using a heat gun to 100-150°C to volatilize and remove any trace moisture from the line. Heat tape was also used but the convenience and speed of using a heat gun proved superior. Once the line was no longer degassing, the primary water trap was isolated from the rest of the vacuum line by closing valve #1 (Figure 3.1) and submerged half-way into a dewar of liquid nitrogen (N_2). 1 micro liters (μL) of water standard was then injected through the septum. Injections were made using *Hamilton* model 7101 1μL syringes (part number 86211). These syringes are made with a trough-the-needle plunger, allowing the water sample to be transferred in its entirety. The efficiency of the water sample transfer was further improved by allowing the needle to remain in the injection port for approximately 30 seconds and heating the injection port and the needle using a heat gun during this time. The glass construction of the primary water trap made it possible to observe the freezing of the water when it was first injected and the subsequent ablation of the ice as the injection port and needle were heated. Once all the water ice was ablated from the needle and the surrounding glass the needle was withdrawn.

During the initial experimentation with water injection, it was observed that some of the water ice did not ablate entirely. In some cases, small crystals of water ice would break off and fall to the bottom of the water trap. By isolating the primary water trap form the rest of the vacuum line these potential aerosols were prevented from being mobilized and removed from the trap. It was also observed that portions of the septum, dislodged by the needle, occasionally fell into the primary water trap. These fragments in the primary water trap had no negative effect on the process but their presence explains the erratic

results of previous experiments in which the septum was placed behind a valve directly over the reaction chamber. In that configuration parts of the septum were falling into the reaction chamber and undergoing fluorination along with the water. For these reasons, it was found that the use of an isolated U trap for initial water injection yielded the most consistent results.

3.3.1.3 Water transport

Once the injection of the water sample was completed valve #2 (Figure 3.1) was closed to isolate the reaction U trap from the rest of the vacuum line. The reaction U trap was then submerged half-way into a dewar of liquid nitrogen. Valve #1 was then opened and the liquid nitrogen dewar, used to freeze the primary water trap, was removed. The primary water trap along with all the plumbing leading up to the reaction U trap was heated to mobilize all the water into vapor so it could condense in the reaction U trap. The primary water trap and the plumbing were heated for 2 minutes to reach a temperature of 100-150°C using a heat gun. It was determined, using an all glass replica of the fluorination line (never used with BrF_5), that under vacuum and at the temperature gradient conditions described above, a 2-minute transfer time was sufficient to move all the water into the reaction U trap without fractionation. After the transfer of water into the reaction U trap the level of liquid nitrogen was raised. This was done to insure complete freezing of any water that may have condensed at or above the previous level of N_2. Valve #2 was then opened allowing any non-condensable gases (melting point $>$-195.8°C) to be vacuumed away. Using a *Pheiffer* quadrupole mass spectrometer attached to the vacuum line it was determined that the non-

Figure 3.1 Schematic view of the water injection, fluorination and oxygen purification line.
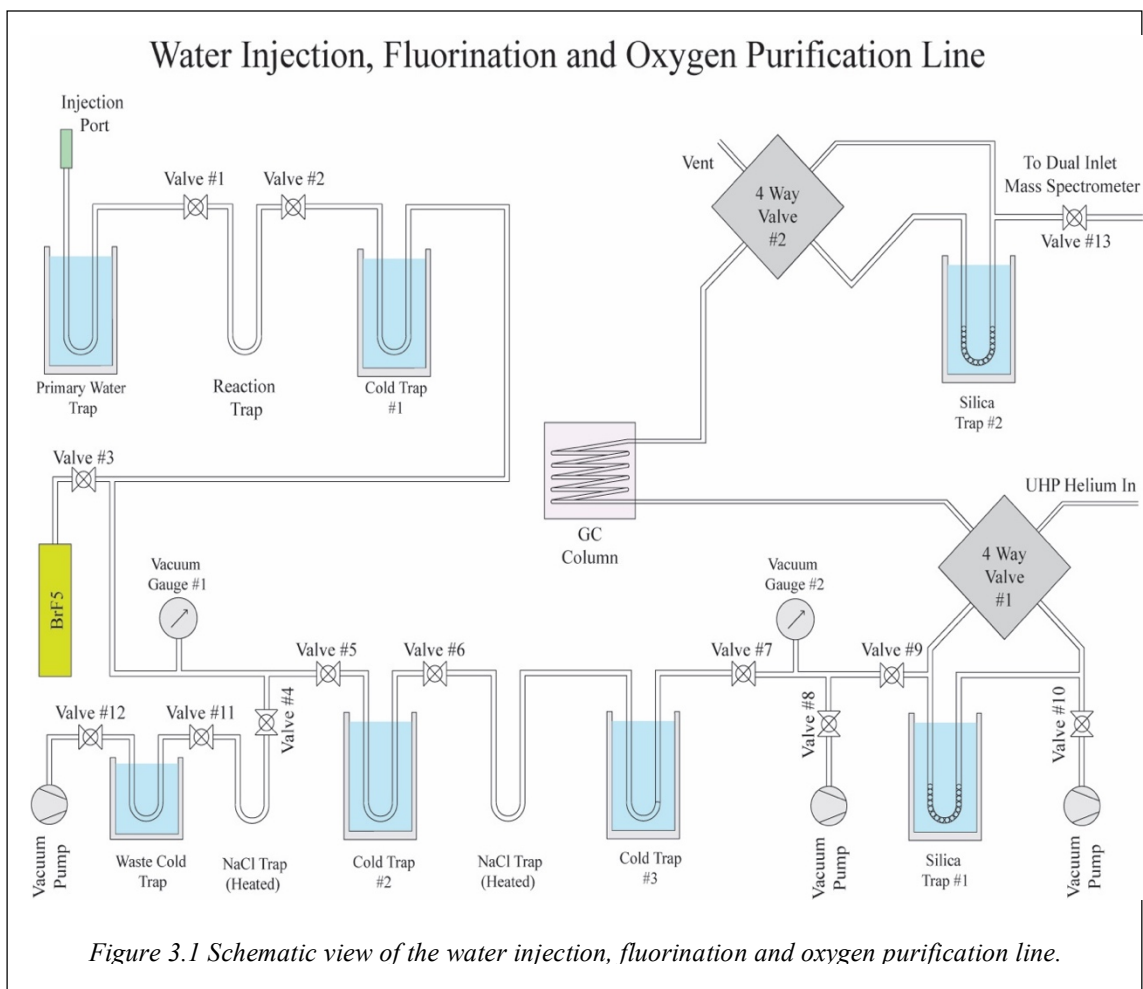
condensable gases observed in this step were nitrogen, oxygen and argon. Essentially, these non-condensable gases were air that leaked through the septum during the injection. By vacuuming away these non-condensable phases potential contribution to the sample from atmospheric O_2 was removed. The pure water sample, now held at a hard vacuum, was then isolated from the rest of the line by closing both valves #1 and #2 (Figure 3.1).

3.3.1.4 Water Fluorination

Refer to figure 3.1 for the location of all components described in this section. To insure complete fluorination of water by the reaction $BrF_5 + H_2O \rightarrow BrF_3 + 2HF + \frac{1}{2}O_2$ a

70

stoichiometric excess of BrF_5 was used. This excess was kept to approximately four time

the stoichiometric balance. BrF_5 reagent was expanded into a known volume by opening

valve #3 and allowed to reach a predetermined pressure needed to provide the appropriate

amount of the reagent. Valve #3 was then closed and the measured amount of BrF_5 was

condensed out of the volume into a U trap (Cold Trap #1) held at liquid nitrogen

temperature. Once the reagent was condensed, the entire volume was open to vacuum and

all the non-condensable gases were removed. It was found that prolonged storage of BrF_5

in a *Kel-F* (Polychlorotrifluoroethylene) container allowed trace amounts of air to leak in

and form a head over the reagent. By purifying the reagent before every fluorination, the

trace contamination was reliably removed. Once the reagent was purified, the metering

volume was again isolated from the vacuum and the liquid nitrogen was removed from the

cold trap and the trap was heated to free the reagent. The reagent was then transferred into

the nickel reaction U trap of the fluorination line, which was still submerged in liquid

nitrogen from the water transfer procedure. This transfer was done by opening valve #2.

Prior to admitting BrF_5 into the reaction U trap the level of liquid nitrogen was again raised

so that the reagent would condense above the previously frozen water. This averted the

possibility of the fluorination reaction starting before the reaction U trap was sealed. The

admittance of the reagent into the reaction chamber was done very quickly. Valve #2 was

opened for only about 5 seconds to allow most the reagent to be transferred. The remaining

reagent in the metering volume was removed as waste. With both valves #1 and #2 closed

securely the liquid nitrogen dewar was removed from the reaction U trap. The entire

reaction chamber assembly, including the valves, was continually heated for 4 minutes

using a heat gun. Care was taken to heat the reaction U trap uniformly to a temperature of

71

approximately 300°C. The valves were kept at a temperature of about 150°C to prevent any of the water sample or reagent from condensing there. It was determined from experimentation as well as reports from previous researchers (O'Neal and Epstein, 1966) that 4 minutes was the ideal time to facilitate the reaction. Allowing the reaction to proceed longer had no benefit. Once the reaction was completed the reactants were expanded into the previously mentioned metering volume. Remaining BrF_5 along with produced BrF_3 and HF were condensed into a cold trap (Cold Trap #1) held at liquid nitrogen temperature and later removed as waste. The produced O_2 gas was further purified.

3.3.2 Oxygen purification

A schematic diagram of the oxygen purification line is included in figure 3.1. Refer to figure 3.1 for the location of all components described in this section. The oxygen purification line follows the design described by Sharp et al, (1996). To remove remaining contaminants produced during fluorination, oxygen was expanded into another cold trap held at liquid N_2 temperature (into Cold Trap #2 by opening Valve #5) Then the remaining gas was passed through a heated NaCl trap to neutralize any molecular Fluorine gas (F_2) potentially produced during the fluorination reaction. Since fluorine gas has a condensation temperature lower than the temperature of liquid nitrogen it had to be captured by the reaction $2NaCl_{(solid)}+F_{2(gas)} \rightarrow 2NaF_{(solid)}+Cl_{2(gas)}$. The Chlorine gas produced by this reaction was collected in another cold trap (Cold Trap #3). The purified oxygen was then collected in molecular sieve trap held at liquid nitrogen temperature (Silica Trap #1). The collection time for oxygen in the molecular sieve trap varied depending on the size of the sample. For

a 1μL injection the collection time was generally between 5 and 10 minutes. Once most

the oxygen was collected in the molecular sieve trap the trap was isolated from the rest of

the purification line by closing valve #9. The 4-way valve (#1) was then switched to allow

UHP (Ultra-High Purity) helium to flow through the molecular sieve trap (Silica Trap #1)

and into the GC (Gas Chromatograph) column. It is important to mention that prior to use

the UHP helium had to be further purified by passing through a molecular sieve trap held

at liquid nitrogen temperature (Not shown in Figure 3.1). 4-Way Valve #2 was also

switched to allow the UHP helium stream coming from the GC column to flow through the

second molecular sieve trap (Silica Trap #2). The second molecular sieve trap (Silica Trap

#2) was then submerged into liquid nitrogen so that any O_2 transported in the helium stream

would become trapped. With the helium transport portion of the line correctly configured

the liquid nitrogen cooling the first molecular sieve trap (Silica Trap #1) was removed and

the trap was heated using a heat gun. The liberated O_2 was transported by the helium stream

trough the 5 Å mol sieve GC column. The purpose of the GC column was to separate the

O_2 from any potential NF_3 contamination. Removal on NF_3 form the sample was essential

because during ionization in the mass spectrometer NF_3 can break down into NF and create

interference at atomic mass 33. Since accurate measurements of mass 33 were essential to

determining the $\delta^{17}O$ of the sample any NF_3 contamination had to be removed. To monitor

the movement of gas through the GC column a TCD (Thermal Conductivity Detector) was

installed inline following the GC column. By monitoring the output of the TCD the arrival

and passage of the O_2 peak was observed. Once all the O_2 gas had cleared the GC column

and passed through the second molecular sieve trap (Silica Trap #2), the second 4-way

valve (#2) was switched to isolate the collected O_2 in the molecular sieve trap and to route

73

the helium stream along with any NF_3 to the vent port. The second molecular sieve trap (Silica Trap #2) was held at liquid nitrogen temperature while the helium was pumped away through the vacuum system of the mass spectrometer (through Valve #13). Once the helium was pumped away the liquid nitrogen was removed from the second molecular sieve trap (Silica Trap #2) and the trap was heated using a heat gun. The oxygen was then admitted into the sample bellows of the dual inlet isotope ratio mass spectrometer.

3.3.3 Isotope ratio mass spectrometer configuration

All the oxygen isotope ratio measurements were made at the Center for Stable Isotopes, University of New Mexico. Much of the preliminary measurements were done using a *ThermoFinnigan Delta Plus XL* IRMS (Isotope Ratio Mass Spectrometer). *ThermoFinnigan MAT 253* IRMS was used to make the high precision isotopic measurements for the VSMOW-SLAP calibration reported herein. No significant variability was observed between the two instruments. Dual inlet configuration was used on both machines to allow for multiple sample/reference comparisons. Fluorination of 1μL of water provided large O_2 samples making it possible to balance the sample and standard at a high pressure allowing for high signal-to-noise ratio. For each of the high precession measurements care was taken to balance both the pressure and the volume of the sample and the reference. This approach reduced the signal amplitude mismatch during sequential sample/reference comparisons and made it possible to run continually for >100 comparison cycles with no analytical drift.

3.3.4 Analytical precision considerations

To meet the accuracy requirements of this study the $\Delta^{17}O$ isotopic ratio measurements had to be made with a standard error of less than 0.005‰ ($\sigma 1$). This was accomplished by increasing the number of sample/reference comparisons for each analysis and by increasing the integration time of each measurement. Using an integration time of 2 seconds the desired standard error was reached only after 450 sample/reference comparisons (figure 3.2). By increasing the integration time to 20 seconds the number of sample/reference comparisons needed to reach the target standard error was reduced to 25 cycles (figure 3.2). $\Delta^{17}O$ values of VSMOW and SLAP reported herein where made with these analytical considerations and exceed the minimum standard error requirement.
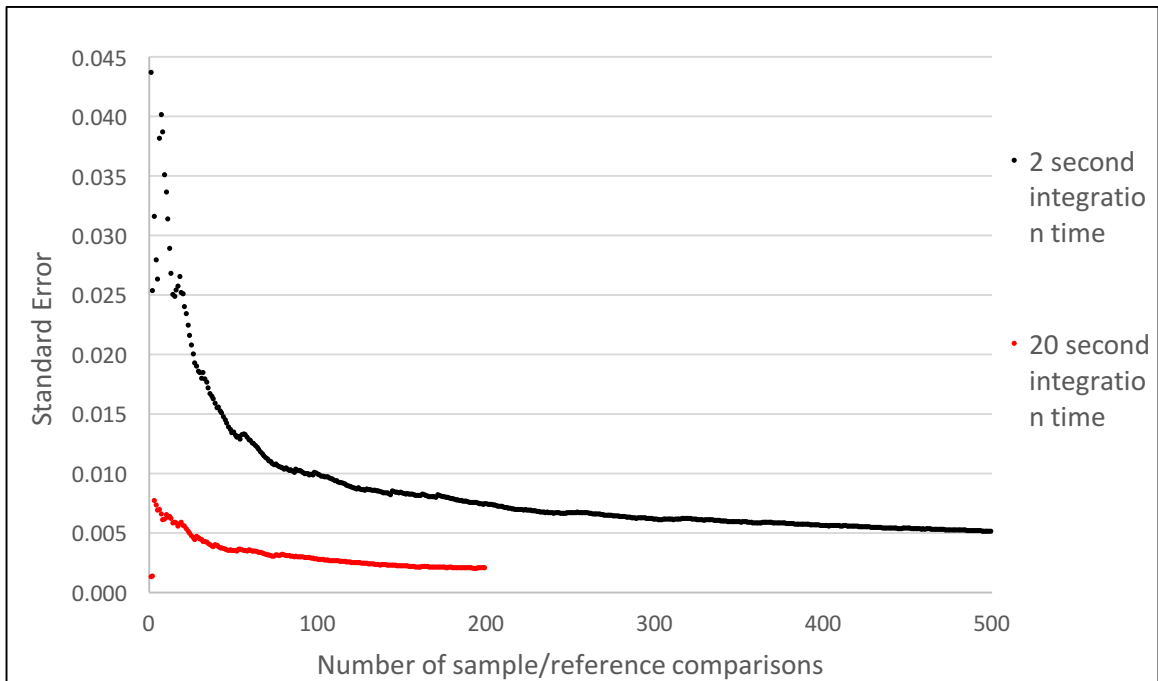

Figure 3.2 Effect of integration time on the measurement standard error.

The results of each multiple-cycle analytical run were also analyzed for instrumental drift. This was done by calculating and plotting the running average of the $\Delta^{17}O$ values of each sample/reference comparison. The slope of the running average was used to calculate the overall instrumental drift for each analysis. Due to careful setup considerations (signal amplitude and gas volume matching) instrument drift was never a major issue. All the analysis used to determine $\Delta^{17}O$ values of VSMOW and SLAP reported herein had running average slopes of less than $4*10^{-5}$. This was equivalent to a maximum instrument drift of 0.004‰ during a 100 sample/reference cycle run. For most of the analytical runs the drift was significantly less (about 0.0008‰ per 100 cycles).

3.4 Results

The raw measured $\delta^{17}O$ and $\delta^{18}O$ values, linearized $\delta'^{17}O$ and $\delta'^{18}O$ values and the calculated $\Delta'^{17}O$ values of each VSMOW and SLAP analysis are presented in Table 3.1. $\Delta'^{17}O$ values shown are calculated by equation $\Delta'^{17}O=\delta'^{17}O-\theta*\delta'^{18}O$ using a terrestrial fractionation line slope (θ) of 0.528. Measurements of VSMOW have a standard deviation of 0.1‰ ($\sigma1$) for $\delta'^{17}O$ and of 0.2‰ ($\sigma1$) for $\delta'^{18}O$. The standard deviation of $\Delta'^{17}O$ for measurements of VSMOW is only 0.01‰ ($\sigma1$). Minute mass-dependent fractionation effects during O_2 extraction and preparation result in measurement deviations of $\delta'^{17}O$ and $\delta'^{18}O$. However, since this variability is caused by mass-dependent fractionation it has no effect on the $\Delta'^{17}O$ values. Thus, the standard deviation of $\Delta'^{17}O$ is smaller than that of $\delta'^{17}O$ and $\delta'^{18}O$. Similarly, $\Delta'^{17}O$ measurements of SLAP have a standard deviation of only 0.01‰ ($\sigma1$). The standard deviation of $\delta'^{17}O$ and $\delta'^{18}O$ is higher for SLAP than it is

Table 3.1 VSMOW and SLAP oxygen isotope analysis data.

VSMOW					
	$\delta^{17}O$	$\delta^{18}O$	$\delta'^{17}O$	$\delta'^{18}O$	$\Delta'^{17}O$
Run #1	-0.163	-0.267	-0.163	-0.267	-0.022
Run #2	-0.012	0.031	-0.012	0.031	-0.028
Run #3	0.002	0.043	0.002	0.043	-0.021
Run #4	-0.274	-0.457	-0.274	-0.457	-0.033
Run #5	-0.033	-0.05	-0.033	-0.050	-0.007
Run #6	-0.028	-0.036	-0.028	-0.036	-0.009
STVDEV	0.11	0.20	0.11	0.20	0.01
Average	-0.085	-0.123	-0.085	-0.123	-0.020

SLAP					
	$\delta^{17}O$	$\delta^{18}O$	$\delta'^{17}O$	$\delta'^{18}O$	$\Delta'^{17}O$
Run #1	-29.537	-55.134	-29.982	-56.712	-0.038
Run #2	-29.262	-54.634	-29.699	-56.183	-0.034
Run #3	-29.807	-55.643	-30.260	-57.251	-0.032
Run #4	-29.964	-55.950	-30.422	-57.576	-0.022
Run #5	-29.924	-55.877	-30.381	-57.499	-0.021
STVDEV	0.30	0.56	0.30	0.59	0.01
Average	-29.699	-55.448	-30.149	-57.044	-0.029

for VSMOW. For SLAP the standard deviation of $\delta'^{17}O$ and $\delta'^{18}O$ is 0.3‰ ($\sigma 1$) and 0.6‰ ($\sigma 1$) respectively. $\delta'^{17}O$ and $\delta'^{18}O$ standard deviation of SLAP is greater than that of VSMOW because SLAP is an extreme negative outlier ($\delta^{18}O = -55.5$) and memory effects during analysis become more prominent. SLAP has a measured $\delta^{17}O$ value of -29.7‰ and a $\delta^{18}O$ value of -55.5‰. Since the measured $\delta^{18}O$ value of SLAP is exactly -55.5‰ no stretch correction is needed for the VSMOW-SLAP scale. Note that the non-linearized value of SLAP is used. Originally the VSMOW-SLAP scale was defined using non-linearized values and here we adhere to that convention. However, linearized $\delta'^{17}O$ and $\delta'^{18}O$ values are used in calculating $\Delta'^{17}O$ of SLAP.

3.5 Discussion

The average measured $\delta'^{17}O$, $\delta'^{18}O$ and $\Delta'^{17}O$ values of VSMOW and SLAP provide a correction reference for all other samples. Since the average measured $\delta'^{17}O$ and $\delta'^{18}O$ values of VSMOW and SLAP are within the standard deviation from the established values no stretch/squeeze correction is required. The primary significance of the VSMOV-SLAP correction is in its application to $\Delta'^{17}O$ measurements. Using the measured $\Delta'^{17}O$ values of VSMOW and SLAP (-0.02‰ and -0.03‰ respectively) a correction factor was established for all other $\Delta'^{17}O$ measurements. The correction factor is the offset between the line plotted by $\Delta'^{17}O_{VSMOW}$ and $\Delta'^{17}O_{SLAP}$ from the terrestrial fractionation line. Mathematically the correction can be expressed as $\Delta'^{17}O_{(corrected)} = \Delta'^{17}O + (0.0002 * \delta'^{18}O - 0.02)$. For most samples ($\delta^{18}O = 0‰ \pm 10‰$) the application of this correction has the effect of adding approximately 0.02‰ to the measured $\Delta'^{17}O$ value. As we attempt to achieve ever higher $\Delta'^{17}O$ resolution, the significance of such a correction becomes more and more crucial. VSMOW-SLAP calibration is ideal for determining such necessary lab-specific corrections and for inter-laboratory standardization of triple oxygen isotopic measurements.

4. Distribution of Hydrous Minerals in Martian Shergottite Zagami

4.1 Abstract

Based on anomalously high concentration of mass 17 oxygen isotope, water extracted from Martian meteorites is thought to be extraterrestrial. Martian meteorite Zagami is the only Martian meteorite that has been subjected to multiple water oxygen isotope analysis. Three separate oxygen isotope studies of the water extracted from this meteorite have produced substantially different results. Thin sections of the meteorite were studied using an ion microprobe to determine if the observed variability is caused by heterogeneous distribution of hydrous minerals within the sample. Hydrous minerals within Zagami were identified, mapped and their distribution was statistically analyzed. Analysis show that hydrous minerals (primarily apatite) are in fact homogeneously distributed within Zagami. According to the mineral distribution data, all the >2 gram samples used for water oxygen isotope analysis were likely representative of bulk fine grain normal Zagami lithology.

4.2 Introduction

All Martian meteorites have been found to contain water (mainly OH) in varying amounts. The oxygen isotope compositions of these waters are distinctly extraterrestrial, with elevated ^{17}O concentration relative to Earth (Karlsson et al., 1992; Agee et al., 2013; Ziegler et al., 2013). Based on this unique isotopic composition, the waters are believed to be at least partially Martian in origin. The study of these waters can thus provide a unique glimpse into the evolution of water on the planet Mars. At present, only two studies

Karlsson et al., (1992) and Agee et al., (2013) have looked at the oxygen isotope composition of water in Martian meteorites. These researchers have shown that the $\Delta^{17}O$ values of water extracted from Martian meteorites range from -0.2 ‰ up to 0.9‰. However, bulk rock oxygen isotope analysis of Martian SNC (Shergottites, Naklites and Chassignites) group meteorites show a tight grouping of $\Delta^{17}O$ values at 0.3±0.1‰ (Clayton and Mayeda, 1983; Franchi et al., 1999). This behavior shows that the waters extracted from the samples are not in isotopic equilibrium (in terms of oxygen) with the bulk rock. It has been proposed that the oxygen isotope disequilibrium is caused by the interaction of the sample with isotopically different and distinct oxygen reservoirs on Mars such as the mantle, crust, hydrosphere and possibly the atmosphere (Karlsson et al. 1992; Agee et al., 2013; Ziegler et al., 2013). The reported $\Delta^{17}O$ values are calculated using the equation $\Delta^{17}O'=\delta^{17}O'-\theta*\delta^{18}O'$ where θ is the slope of the terrestrial fractionation line. A kinetic fractionation value of 0.52 is used for θ in the calculation because the water is extracted by heating which is a kinetic process.

Because of the limited availability of Martian material and the low water content of most samples (about 300ppm) no comprehensive work has yet been done on evaluating the reproducibility of the Martian water $\Delta^{17}O$ measurements. In fact, the only Martian meteorite that has been analyzed more than once is Zagami. So far, three different masses of Zagami have been analyzed for water oxygen isotope composition. Karlsson et al., (1992) analyzed two samples of Zagami, one 2.93g sample and one 3.43g sample. The third 3.5g sample was analyzed as part of this study on the oxygen isotope composition of water in Martian meteorites. Interestingly, one of the samples measured by Karlsson et al.,
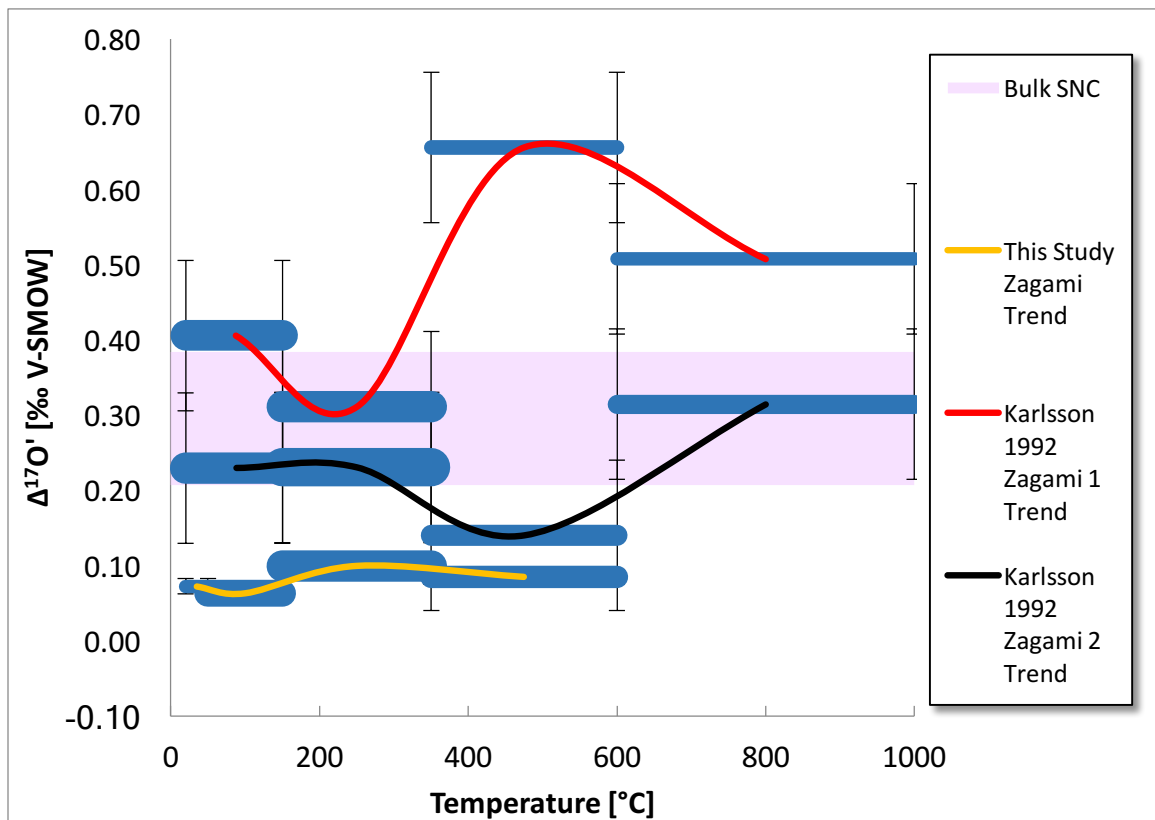
Figure 1. Zagami water data. Horizontal bars indicate the temperature range for each extraction step and the thickness of the horizontal bars indicates the relative amount of water extracted for that interval. The Bulk SNC area represents the range of $\Delta^{17}O$ values measured from the bulk silicate portion of SNC group meteorites.

(1992) produced substantially different results (Figure 4.1). Note that the water was extracted using step-wise heating to differentiate between absorbed water and low/high temperature mineral phases. It is not likely that the analytical method is the cause of the problem. When the method is applied to terrestrial standards the reproducibility of $\Delta^{17}O$ is within 0.05‰ (σ1). It is possible that the observed difference in the oxygen isotopic composition of waters extracted from Zagami is due to heterogeneity in the distribution of water within the sample. The possible existence of heterogeneity in the distribution of hydrous phases within Zagami is quite intriguing and is the focus of this work.

81

The main mass of Zagami consists of several distinct lithologies. Most of the sample is dominated by the fine to coarse-grained (0.24-0.36mm) basaltic lithology referred to as normal Zagami (Stolper and McSween 1979). Zagami also includes a dark-mottled-lithology which has been found to contain higher concentration of shock melt (Marti et al. 1995) and a Fe-rich lithology which has been described as residual melt by McCoy et al. 1993. This study will focus on the fine-grained normal Zagami lithology because it is by far the most abundant.

The mineralogy of the fine-grained normal Zagami lithology consists primarily of pyroxene and plagioclase that has been shocked to amorphous maskelynite (Easton and Elliott, 1977). The lithology also contains amphibole (Treiman, 1985a), phosphates (McCoy et al. 1992), sulfides (McCoy et al. 1999), oxides (Stolper and McSween, 1979) and glass veins (McCoy et al. 1992). Amphibole and phosphates are the most important mineral phases for this discussion since they are the only hydrous phases present in the fine-grained normal Zagami lithology. Amphibole is reported to be present in Zagami melt inclusions in the form of kaersutite $((Na)(Ca_2)(Mg_4Ti)(Si_6Al_2)(O_{22})(OH,F)_2)$ and actinolite $((Ca_2)(Fe_5)(Si_8)(O_{22})(OH,F)_2)$ (Treiman, 1985a). Phosphates make up between 0.5 and 1.3 wt% of Zagami and occur as merrillite $(Ca_9NaMg(PO_4)_7)$ and apatite $(Ca_{10}(PO_4)_6(OH,F,Cl)_2)$ (Wang et al. 1999; Shearer et al. 2015). The phosphate assemblage in Zagami is dominated by merrillite. Apatite, which is the only phase relevant to OH budget, is relatively rare (Shearer et al. 2015). Karlsson et al., (1992) reported the bulk H_2O content of Zagami to be 430 ppm. This value agrees with H_2O concentrations reported for other Martian shergottites. Based on available mineralogical data most of the 430 ppm H_2O budget of Zagami is likely stored in the minerals kaersutite, actinolite and apatite. Since

these minerals have very distinct compositions it was possible to identify them and to map their spatial distribution using an electron microprobe. This data was then used to conduct statistical analysis of the distribution of the different hydrous minerals within Zagami and to determine if the observed heterogeneity in the oxygen isotope composition of the water extracted from different specimens of Zagami can be explained by the distribution of the hydrous phases within bulk Zagami.

4.3 Methods

Six thin sections of Zagami from the University of New Mexico Institute of Meteoritics collection were initially considered for this work. The thin sections were first studied using a petrographic microscope to determine if any significant differences in mineralogy or grain size existed between them. It was determined that no significant differences existed between the six thin sections. Based on mineralogy and grain size it was also determined that all six thin sections were representative of the fine-grained normal Zagami lithology. The physical condition of the thin sections was considered and two thin sections (998 and 1094), with the least surface damage, were finally chosen for microprobe analysis. The carbon coat on the Zagami 998 thin section was beginning to degrade so the thin section was re-polished to a 0.05-micron finish and carbon coated. Zagami thin section 1094 was in good condition and did not require any additional prep-work.

Microprobe analytical work on the thin sections was done using the *JOEL 8200 electron probe* at the Earth and Planetary Science department of the University of New Mexico. Full thin section qualitative maps of elements Ca, Cl, F, P and Ti were made for

both Zagami thin sections (998 and 1094). These elements were chosen to identify the minerals of interest for this study (kaersutite, actinolite, merrillite and apatite). Thin section 889 was mapped using 10μm steps with a dwell time of 30mSec per step. The final dimensions of the large-scale map of thin section 998 ended up being 8998x17996μm. Thin section 1094 was also mapped using 10μm steps with a dwell time of 30mSec per step and the final dimension of the map was 5266x10786μm. *JOEL* software was used to set the mapping conditions for the initial qualitative mapping of the thin sections. The qualitative
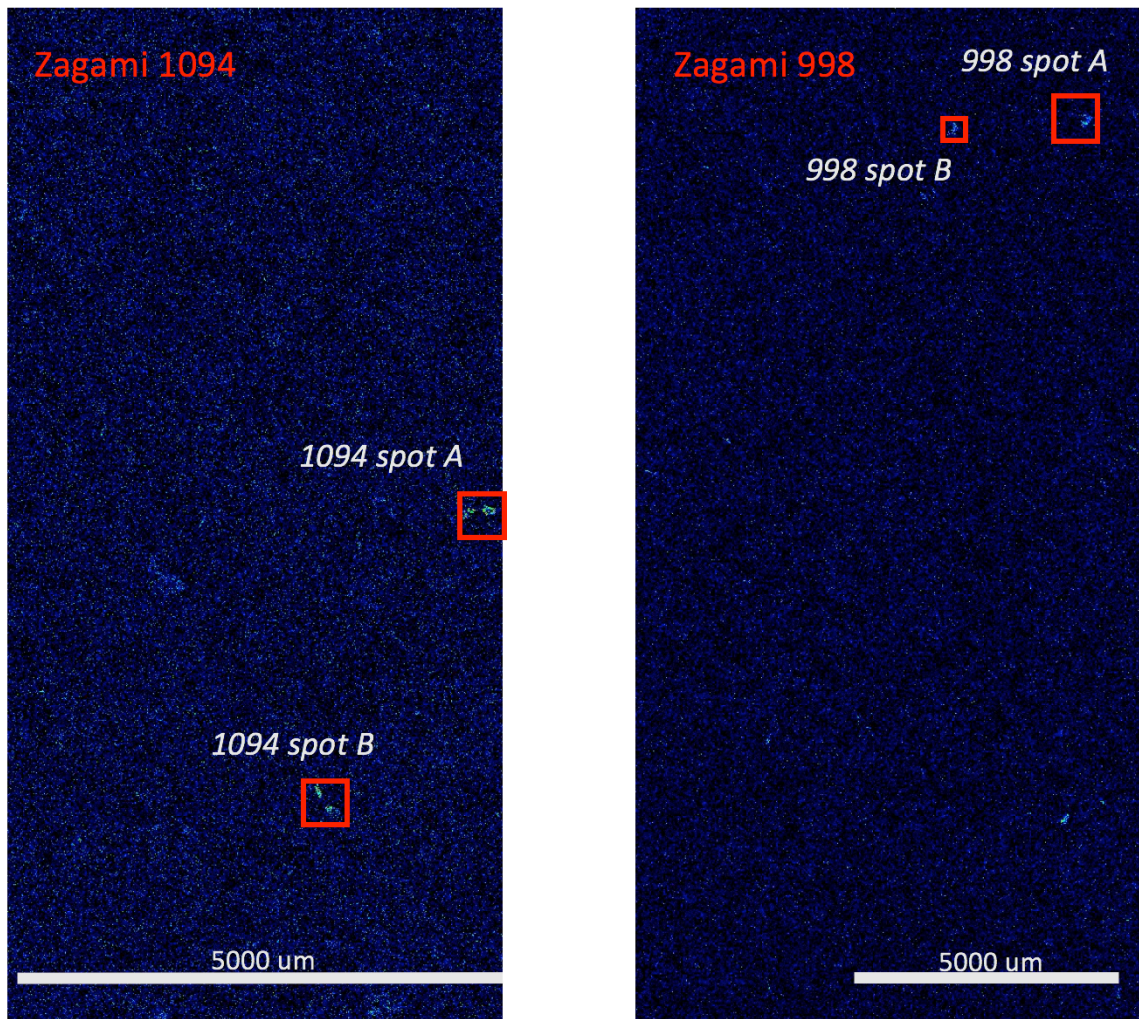

Figure 4.2. Qualitative F maps of Zagami thin sections 1094 and 998 showing the F-rich apatite areas selected for single-point analysis and qualitative mapping.

maps were then used to determine the relative distribution of the hydrous minerals in the thin sections. Based on the qualitative data, four (two per thin section) areas of interest (Figure 4.2) were identified based on elevated concentration of Fluorine and Chlorine (characteristic of kaersutite, actinolite and apatite). The selected areas on Zagami thin section 1094 were designated 1094 spot A and 1094 spot B. Selected areas on Zagami thin section 998 were designated 998 spot A and 998 spot B. All four of the selected areas were roughly 300x300 microns. The selected areas were then imaged using BSE (Back Scatter Electrons). The BSE images were linked to the microprobe stage coordinates through *Probe for EPMA ImageSnap* software to allow for more efficient sample navigation and analytical automation. Once the BSE images were synchronized for stage navigation *Probe for EPMA* software was used to create and automate multiple qualitative single-point analysis of various mineral grains (Figures 4.3a-4.3d). This was done to accurately determine the mineral chemistry of the phases in question. Measured X-ray spectra where compared against known standards by the *Probe for EPMA* software to insure the accuracy of the measurements. The following standards were used: 204 Albite Taylor std. 4, 210 Rutile Taylor std. 10, 214 Apatite-F (wiberforce) Taylor std. 14, 215 Diopside Taylor std. 2, 406 Sodalite std. 2, and 412 Almandine Oxygen std. 2. The average of 29 quantitative single-spot analyses of multiple apatite grains in Zagami was used to determine the actual chemical makeup of the grains. The measured values were normalized to the atomic concentration of oxygen in apatite to calculate normalized abundance for the constituent elements. The calculated normalized abundance was then used to determine the formula of Zagami apatite. This data, along with measured concentrations of fluorine and chlorine,
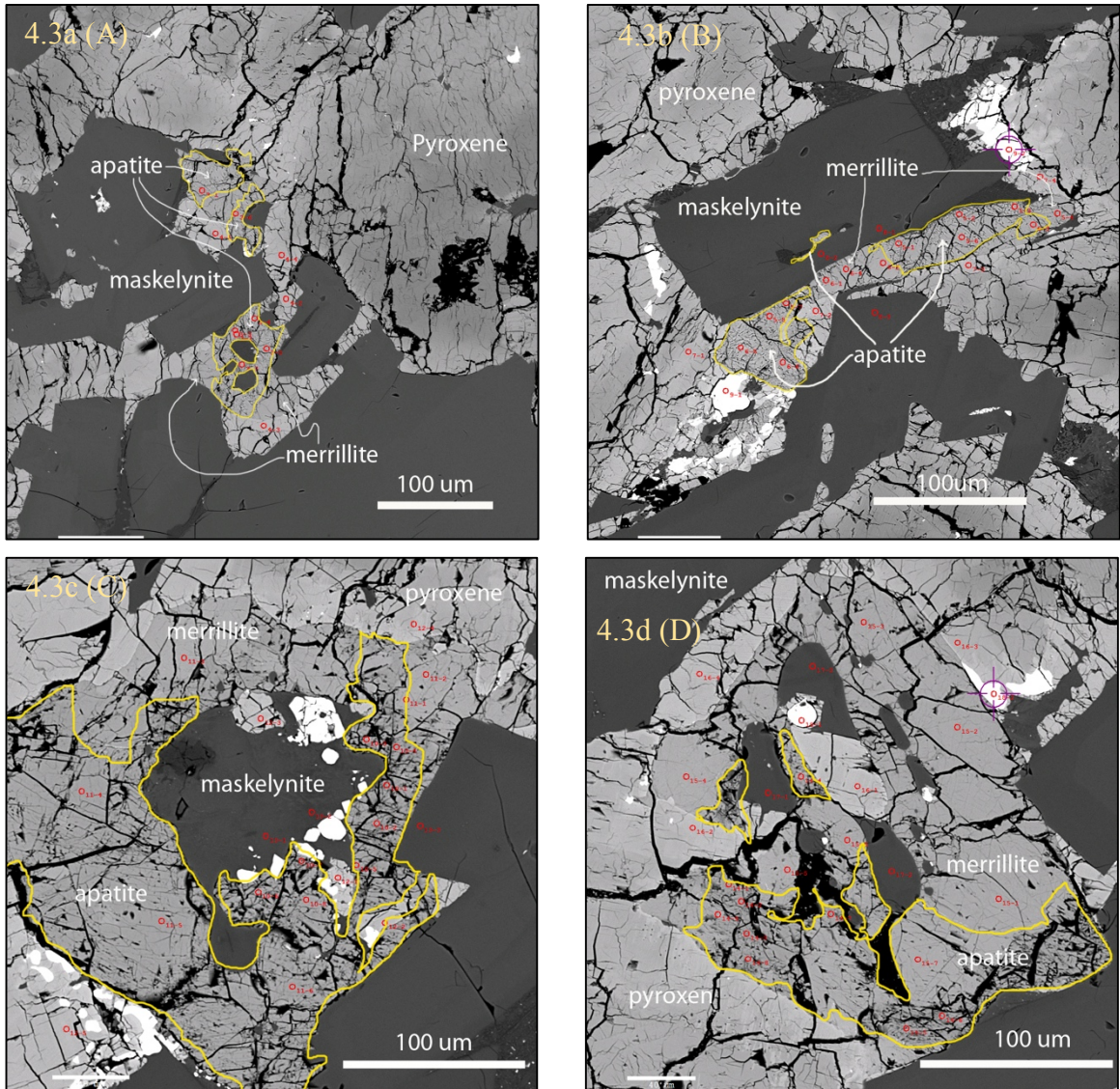
Figure 4.3a-4.3d. BSE images of 1094 spot A, B, C and D showing the distribution of mineral grains and the location of quantitative single point analyses. Apatite grains are outlined in yellow.

was also used to determine the ratio of HO to F to Cl in the apatite ($Ca_{10}(PO_4)_6(HO,F,Cl)_2$).

Once the minerals in the assemblages were identified, the four areas of interest were quantitatively mapped at higher magnification (Figures 4.4a-4.4d). These maps identified the distribution of Ca, Cl, F, P and Mg in the areas of interest. Quantitative mapping was done using *JOEL* software. The same set of standards was used for quantitative mapping
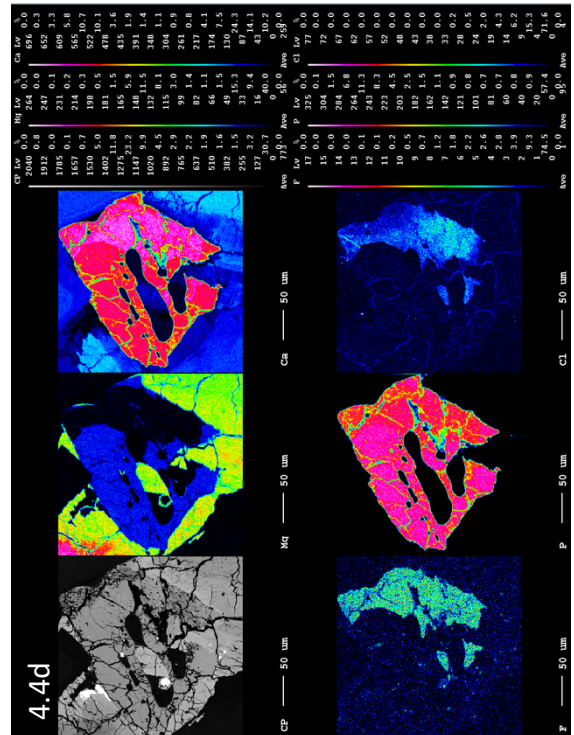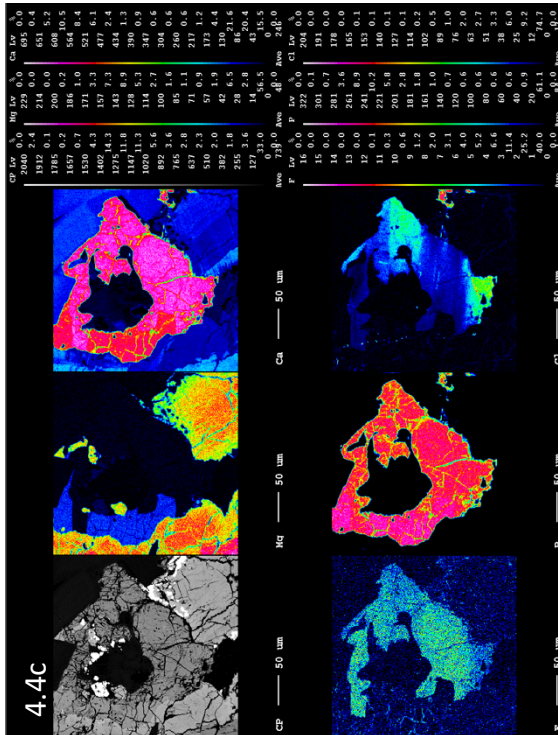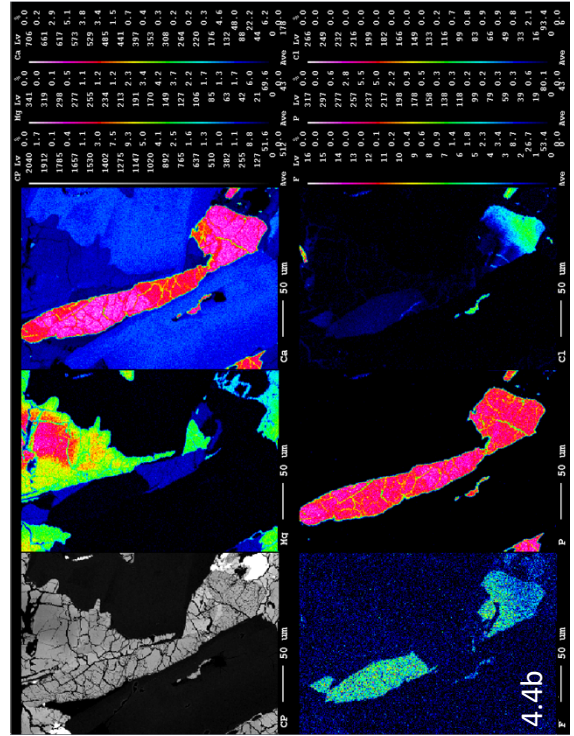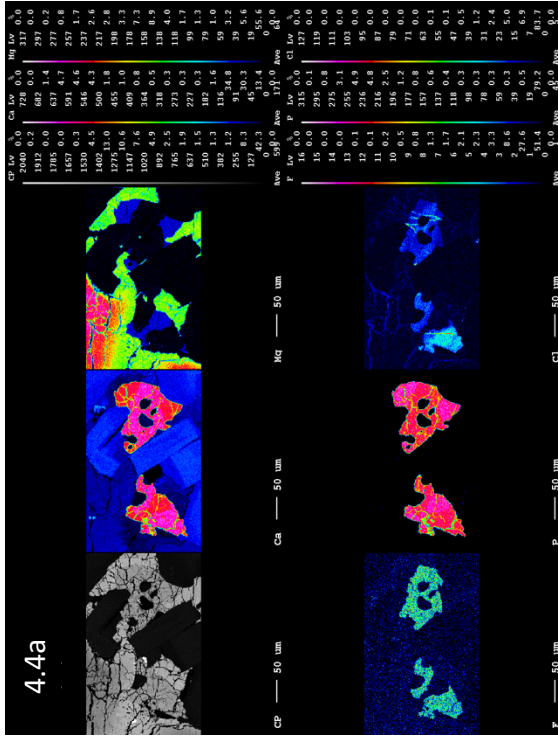
Figure 4.4a-4.4d. Qualitative maps of 1094 spots A, B, C and D showing a BSE image of the area and the distribution of Ca, Mg, F, P and Cl.

as for the single point analysis except for 210 Rutile Taylor std. 10. 210 Rutile Taylor std. 10 was excluded from the quantitative analytical setup because Ti was not measured. 215 Diopside Taylor std. 2 was used as the standard for Mg analysis during quantitative mapping.

Graphical data was exported using both the *JOEL* software and *ImageJ* software. The numerical data from the single point analyses was exported to and analyzed using *Microsoft Excel.* To determine the overall distribution of hydrous grains within Zagami the qualitative maps were statistically analyzed using *ImageJ* software. The same statistical approach was also used to study the quantitative maps but with the purpose of understanding F and Cl zoning in the apatite grains. The numerical data was processed and normalized using *Microsoft Excel.*

4.4 Results

Statistical analysis of mineral distribution in the qualitative maps of Zagami thin sections is presented in table 4.1. Majority of the phosphate assemblage in both thin sections is made up of anhydrous mineral merrillite. 0.17% of the area of the thin sections is occupied by apatite (possibly containing OH). Of the apatite present, 0.11A% is Cl-rich apatite while 0.06A% is F-rich apatite. No amphibole minerals were observed on the large-scale qualitative maps of Zagami thin sections 998 and 1094. The mineral grains in the samples showed uniform distribution. Typical fine-grain normal Zagami foliated texture

Table 2.4 Mineral composition of Zagami thin sections 998 and 1094 reported in area percent (A%)				
Thin Section	**Pyroxene**	**Maskelynite**	**Iron-titanium oxides**	**Phosphate minerals**
998	78.23	19	1.27	1.5
1094	78.28	19.1	1.12	1.5

produced by preferential orientation of pyroxene and maskelynite grains, originally reported by Stolper and McSween 1979 and McCoy et al. 1992, was also observed in the samples.

Based on data collected from single-point quantitative analysis a ratio of apatite OH site occupancy in the F-rich portion was calculated to be $OH_{0.122}$, $F_{1.679}$, $Cl_{0.199}$. This indicates that OH sites in the F-rich apatite are occupied by 83.9% fluorine 6.1% OH and 10% chlorine. By combining the calculated percentage of OH in the F-rich apatite grains and the distribution of F-rich apatite in Zagami, it was determined that F-rich apatite-bound OH makes up 0.013 wt% of Zagami (130 ppm). By applying the same OH occupancy value to the Cl-rich apatite portion in Zagami it was calculated that the Cl-rich portion could store 0.0238 wt% (238 ppm) OH. In total the apatite OH storage capacity in Zagami was determined to be 0.0369 wt% (369 ppm).

Quantitative maps of F-rich apatite grains within 1094 spot A, 1094 spot B, 998 spot A and 998 spot B showed that F is not distributed evenly with in the grains (Figures 4a-4d). It appeared that in portions of the grains significant amounts of Cl are present. The distribution of F and Cl did not show any systematic zoning behavior. In 1094 spot A (Figure 4a) Cl was observed to be concentrated in linear features that appeared to be fractures. However, the features did not follow any actual fractures observed in the BSE image of 1094 spot A. In 998 spot A (Figure 4c) the apatite grain showed alternating bands between the Cl-rich and F-rich zones arranged linearly across the grain.

4.5 Discussion

Zagami thin sections analyzed in this study are conclusively typical of the fine-grain normal Zagami lithology. The textural and mineralogical measurements are in good agreement with Zagami literature data (Easton and Elliot, 1977; McCoy et al. 1992; McCoy et al. 1999; Stolper and McSween, 1979). The amphibole minerals reported by Treiman, 1985a were likely not observed in this study due to their small size. Since the focus of this study is the understanding of the broad distribution of large mineral grains in the sample, it is not surprising that the smaller grains were not identified. This however, is not a problem because, the reported amphibole grain account for a small portion of Zagami and are not likely to have much impact on the total OH budget. The calculated 369 ppm OH storage capacity of apatite in Zagami agrees with the 430 ppm value reported by Karlsson et al., (1992) value of 430 ppm which includes the absorbed water and crystal defect OH groups in addition to mineral bonded OH. For this reason, it is appropriate that their reported value is higher than the storage capacity of apatite alone.

The fluorine/chlorine zoning observed in the apatite grains within Zagami is most likely due to fractional crystallization. A study by Mccubbin et al. (2015) determined that for a basaltic melt the mineral-melt partition coefficients (D values) for OH site elements in apatite are $D_F^{Ap.-melt} = 4.4\text{-}19$, $D_{Cl}^{Ap.-melt} = 1.1\text{-}5$, $D_{OH}^{Ap.-melt} = 0.07\text{-}0.24$. Since F has a much higher partition coefficient than Cl and OH it is preferentially incorporated into the apatite grain as the melt begins to crystalize. Once F is exhausted Cl becomes the dominant element in the OH site of apatite grains. The apatite grains in Zagami are interstitial and element partitioning occurs on a small scale within isolated pockets of grain boundary melt. This produces the irregular zoning characteristics observed in Zagami apatite. Essentially, the distribution of F and Cl follows the cooling history of each individual apatite grain. The

partitioning of OH into the apatite remains relatively constant up to the point where Cl occupancy in the apatite OH site reaches approximately 80% at which point the OH partitioning drastically decreases until Cl is exhausted (McCubbin et al., 2016). Once Cl is exhausted OH dominates the structure of the apatite until OH is no longer available and merrillite ($Ca_9NaMg(PO_4)_7$) becomes the dominant phosphate mineral (McCubbin et al., 2016). This transition to merrillite is exactly what is observed in Zagami and indicates complete removal of the volatile components OH, F and Cl from the melt. Since we see a complete gradient from F-rich to Cl-rich apatite and a transition to merrillite, the removal of volatiles from the melt is most likely due to their incorporation into the apatite. If most the OH available in the melt is incorporated into the apatite grains of Zagami we should expect a very uniform Martian mantle-like oxygen isotope composition from the OH extracted from the sample.

The physical distribution of apatite grains within Zagami is very uniform, showing no preferential grouping. Based on the statistical analysis of apatite grain distribution, Zagami shows remarkable textural homogenate even on μm size scale. Therefore, it would be unlikely that a 3g sample (used for H_2O analysis) would contain any significant heterogeneity in hydrous mineral distribution. However, due to the large sample size, it is possible that an impact melt inclusion could have been overlooked during sample preparation. If such an inclusion was present it could contain isotopically different water. It is possible that one of the samples of Zagami measured by Karlsson et al., (1992) contained Martian crustal/near-surface water component trapped in the shock melt during the sample ejection event. The proposed elevated [17]O concentration of Martian near surface water (Karlsson et al., 1992; Romanek et al., 1994; Clayton and Mayeda, 1996; Farquhar

et al., 1998; Franchi et al., 1999; Farquhar and Thiemens, 2000; Agee et al., 2013) could explain the elevated $\Delta^{17}O$ of the waters extracted from the outlier Zagami sample.

References

Agee, C.B., Wilson, N.V., McCubbin, F.M., Ziegler, K., Polyak, V.J., Sharp, Z.D., Asmerom, Y., Nunn, M.H., Shaheen, R., Thiemens, M.H., Steele, A., Fogel, M.L., Bowden, R., Glamoclija, M., Zhang, Z., Elardo, S.M. (2013). Unique meteorite from the Early Amazonian epoch on Mars: Water-rich basaltic breccia NWA 7034. *Science* **339,** 780-785.

Anderson, D.E. and Hord, C.W. (1971). Mariner 6 and 7 ultraviolet spectrometer experiment: Analysis of hydrogen Lyman-alpha data. *Geophys. Res.,* **76**, 6666-6673. Andrews-Hanna J. C., Phillips R. J. (2007). Hydrological modeling of outflow channels and chaos regions of Mars *J. Geophys. Res* **112** E08001

Andrews-Hanna J. C., Phillips R. J. (2007). Hydrological modeling of outflow channels and chaos regions of Mars *J. Geophys. Res* **112** E08001

Ashworth, J.R., Hutchison, R., 1975. Water in non-carbonaceous stony meteorites. *Nature* **256**, 714–715.

Ball, S.M., Hancock, G., Martin, S.E., Pinot de Moira, J.C. (1997). A direct measurement of the O(1D) quantum yields from the photodissociation of ozone between 300 and 328 nm. *Chem. Phys. Lett.,* **264**, 531-538.

Barth, C.A. The Atmosphere of Mars. *Annual Review of Earth and Planetary Science,* **2**, 333-367.

Barkan E. and Luz B. (2005) High precision measurements of $^{17}O/^{16}O$ and $^{18}O/^{16}O$ ratios in H_2O. *Rapid Commun. Mass Spectrom.* **19**, 3737-3724.

Bibring, J.-P., Langevin, Y., Mustard, J.F., Arvidson, R., Gendrin, A., Gondet, B., Mangold, N., Pinet, P., Forget, F. and the OMEGA team (2006). Global mineralogical and aqueous Mars history derived from OMEGA/Mars Express data. *Science* **312**, 400-404.

Bishop, J. L., Pieters, C. M., Edwards, J. O. (1994), Infrared spectroscopic analyses on the Nature of water in montmorillonite, *Clays Clay Miner* **42**, 702–716.

Bjoraker, G.L., Mumma, M J., Larson, H. P. (1989). Isotopic abundance ratios for hydrogen and oxygen in the Martian atmosphere. *Bull. Amer. Astron. Soc.* **21**, 991.

Brain D.A. and Jakosky, B.M. (1998). Atmospheric loss since the onset of the Martian geologic record: Combined role of impact corrosion and sputtering. *Geophys. Res.,* **103**, 22689-22694.

Brandon, A.D., Walker, R.J., Morgan, J.W., Goles, G.G. (2000). Re-Os isotopic evidence for early differentiation of the Martian mantle. *Geochimica et Cosmochimica Acta*

64, 4083-4095.

Brandon, A.D., Puchtel, I.S., Walker, R.J., Day, J.M.D., Irving, A.J., Taylor, L.A. (2012). Evolution of the Martian mantle inferred from the 187Re–187Os isotope and highly siderophile element abundance systematics of shergottite meteorites. *Geochimica et Cosmochimica Acta* **76**, 206-235.

Bridges, J.C., Catling, D.C., Saxton, J.M., Swindle, T.D., Lyon, I.C., Grady, M.M. (2001). Alteration Assemblages in Martian Meteorites: Implications for Near-Surface Processes. *Space Sci Rev*. **96**, 365-392.

Bridges, J.C., Grady, M.M. (1999). A halite-siderite-anhydrite-chlorapatite assemblage in Nakhla: Mineralogical evidence for evaporites on Mars. *Meteoritics & Planetary Science* **34**, 407-415.

Bridges, J.C., Grady, M.M. (2000) Evaporite mineral assemblages in the Nakhla (Martian) meteorite. *Earth Planet. Sci. Lett.* **176**, 267-279.

Bunch, T.E., Reid, A.M. (1975). The nakhlites, part 1: petrography and mineral chemistry. *Meteoritics* **10**, 303–315.

Borg, L.E., Nyquist, L.E., Taylor, L.A., Wiesmann, H., Shih, C-Y. (1997). Constraints on Martian differentiation processes from Rb-Sr and Sm-Nd isotopic analyses of the basaltic Shergottite QUE94201. *Geochimica et Cosmochimica Acta* **61**, 4915-4931.

Carr M. H. (1979). Formation of Martian flood features by release of water from confined aquifers. *J. Geophys. Res* **84**, 2995-3007.

Carr, M. H. (2012). The fluvial history of Mars. *Phil. Trans. R. Soc. A.* **370**, 2193-2215.

Chassefiere, E. and Leblanc, F. (2004). Mars atmospheric escape and evolution; interaction with the solar wind. *Planet. Space Sci.,* **52**, 1039-1058.

Chaufray, J.Y., Modolo, R., Leblanc, F., Chanteur, G., Johnson, R.E., Luhmann J.G. (2007). Mars solar wind interaction: Formation of the Martian corona and atmospheric loss to space. *Journal of Geophysical Research* **112**, E09009, doi:10.1029/2007JE002915.

Chennaoui Aoudjehane, H., Avice, G., Barrat, G.-A., Boudouma, O., Chen, G., Duke, M.J. M., Franchi, I.A., Gattacceca, J., Grady, M.M., Greenwood, R.C., Herd, C.D.K., Hewins, R., Jambon, A., Marty, B., Rochette, P., Smith, C.L., Sautter, V., Varchovsky, A., Weber, P., Zanda, B (2012). Tissint Matrian Meteorite: A Fresh Look at the Interior, Surface, and atmosphere of Mars. *Science,* **338**, 785-788.

Clayton, R.N., Grossman, L., Mayeda, T. K. (1973). A component of primitive nuclear

composition in carbonaceous meteorites. *Science* **182**, 485.

Clayton, R.N., Mayeda, T.K. (1983). Oxygen isotopes in eucrites, shergottites, nakhlites, and chassignites. *Earth and Planetary Science Letters* **62**, 1-6.

Clayton R. N. and Mayeda T. K. (1996) Oxygen isotope studies of achondrites. *Geochim. Cosmochim. Acta.* **60**, 1999-2017.

Cliff, S.S and Thiemens, M.H. (1997). The $^{18}O/^{16}O$ and $^{17}O/^{16}O$ ratios in atmospheric nitrous oxide: A mass-independent anomaly. *Science,* **278**, 1774-1776.

Coplen T. B. (1994) Reporting of stable hydrogen, carbon, and oxygen isotopic abundances (Technical Report). *Pure Appl. Chem.* **66**, 273-276.

Debaille, V., Yin, Q.Z., Brandon, A.D., Jacobsen, B. (2008). Martian mantle mineralogy investigated by the 176Lu–176Hf and 147Sm–143Nd systematics of shergottites. *Earth and Planetary Science Letters* **269**, 186-199.

Donahue, T.M. (1995) Evolution of water reservoirs on Mars from D/H ratios in the atmosphere and crust *Nature,* **374**, 432–434.

Dreibus, G., Wänke, H. (1987). Volatiles on Earth and Mars: A comparison. *Icarus* **71**, 225-240.

Easton, A. J. and Elliott C. J. (1977). Analyses of some meteorites from the British Museum (Natural History) collection. *Meteoritics,* **vol. 12,** 409-416.

Eiler, J.M., Valley, J.W., Graham, C.M., Fournelle, J. (2002). Two populations of carbonate in ALH84001: geochemical evidence for discrimination and genesis. *Geochimica et Cosmochimica Acta* 66, 1285-1303.

Farmer, C. B., Davies, D.W., Holland, A. L., Laporte, D. D., Doms, P. E. (1977). Mars – Water Vapor observations from the Viking orbiters. *Geophys. Res.,* **82**, 2445-4248.

Farquhar, J., Thiemens, M. H., and Jackson, T. (1998). Atmosphere-surface interaction on Mars: $\Delta^{17}O$ measurement of carbonate from ALH 84001. *Science,* **284**, 1580-1582.

Farquhar, J. and Thiemens M. H. (2000). Oxygen cycle of the Martian atmosphere-regolith system: $\Delta^{17}O$ of secondary phases in Nakhla and Lafayette. *Journal of Geophysical Research* **105**, 11991-11997.

Feldman, W.C., Prettyman, T.H., Maurice, S., Plaut, J.J., Bish,D.L., Vaniman, D.T., Mellon, M.T., Metzger, A.E., Squyres, S.W., Karunatillake, S., Boynton, W.V., Elphic, R.C., Funsten, H.O., Lawrence, D.J., Tokar, R.L. (2004). Global distribution of near-surface hydrogen on Mars. *Journal of Geophysical Research*

31, E09006, doi:10.1029/2003JE002160.

Filiberto, J., Treiman, A.H. (2009). Martian magmas contained abundant chlorine, but little water. *Geology* **37**, 1087-1090.

Franchi, I.A., Wright, I.P., Sexton, A.S. and Pillinger, C.T. (1999). The oxygen-isotopic composition of Earth and Mars. *Meteorit. & Planet. Sci*. **34**, 657-661.

Frost, R. L., Ruan, H., Kloprog ge, J. T., Gates, W. P. (2000). Dehydration and dehydroxylation of nontronites and ferruginous smectite. *Thermochim. Acta,* **346**, 63–72.

Gooding, J.L., Wentworth, S.J., Zolensky, M.E. (1991). Aqueous alteration of the Nakhla meteorite. *Meteoritics* **26**, 135-143.

Goodrich, C. (2002). Olivine-phyric Martian basalts: A new type of Shergottite. *Meteorit. & Planet. Sci*. **37**, B31-34.

Grim, R. E., and G. Kulbicki (1961), Montmorillonite - high temperature reactions and classification, *Am. Mineral* **46**, 1329–1369.

Grinspoon, D.H. and Lewis, J.S. Cometary water on Venus: Implications of stochastic impacts. *Icarus,* **74**, 21-35.

Gross, J., Filiberto, J., Bell, A.S. (2013). Water in the Martian interior: Evidence for terrestrial MORB mantle-like volatile contents from hydroxyl-rich apatite in olivine–phyric shergottite NWA 6234. *Earth and Planetary Science Letters* **369-370, 120-128.**

Halevy, I., Fischer, W.W., Eiler, J.M. (2011). Carbonates in the Martian meteorite Allan Hills 84001formed at 18 ± 4 °C in a near-surface aqueous environment. *Proceedings of the National Academy of Sciences* **108**, 16895-16899.

Hallis, L.J., Taylor, G.J., Nagashima, K., Huss, G.R. (2012). Magmatic water in the Martian Meteorite Nakhla. *Earth and Planetary Science Letters* **359–360**, 84-92.

Hanna J. C., Phillips R. J. (2005). Hydrological modeling of the Martian crust with application to the pressurization of aquifers. *J. Geophys. Res **110, E01004.*

Hardgrove, C., Moersch, J., Drake, D., Mitrofanov, I., Litvak, M., Behar, A., Boynton, W.V., Deflores, L., Fedosov, F., Golovin, D., Jun, I., Harshman, K., Kozyrev, A.S., Malakhov, A., Milliken, R., Kuzmin, R.O., Mischna, M., Mokrousov, M., Nikiforov, S., Sanin, A.B., Tate, C., Varenikov, A., and the MSL Science Team (2013). Chlorine and hydrogen contents from the first 90 sols of MSL DAN active measurements. *LPSC* abstract# **1752**.

Hartmann, W.K., Neukum, G. (2001). Cratering chronology and the evolution of Mars, *Space Sci. Rev.* **96**, 165-194.

Herd, C.D.K., Borg, L.E., Jones, J.H., Papike, J.J. (2002). Oxygen fugacity and geochemical variations in the Martian basalts: implications for Martian basalt petrogenesis and the oxidation state of the upper mantle of Mars. *Geochimica et Cosmochimica Acta* **66**, 2025-2036.

Huff, A.K. and Thiemens, M.H. (1998). $^{17}O/^{16}O$ and $^{18}O/^{16}O$ isotope measurements of atmospheric carbon monoxide and its sources. *Geophy. Res. Lett.,* **25**, 3509-3512.

Hut G. (1987) *Consultants' group meeting on stable isotope reference samples for geochemical and hydrological investigations.* International Atomic Energy Agency, Vienna.

Inoue, T., Wada, T., Sasaki, R., Yurimoto, H. (2010). Water partitioning in the Earth's mantle. *Physics of the Earth and Planetary Interiors* **183**, 245-251.

Irving, A. (2012). Martian Meteorites. http://www.imca.cc/mars/Martian-meteorites.htm.

Jabeen, I. and Kusakabe, M. (1997). Determination of $\delta^{17}O$ Values of reference water samples VSMOW and SLAP. *Chemical Geology,* **143**, 115-119.

Jakosky , B.M. and Farmer, C.B. (1982). The seasonal and global behavior of water vapor in the Mars atmosphere – Compleate global results of the Viking atmospheric water detector experiment. *Geophys. Res.* **87,** 2999-3019.

Jakosky, B.M., Zent, A.P., Zurek, R.W. (1997). The mars Water Cycle: Determining the Role of Exchange with the Regolith. *Icarus,* **130**, 87-95.

Jakosky, B.M., Phillips, R.J. (2001). Mars' volatile and climate history. *Nature* **412**, 237-244.

Johnson, M.C., Rutherford, M.J., Hess, P.C. (1991). Chassigny petrogenesis: Melt compositions, intensive parameters, and water contents of Martian (?) magmas. *Geochimica et Cosmochimica Acta* **55**, 349-366.

Johnston, J.C. and Thiemens, M.H. (1997). The isotopic composition of tropospheric ozone in three environments. *Geophys. Res.,* **102**, 25395-25404.

Karlsson, H. R., Clayton, R. N., Gibson Jr. E. K., Mayeda, T. K. (1992). Water in SNC Meteorites: Evidence for a Martian Hydrosphere. *Science* **255**, 1409-1411.

Koizumi, E., Mikouchi, T., Mcay, G., Monkawa, A., Chokai, J., Miyamoto, M. (2004). Yamato 980459: crystallization of Martian magma. *Lunar Planet. Sci.XXXV.* Lunar Planet inst., Houston abstract# **1494.**

Krasnopolsky, V.A. Mars' upper atmosphere and ionosphere at low, medium, and high solar activities: Implications for evolution of water. *Journal of Geophysical Research (Planets),* **107**, 11-1-11-11.

Kuebler, K. E. (2013). A combined electron microprobe (EMP) and Raman spectroscopic study of the alteration products in Martian meteorite MIL 03346, *Journal of Geophysical Research: Planets* **118**, 347-368.

Kuzmin, R.O., Zabalueva, E.V., Mitrofanov, I.G., Litvak, M.L., Rodin, A.V., Boynton, W.V., Saunders, R.S. (2007). Seasonal Redistribution of Water in the Surficial Martian Regolith: Results from the *Mars Odyssey* High-Energy Neutron Detector (HEND). *Solar System Research* **41***,* 89–102.

Lantz L. L. (1967) A mass spectrometric analysis of oxygen isotopes of water via the cobalt(III) fluoride-water reaction. *MS thesis,* Iowa State University.

Lécuyer, C., Gillet, P., Robert, F. (1998). The hydrogen isotope composition of seawater and the Global water cycle. *Chem. Geol.* **145**, 249–261.

Lapen, T.J., Righter, M., Brandon, A.D., Debaille, V., Beard, B.L., Shafer, J.T., Peslier, A.H., (2010). A younger age for ALH84001 and its geochemical link to shergottite sources in Mars. *Science* **328**, 347-351.

Lee, C.W., Savarino, J., Thiemens, M.H. (1998). Multiple stable oxygen isotope studies od sulfate and hydrogen peroxide collected from rain water: A new way to investigate in-situ S(IV) oxidation chemistry by dissolved H_2O_2 in aqueous solution. *Eos Trans. 79(45) fall meet. Abstract,* **F91**.

Leshin, L.A. (2000). Insight into Martian water resovoirs from analyses of Martian meteorite QUE94201. *Geophys. Res. Lett.* **27**, 2017-2020.

Leshin, L.A., Vicenzi, E. (2006). Aqueous processes recorded by Martian meteorites: Analyzing Martian water on Earth. *Elements* **2**, 157-162.

Leshin, L.A., Epstein, S., Stolper, E.M. (1996). Hydrogen isotope geochemistry of SNC meteorites. *Geochimica et Cosmochimica Acta* **60**, 2635-2650.

Leshin, L.A., Webster, C.R., Mahaffy, P.R., Flesch, G.J., Christensen, L.E., Stern, J.C., Franz H.B., McAdam, A.C., Niles, P.B., Archer, P.D. Jr., Sutter, B., Jones, J.H., Ming, D.W., Atreya, S.K., Owen, T.C., Conrad, P. and the MSL Science Team (2013). Hydrogen isotopic composition of water in the Martian atmosphere and released from Rocknest fines. *LPSC* abstract# **2234**.

Lundin, R., Zakharov, A., Pellinen, R., Borg, H., Hultqvist, B., Pissarenko, N., Dubinin, E. M., Barabash, S.W., Leide, I., Koskinen, H. (1989). First measurements of the

ionospheric escape from Mars. *Nature,* **341**, 609-612.

Luz, B. and Barkan, E. (2010). Variations of $^{10}O/^{16}O$ and $^{18}O/^{16}O$ in meteoric waters. *Geochimica et Cosmochimica Acta.* **74**, 6276-6286.

Maltagliati, L., Titov, D.V., Encrenaz, T., Melchiorri, R., Forget, F., Keller, H.U., Bibring, J.-P. (2011). Annual survey of water vapor behavior from the Omega mapping spectrometer on board Mars Express. *Icarus,* **213**, 480-495.

Maltagliati, L., Montmessin, F., Korablev, O., Fedorove, A., Forget, F., Maattanen, A., Lefevre,F., Bertaux, J.-L. (2013). *Icarus,* **223**, 942-962.

Malin M. C. and Edgett, K. S. (2000). Evidence for Recent Groundwater Seepage and Surface Runoff on Mars. *Science* **288**, 2330-2335.

Marti, K., Kim, J. S., Thakur, A. N., McCoy, T. J. and Keil, K. (1995). Signature of the martial atmosphere in glass of the Zagami meteorite. *Science* **267,** 1981-4.

Mason, H.E., McCubbin, F.M., Smirnov, A., Phillips, B.L. (2009). Solid-state NMR and IR Spectroscopic investigation of the role of structural water and F in carbonate-rich fluoroapatite. *Am. Mineral.* **94**, 507-516.

McCoy, T. J., Taylor, G. J. and Keil, K. (1992). Zagami: Product of two-stage magmatic history. *Geochimica et Cosmochimica Acta,* **56,** 3571-3582.

McCoy, T. J., Wadhwa, M. and Keil, K. (1993). Zagami: Another new lithology and a complex near-surface magmatic history. *LPS XXVI,* 925-926.

McCoy, T. J. and Lofgren G. E. (1999). Crystallization of the Zagami Shergottite: An experimental study. *Earth and Planet. Sci. Lett.* **173,** 397-411.

McCubbin, F. M., Boyce, J. W., Srinivasan, P., Santos, A. R., Elardo S. M., Filiberto, J., Steele, A. And Shearer, C. K. (2016). Heterogeneous distribution of H_2O in the Martian interior: Implications for the abundance of H_2O in depleted and enriched mantle sources. *Meteoritics & Planetary Science.* Volume 51, **11,** 2036-2060.

McCubbin, F.M., Hauri, E.H., Eldardo, S.M., VanderKaaden, K.E., Wang, J., Shearer, C.K. (2012). Hydrous melting of the Martian mantle produced both depleted and enriched Shergottites. *Geology* **40**, 683-686.

McCubbin, F. M., Vander Kaaden, K. E., Tartese, R., Boyce, J. W., Mikhail, S., Whitson, E. S., Bell, A. S., Anand, M., Franchi, I. A. (2015). Experimental investigation of F, Cl, and OH partitioning between apatite and Fe-rich basaltic melt at 1.0-1.2 GPa and 950-1000C. *American Mineralogist,* **100,** 1790-1802.

McKeegan , K.D. and Leshin, L.A. (2001) Stable isotope variability in extraterrestrial

materials. *Stable Isotope Geochemistry* (eds. J. W. Valley and D. R. Cole). Mineralogical Society of America, Washington, D. C. pp. 279-318.

McKeegan, K.D., Aleon, J., Bradley, J., Brownlee, D., Busemann, H., Butterworth, A., Chaussidon, M., Fallon, S., Floss, C., Gilmour, J., Gounelle, M., Graham, G., Guan, Y., Heck, P.R., Hoppe, P., Hutcheon, I.D., Huth, J., Ishii, H., Ito, M., Jacobsen, S.B., Kearsley, A., Leshin, L.A., Liu, M.-C., Lyon, I., Marhas, K., Marty, B., Matrajt, G., Meibom, A., Messenger, S., Mostefaoui, S., Mukhopadhyay, S., Nakamura-Messenger, K., Nittler, L., Palma, R., Pepin, R.O., Papanastassiou, D.A., Robert, F., Schlutter, D., Snead, C.J., Stadermann, F.J., Stroud, R., Tsou,P., Westphal, A., Young, E.D., Ziegler, K., Zimmermann, L., Zinner, E. (2006) Isotopic composition of cometary matter returned by Stardust. *Science,* **314**, 1724-1728.

McSween, H.Y., Harvey, R.P. (1998). An Evaporation Model for Formation of Carbonates in the ALH84001 Martian Meteorite. *International Geology Review* **40**, 774-783.

McSween, H.Y.J., Treiman, A.H. (1998). Martian Meteorities, in: Papike, J.J. (Ed.), Planetary Materials. *Mineralogical Society of America*, Washington, D.C., pp. 6.1-6.53.

McSween, H.Y., Grove, T.L., Lentz, R.C.F., Dann, J.C., Holzheid, A.H., Riciputi, L.R., Ryan, J.G. (2001). Geochemical evidence for magmatic water within Mars from pyroxenes in the Shergotty meteorite. *Nature* **409**, 487-490.

Melwani Daswani, M., Schwenzer, S.P., Wright, I.P., Grady, M.M. (2013). Low temperature near-surface thermochemical modelling of the alteration assemblage in Martian meteorite ALH84001. *LPSC* abstract# **2713**.

Meijer H. A. J. and Li W. J. (1998) The use of electrolysis for accurate $\delta^{17}O$ and $\delta^{18}O$ isotope measurements in water. *Isotopes in Environmental and Health Studies.* **34:4**, 349-369.

Miller M. F. (2002) Isotopic fractionation and the quantification of ^{17}O anomalies in the Oxygen three-isotope system: an appraisal and geochemical significance. *Geochimica et Cosmochimica Acta.* **66**, 1881-1889.

Mitrofanov, I., Litvak, M., Lisov, D., Behar, A., Boynton, W., Deflores, L., Fedosov, F., Golovin, D., Hardgrove, C., Harshman, K., Jun, I., Kozyrev, A., Kuzmin, R., Malakhov, A., Mischna, M., Moersch, J., Mokrousov, M., Nikiforov, S., Sanin, A., Shvetsov, V., Starr, R., Tate, C., Tret'yakov, V., Varenikov, A., Vostrukhin, A. and the MSL Team (2013). Content of Hydrogen at testing spots of the Gale crater: the first data from DAN onboard the Curiosity Mars Rover. *LPSC* abstract# **1487**.

Mittlefehldt, D.W. (1994). ALH84001, a cumulate orthopyroxenite member of the Martian meteorite clan. *Meteoritics* **29**, 214-221.

Murchie, S.L., Mustard, J.F., Ehlmann, B.L., Milliken, R.E., Bishop, J.L., McKeown, N.K., Noe Dobrea, E.Z., Seelos, F.P., Buczkowski, D.L., Wiseman, S.M., Arvidson, R.E., Wray, J.J., Swayze G., Clark, R.N., Des Marais, D.J., McEwen, A.S., Bibring, J.-P. (2009). A synthesis of Martian aqueous mineralogy after one Mars year of observations from the Mars Reconnaissance Orbiter. *Journal of Geophysical Research* **114,** E00D06, doi:10.1029/2009JE003342.

Muttik, N., McCubbin, F.M., Keller, L.P., Santos, A.R., McCutcheon, W.A., Provencio, P.P., Rahman, R., Shearer, C.K., boyce, J.W., Agee, C.B. (2014). Inventory of H_2O in the ancient Martian regolith from Northwest Africa 7034: The important role of Fe oxides. *Geophysical Research Letters* **41**, 8235-8244.

Nair, H., Allen, M., Anbar, A.D., Yung, Y.L., Clancy, R.T. (1994). A photochemical Model of the Martian Atmosphere. *Icarus,* **111**, 124-150.

Nakamura, T., Noguchi, T., Tsuchiyama, A., Ushikubo, T., Kite, N.T., Valley, J.W., Zolensky, M.E., Kakazu, Y., Sakamoto, K., Mashio, E., Uesugi, K., Nakano, T. (2008) Chondrulelike objects in short–period comet 81P/Wild 2. *Science,* **321**, 1664-1667.

Nakashima, D., Ushikubo, T., Zolensky, M.E., Kita, N.T. (2012). High precision oxygen three-isotope analyses of anhydrous chondritic interplanetary dust particles. *Meteorit. Planet. Sci.,* **47**, 1997-208.

Norman, D.I. and Palin, J.M. (1982). Volatiles in phyllosilicate minerals. *Nature* **296**, 551-553.

Ogliore, R.C., Huss, G.R., Nagashima, K., Butterworth, A.L., Gainsforth, Z., Stodolna, J., Westphal, A.J., Joswiak, D., Tyliszczak, T. (2012). Incorporation of a late-forming chondrule into comet Wild 2. *Astrophysics,* **745**, L19.

O'Neil J. R. and Epstein S. J. (1966) A method for oxygen isotope analysis of milligram quantities of water and some of its applications. *Journal of Geophysical Research.* **71**, 4955-4961.

Owen, T., Bieman, K., Rushneck, D.R., Biller, J.E., Howarth, D.W., Lafleur, A.L. (1977). The Composition of the atmosphere at the surface of Mars. *Geophys. Res.,* **82**, 4635-4639.

Owen, T., Bar-Nun, A., Kleinfelf, I. (1992). Possible cometary origin of heavy noble gases in the atmosphere of Venus, Earth and Mars. *Nature.* **358**, 43-46.

Owen, T., Maillard, J.P., de Bergh, C., Lutz, B.L. (1988). The abundance of HDO and the value of D/H *Science.* **240**, 1767–1771.

Pankine, A.A., Tamppari, L.K., Smith, M.D. (2010). MGS TES observations of the water vapor above the seasonal and perennial ice caps during northern spring and summer. *Icarus,* **210**, 58-71.

Papike, J.J., Karner. C.K., Sharer, P.V., Burger, P.V. (2009). Silicate mineralogy of Martian meteorites. *Geochimica et Cosmochimica Acta.* **73**, 7443-7485.

Phillip, R. J., Zuber, M. T., Solomon, S. C., Golombek, W. P., Jakosky, B. M., Banerdt, W. B., Smith, D. E., Williamn, R. M. E., Hynek, B. M., Aharonson, O., Hauck II, A. S. (2001). Ancient Geodynamica and Global-Scale Hydrology on Mars. *Science* **291**, 2687-2591.

Rahmati, A., Larson, D.E., Cravens, T.E., Jillis, R.J., Dunn, P.A., Halekas, J.S., Connerney, J.E., Eparvier, F.G., Thiemenn, E.M.B., Jakosky, B.M. (2015). MAVEN insight into oxygen pickup at Mars. *Geophysical Research Letters,* **42**, 8870-8876.

Reid, A.M., Bunch, T.E., 1975. The nakhlites II: where, when, and how. *Meteoritics* **10**, 317–324.

Rockmann, T., Brenninkmeijer, C.A.M., Neeb, P., Crutzen, P.J. (1998). Ozonolysis of nonmethane hydrocarbons as a source of the observed mass independent oxygen isotope enrichment in troposphere. *Geophys. Res.,* **103**, 1463-1470.

Romanek, C.S., Grady, M.M., Wright, I.P., Mittlefehldt, D.W., Socki, R.A., Pillinger, C.T., Gibon Jr, E.K. (1994). Record of fluid-rock interactions on Mars from ALH84001. *Nature* **372**, 655-657.

Ruzicka, A., Grossman, J.N., Garvie, L. (2014). *The Meteoritical Bulletin,* **100,** 54-55.

Savarino, J., Bhattacharya, S.K., Thiemens, M.H. (1998). Isotopic study of photodissociation of Carbon dioxide: An unusual oxygen mass-independent fractionation and its implications to atmospheres of Mars and Early Earth. *Eos Trans., 79(45), fall meet. Suppl., Abstract,* **F93**.

Sawyer, D.J., McGehee, M.D., Canepa, J., Moore, C.B. (2000). Water soluble ions in the Nakhla Martian meteorite. *Meteoritics & Planetary Science* **35**, 743-747.

Sharp Z. D., Gibbons J. A., Maltsev O., Atudorei V., Pack A., Sengupta S., Shock E. L., Knauth L. P. (2016) A calibration of the ripple oxygen isotope fractionation in the SiO_2-H_2O systems and applications to natural samples. *Geochimica et Cosmochimica Acta.* **186**, 105-119.

Shearer, C. K., Burger, P. V., Papike, J. J., McCubbin, F. M. and Bell, A. S. (2015). Crystal chemistry of merrillite from Martian meteorites: Mineralogical records of magmatic processes and planetary differentiation. *Meteoritics & Planetary Science,* **50,** 649-673.

Smykatz-Kloss, W. (1974). Differential Thermal Analysis. *Springer-Verlag, New York.*

Smith M.D. Interannual variability in TES atmospheric observations of Mars during 1999-2003. *Icarus,* **167**, 148-165.

Smith M.D., Wolff, M.J., Clancy. R.T., Murchie, S.L. (2009). Compact reconnaissance imaging spectrometer observations of water vapor and carbon monoxide. *Geophys. Res. (Planets),* **114**, 0.

Stolper, E. and McSween, Y. H. (1979). Pertology and origin of the shergottite meteorites. *Geochimica et Cosmochimica Acta.* **V43 n4**, 589-602.

Tanaka K. L., Skinner J. A. Jr., Hare T. M. (2005) Geologic map of the northern plains of Mars. *Scientific Investigations Map* 2888, US Geological Survey.

Thiemens, M.H. and Heidenreich, J.E.III. (1983). The Mass-independent fractionation of oxygen - A novel isotope effect and its possible cosmochemical implications. *Science,* **219**, 1073-1075.

Thiemens, M.N. (1999). Mass-independent isotope effects in planetary atmospheres and the early solar system. *Science,* **283**, 341-345.

Thiemens, M.H., Chakraborty, S., Dominguez, G. (2012). The physical chemistry of mass-Independent isotope effects and their observation in nature. *Annu. Rev. Phys. Chem.,* **63**, 155-177.

Treiman, A. H. (1985a) Amphibole and hercynite spinel in Shergotty and Zagami: Magmatic water, depth of crystallization, and metasomatism. *Meteoritics,* **20**, 229-243.

Treiman, A.H. (2005). The nakhlite meteorites: Augite-rich igneous rocks from Mars. *Chemie der Erde* **65**, 203-270.

Treiman, A.H., Barrett, R.A., Gooding, J.L. (1993). Preterrestrial aqueous alteration of the Lafayette (SNC) meteorite. *Meteoritics* **28**, 86-97.

Tschimmel, M. Ignatiev, N.I., Titov, D.V., Lellouch, E., Fouchet, T., Giuranna, M. and Formisano, V. (2008). Investigation of water vapor on Mars with PFS/SW of Mars Experss. *Icarus,* **195**, 557-575.

Usui, T., Alexander, C.M.O.D., Wang, J., Simon, J.I., Jones, J.H. (2012). Origin of water and mantle-crust interactions on Mars inferred from hydrogen isotopes and volatile element abundances of olivine-hosted melt inclusions of primitive shergottites. *Earth and Planetary Science Letters* **357–358**, 119-129.

Usui, T., McSween H. Y., Floss, C. (2008). Pertogenesis of olivine-phyric shergottite Yamato 980459, revisited. *Geochimica et Cosmochimica Acta.* **72**, 1711-1730.

Velivetskaya, T.A., Ignatiev, A.V., Budnitskiy, S.Y., Yakovenko, V.V., Vysotsky, S.V. (2016). Mass-independent fractionation of oxygen isotopes during H_2O_2 formation by gas-phase discharge from water vapor. *Geochimica et Cosmochimica Acta,* **193**, 54-65.

Wang, A., Jolliff, B. and Haskin, A. L. (1999) Raman spectroscopic characterization of a Martian SNC meteorite: Zagami. *Journal of Geophysical Research Atmospheres,* **104,** 8509-8520.

Wänke, H., Dreibus, G. (1988). Chemical composition and accretion history of terrestrial planets. *Phil. Trans. Roy. Soc. London* **A325**, 545-557.

Ziegler K., Sharp Z. D. and Agee C. B. (2013) The unique NWA 7034 Martian meteorite: evidence for multiple oxygen isotope reservoirs. *LPSC abstract#* **2639**.